CARBON AND NITROGEN ISOTOPE RECORDS OF THE HIRNANTIAN GLACIATION

A Thesis Submitted to the College of
Graduate Studies and Research
In Partial Fulfillment of the Requirements
For the Degree of Master of Science
in the Department of Geological Sciences
University of Saskatchewan
Saskatoon

Daniel F. LaPorte

PERMISSION TO USE

In presenting this thesis in partial fulfilment of the requirements for a postgraduate degree from the University of Saskatchewan, I, Dan LaPorte, agree that the Libraries of this University may make it freely available for inspection. I further agree that permission for copying of this thesis in any manner, in whole or in part, for scholarly purposes may be granted by myself, Dr. Chris Holmden, Dr. William P. Patterson, or in my absence or Drs. Holmden and Patterson's absence, by the Head of the Department of Geological Sciences or the Dean of the College in which my thesis work was done. It is understood that any copying or publication or use of this thesis or parts thereof for financial gain shall not be allowed without my written permission. It is also understood that due recognition shall be given to me and to the University of Saskatchewan in any scholarly use which may be made of any material in my thesis titled: *Isotopic Records from Epeiric Sea Settings during the Hirnantian Glaciation: Implications for Carbon Isotope Gradients.*

Requests for permission to copy or to make other use of material in this thesis in whole or part should be addressed to Daniel F. LaPorte or:

Head of the Department of Geological Sciences
University of Saskatchewan
Saskatoon, Saskatchewan
S7N 5E2
Canada

UNIVERSITY OF SASKATCHEWAN
College of Graduate Studies and Research

ABSTRACT
Submitted in partial fulfillment
of the requirements of the

DEGREE OF MASTER OF SCIENCE
By

Daniel F. LaPorte
Department of Geological Sciences
University of Saskatchewan
December 2008

Examining Committee:

Dr. K. Ansdell	Chair of Committee
Dr. C. Holmden	Co-Supervisor, Department of Geological Sciences
Dr. W. Patterson	Co-Supervisor, Department of Geological Sciences
Dr. L. Buatois	Department of Geological Sciences
Dr. M. Mangano	Department of Geological Sciences

CARBON AND NITROGEN ISOTOPE RECORDS OF THE HIRNANTIAN GLACIATION

The Hirnantian mass extinction was the second largest of the Phanerozoic. A global sea level fall resulting from a glaciation on Gondwanaland caused significant changes in ocean circulation patterns and nutrient cycling that is recorded as a worldwide positive $\delta^{13}C$ excursion.

In chapter 2, carbon and nitrogen isotope profiles were reconstructed from two North American carbonate platforms in Nevada and one in the Yukon with the purpose of gaining a better understanding of proximal to proximal gradients in $\delta^{13}C$ values from Hirnantian epeiric seaway sediment. Positive $\delta^{13}C$ excursions are recorded in bulk inorganic and organic carbon fractions from all three sections, and in graptolite periderms from one section. A larger positive excursion is recorded in the proximal sediment (7‰) compared to proximal sediment (3-4‰). This gradient appears to reflect differences in surface water dissolved inorganic carbon $\delta^{13}C$ values across epeiric seas. These findings are consistent with the carbonate weathering hypothesis, that predicts larger positive $\delta^{13}C$ shifts in proximal settings of tropical epeiric seas resulting from changes in the *local* carbon weathering flux caused by the exposure of vast areas of carbonate sediment during glacioeustatic sea level fall and restricted shelf circulation. A 2‰ positive excursion in $\delta^{15}N$ is interpreted to result from increased ocean ventilation, greater partitioning of atmospheric oxygen into downwelling surface waters, oxygen minimum zone shrinkage, and declining denitrification rates. This allowed for upwelling of recycled nitrogen with high $\delta^{15}N$ values into the photic zone that forced exported organic matter from the photic zone to higher $\delta^{15}N$ values, consistent with the observed positive shift in $\delta^{15}N$ during the Hirnantian glaciation. This study presents a conceptual model to explain secular changes in $\delta^{13}C$ and $\delta^{15}N$ during the transition from a greenhouse to icehouse climate.

The second focus of this research, presented in chapter 3, was on improving the chemical and analytical methods for $\delta^{18}O$ analysis of biogenic apatites. The technique applies cation exchange chromatography that allows for small sample sizes of apatite (200 µg) to be used for chemical conversion to Ag_3PO_4. The precision (0.15‰, 1σ) of $\delta^{18}O$ analysis obtained using a Thermal Conversion Elemental Analyser Continuous Flow – Isotope Ratio Mass Spectrometer (TC/EA CF-IRMS), and the ability to collect multipe isotopes (O, Ca, Sr, REE) using a cation

exchange column, makes this technique valuable for high-resolution, multi-isotope studies of biogenic apatites.

Keywords: $\delta^{13}C$, $\delta^{15}N$, $\delta^{18}O$, Hirnantian, mass extinction, epeiric sea, apatite, mass spectrometry.

Acknowledgements

First, I would like to acknowledge the support of my co-supervisors Chris Holmden and William Patterson. I am very grateful for the knowledge they have shared as well as the passion they invoke for science. I thank Tim Prokopiuk for his honesty, problem solving abilities, reading early drafts of the manuscript and assistance with analyses at the Saskatchewan Isotope Laboratory. I also thank Bruce Eglington, Ngat Mee Choo, Blaine Novokavski, Jim Rosen, Stan Finney, Charles Mitchell, and Mike Melchin for all their expertise, assistance and sharing of knowledge during my studies. Finally, I would like to thank my wife Jill; without her love, patience and constant support I surely would not have made it through.

This research was supported by a University of Saskatchewan Graduate Scholarship and a Geologic Society of America Graduate Research Grant to D. LaPorte, and National Sciences Foundation Grant #EAR0418790 to C. Holmden.

TABLE OF CONTENTS

LIST OF TABLES

LIST OF FIGURES

APPENDICES

CHAPTER 1 INTRODUCTION

1.1 Overview and Motivation

1.1.1 Hirnantian Mass Extinction

The Hirnantian stage (~444 Ma) marks the first of five major mass extinctions during the Phanerozoic and has been associated with a continental glaciation on Gondwanaland. Based on biostratigraphic (Melchin and Mitchell, 1991; Brenchley et al., 1994; Finney et al., 1997; Finney et al., 1999; Storch, 2006) and sedimentological studies (Ghienne, 2003; Le Heron et al., 2006; Brenchley et al., 2006), it is believed that the Hirnantian glaciation lasted approximately 0.5 – 2 Ma. In general, the glaciation is characterized by a positive $\delta^{13}C$ excursion that occurs over an interval of 1.5 graptolite biozones (Brenchley et al., 1994; Finney et al., 1997, 1999; Sheehan, 2001; Brenchley et al., 2003) and coincides with atmospheric levels of CO_2 that are estimated to have been approximately 12 to 16 times Present Atmospheric Level (PAL) (Yapp and Poths, 1992). Until recently, the Hirnantian was considered to be a single glacial event during a stable early Paleozoic greenhouse climate period. However, more detailed studies of Ordovician and Silurian stratigraphic sections have revealed greater fluctuations in early Paleozoic climate than was previously assumed, with several geological intervals characterized by positive $\delta^{13}C$ excursions similar to the Hirnantian (Fanton et al., 2002; Saltzman, 2003; Munnecke et al., 2003; Cramer and Saltzman, 2005; Melchin and Holmden, 2006a, b) and, in several cases, evidence of glacioeustatic sea level fall (Grahn and Caputo, 1992; Díaz-Martínez and Grahn, 2007).

The majority of Paleozoic ocean and climate change is recorded in the preserved stratigraphic sections of ancient epeiric seas, defined as relatively shallow seas that cover vast areas of continental landmass during periods of high sea level. Reconstruction of stratigraphic carbon isotope ($\delta^{13}C$) profiles of inorganic and organic carbon sediment and nitrogen isotope ($\delta^{15}N$) profiles of the sedimentary organic matter are two methods that can be used to interpret changes in the Paleozoic ocean and climate systems through the carbon ($\delta^{13}C$) and nutrient ($\delta^{15}N$) cycles.

Traditionally, $\delta^{13}C$ stratigraphic profiles from epeiric sea sediment have been considered representative of the composition of global ocean water $\delta^{13}C$ values of dissolved inorganic

carbon ($\delta^{13}C_{DIC}$). This approach allows for the interpretation of $\delta^{13}C$ from epeiric sea stratigraphic profiles to be used to track changes in global carbon cycling, glaciations, ocean circulation, nutrient availability, and extinction events (Bickert et al., 1997; Veizer et al., 1999; Saltzman, 2002; Saltzman, 2003). The traditional interpretation relies on the assumptions: 1) the residence time of carbon is long enough to ensure a homogeneous isotopic composition within the ocean and contemporaneous epeiric seas, and 2) the size of the ocean DIC reservoir is large enough that it dominates the $\delta^{13}C_{DIC}$ of epeiric seas. In contrast to this view, other studies have suggested that epeiric seas may have been decoupled from the contemporaneous open ocean and local conditions within epeiric seas may have more greatly affected $\delta^{13}C_{DIC}$ than was previously assumed (Patterson and Walter, 1994; Holmden et al., 1998; Fanton et al., 2002; Melchin and Holmden, 2006; Panchuk et al., 2006). For example, Patterson and Walter (1994) determined that lower $\delta^{13}C$ values characterize DIC in relatively restricted waters of Florida Bay/Bahamas Banks compared to waters adjacent to the Florida Reef Tract/Florida Straits that are better mixed with open marine water. Restricted circulation coupled with input of terrestrial organic matter such as mangrove and sea grass detritus from the Everglades with low $\delta^{13}C$ values (Lloyd, 1964; Patterson and Walter, 1994) are the most likely causes. Another study of the Bahamas Bank noted that the $\delta^{13}C_{DIC}$ of the shelf surface waters were on average 0.5‰ higher than the adjacent open marine water (Swart et al., in press). This increased $\delta^{13}C_{DIC}$ was attributed to the difference in fractionation between aragonite and calcite and the high productivity on the shelf. If local control of carbon cycling (C-cycling) on modern day platforms is analogous to ancient epeiric seas, in spite of the vast differences in area between them, carbon cycling processes in Florida Bay and Bahamas Bank could serve as analogues for C-cycling in Ordovician epeiric seas (Patterson and Walter, 1994; Holmden et al., 1998; Panchuk et al., 2005a, b).

Recent studies of ancient epeiric sea C-cycling have shown that changes in C-cycling may have been decoupled from that of the open ocean. If this was the case, then localized changes in circulation, climate, water column depth, and nutrient cycling may have had a greater effect on stratigraphic variations in $\delta^{13}C$ values than has been previously assumed (Holmden et al., 1998; Fanton et al., 2003; Panchuk et al., 2005; 2006; Melchin and Holmden, 2006a, b). A study by Panchuk et al. (2005) showed that it was possible to model a ~4‰ $\delta^{13}C$ gradient across a time-slice of the Mohawkian Sea (Ordovician in age) where lower $\delta^{13}C$ values were found in

proximal locations compared to higher values in locations closer to the open ocean. In order to reproduce the observed gradient, the epeiric sea was divided into two sections (inner and outer region) and circulation was restricted between the two sections and the open ocean. A steady source of low $\delta^{13}C$, possibly from terrestrial sources, was added to the inner region thus driving the $\delta^{13}C_{DIC}$ to lower values compared to the outer region and open ocean. Studies of $\delta^{13}C$ profiles from Hirnantian stratigraphic sections have also noted a gradient in $\delta^{13}C$ across epeiric seas however, the gradient is opposite to that reported by Panchuk et al. (2005) such that proximal settings record larger positive $\delta^{13}C$ excursions than coincident distal setting $\delta^{13}C$ excursions (Finney et al., 1999; Kaljo et al., 2004; Melchin and Holmden, 2006a). This trend exists in three separate basins (Nevada, Cape Phillips, Estonia-Baltica) from two paleocontinents (Laurentia, Baltica). Gaining a better understanding of the causes for the observed carbon isotope gradients in Hirnantian epeiric seas is one of the motivations for conducting this research.

Nitrogen, phosphorous, and iron are considered the major limiting nutrients for productivity in the ocean. The availability of these nutrients controls the strength of the biological carbon pump and consequently the role of the oceanic system on atmospheric CO_2 concentrations. Since the residence time of nitrogen in the modern oceans is only ~3000 years (Gruber, 2004), small changes in the magnitude of the sources (N_2 fixation) and sinks (denitrification) of fixed, or biologically available, nitrogen can have a substantial impact on the marine nitrogen reservoir (Ganeshram et al., 1995).

Nitrogen isotopes have proven to be valuable proxies of climate driven circulation changes in ocean redox state through the Pleistocene glaciations. Down core trends in sedimentary $\delta^{15}N$ records beneath modern upwelling zones reveal increased water column denitrification during warm interglacials ($\delta^{15}N$ = 7–8‰; oxygen minimum zone expansion) and reduced denitrification during cooler glacials ($\delta^{15}N$ = 4–5‰; oxygen minimum zone shrinkage) (Altabet et al., 1995; Ganeshram et al., 1995; Lyle et al., 2000; Ganeshram et al., 2000; Altabet et al., 2002; Dean, 2007). Sedimentary nitrogen isotopes ($\delta^{15}N$) have never been studied through the Hirnantian glaciation and few studies of $\delta^{15}N$ have been reported for the Paleozoic (Calvert et al., 1996). This is mostly because modern nitrogen cycling is still poorly understood and the possibility that the nitrogen cycle had different primary components prior to significant terrestrial

biomass. Changes in the redox state of the Ordovician oceans may have occurred during the transition from a greenhouse to icehouse climate during the Hirnantian. Gaining a better understanding of the N-cycle was the motivation for studying stratigraphic changes in $\delta^{15}N$ from the two sections located in Nevada.

1.1.2 Biogenic apatite $\delta^{18}O$: Chemical and Analytical Procedure

Biogenic apatite $\delta^{18}O$ has been used in modern and palaeoenvironmental research for decades (Longinelli and Nuti, 1973; Kolodney et al., 1983; Longinelli, 1984; Luz et al., 1984; Shemesh et al., 1984; Lécuyer et al., 1996; Stephan, 2000) as an alternative to calcite $\delta^{18}O$. Similar to calcite, the $\delta^{18}O$ value of biogenic apatite reflects the temperature and $\delta^{18}O$ value of the water from which the mineral grew. However, $\delta^{18}O$ values in apatite exhibit a smaller temperature dependence of ~0.23‰/°C, compared to 0.28‰/°C for calcite. For this reason improved isotopic measurement precision, especially for sub-milligram samples of apatite, would benefit the study of biogenic apatites $\delta^{18}O$. The high precision of calcite $\delta^{18}O$ analysis (±0.1‰, 1σ) on samples as small as 10 μg has only been possible for $\delta^{18}O_{PO4}$ measurements of much larger apatite samples in the range of 10–30 mg, using nickel bomb fluorination (Crowson et al., 1991), and offline silica-tube graphite reduction (O'Neil et al., 1994) for converting phosphate oxygen to CO_2 gas prior to mass spectrometric analysis. The large sample sizes practically excludes analysis of a preferred Paleozoic apatite substrate (conodonts) or detailed life history studies using $\delta^{18}O_{PO4}$ time-series reconstructions from mammalian or reptilian teeth. Conodonts are small tooth-like microfossils that weigh between 5 and 100 μg and are preserved in marine sediment from the Cambrian to the Triassic. Because conodonts are composed of apatite, they are a promising proxy for seawater paleotemperature reconstructions (Luz et al., 1984; Joachimski et al., 2006). Life history studies would also benefit from smaller sample sizes and greater precision that would allow for more detailed time-series reconstruction.

1.2 Methodology

My research is divided into two main chapters (2 and 3), each a separate article submitted for peer-review in scientific journals. Chapter 2 has been submitted for publication in *Palaeogeography, Palaeoclimatology, Palaeoecology* and Chapter 3 has been accepted for

publication in *Journal of Mass Spectrometry*. Each article consists of original work by the author with supervision by the author's co-advisors. Chapter 2 uses carbon and nitrogen isotope stratigraphic profiles from proximal and distal settings to gain a better understanding of $\delta^{13}C$ gradients in epeiric sea dissolved inorganic carbon that occurred during the Hirnantian and nutrient cycling during a change from greenhouse to icehouse climate. The additional use of $\delta^{13}C$ of graptolites, and supporting geochemical data assists in identifying changes in the primary productivity, source mixing of isotopically distinct watermasses, and potential diagenetic effects as well as adding constraints on a conceptual model.

Chapter 3 then discusses a chemical and analytical technique developed by the author for the $\delta^{18}O$ analysis of apatite that results in small sample sizes (200 μg), limits fractionation during processing, attains precise $\delta^{18}O$ analysis (0.15‰, 1σ), and allows for collection of multiple isotope systems (Ca, Sr, REE). Although the chapter contents are treated separately, both chapters make contributions to the study and interpretation of preserved ancient epeiric sea isotope stratigraphic profiles and their relation to palaeoceanography and palaeoclimatology.

1.3 References

Altabet, M.A., Francois, R., Murray, D.W., and Prell, W.L. 1995. Climate-related variations in denitrification in the Arabian Sea from sediment $^{15}N/^{14}N$ ratios. Nature, v. 373, p. 506-509.

Altabet M.A., Higginson, M.J., and Murray, D.W. 2002. The effect of millennial-scale changes in Arabian Sea denitrification on atmospheric CO_2. Nature, v. 415, p. 159-162.

Bickert, T., Patzold, J., Samtleben, C., and Munnecke, A. 1997. Paleoenvironmental changes in the Silurian indicated by stable isotopes in brachiopod shells from Gotland, Sweden. Geochimica et Cosmochimica Acta, v. 61, p. 2717-2730.

Brenchley, P.J., Marshall, J.D., Carden, G.A.F., Robertson, D.B.R., Long, D.G.F., Meidla, T., Hints, L., and Anderson, T.F. 1994. Bathymetric and isotopic evidence for a short-lived Late Ordovician glaciation in a greenhouse period. Geology, v. 22, p. 295-298.

Brenchley, P.J., Carden, G.A., Hints, L., Kaljo, D., Marshall, J.D., Martma, T., Meidla, T., and Nõlvak, J. 2003. High-resolution stable isotope stratigraphy of Upper Ordovician sequences: Constraints on the timing of bioevents and environmental changes associated with mass extinction and glaciation. GSA Bulletin, v. 115, p. 89-104.

Brenchley, P.J., Marshall, J.D., Harper, D.A.T., Buttler, C.J., and Underwood, C.J. 2006. A late Ordovician (Hirnantian) karstic surface in a submarine channel, recording glacio-eustatic sea-level changes: Meifod, central Wales. Geological Journal, v. 41, p. 1-22.

Calvert, S.E., Bustin, R.M., and Ingall, E.D. 1996. Influence of water column anoxia and sediment supply on the burial and preservation of organic carbon in marine shales. Geochimica et Cosmochimica Acta, v. 60, p. 1577-1593.

Cramer, B.D., and Saltzman, M.R. 2005. Sequestration of ^{12}C in the deep ocean during the early Wenlock (Silurian) positive carbon isotope excursion. Palaeogeography, Palaeoclimatology, Palaeoecology, v. 219, p. 333-349.

Crowson, R.A., Showers, W.J., Wright, E.K., and Hoering, T.C. 1991. Preparation of phosphate samples for oxygen isotope analysis. Analytical Chemistry, v. 63, p. 2397-2400.

Dean,W.E. 2007. Sediment geochemical records of productivity and oxygen depletion along the margin of western North America during the past 60,000 years: teleconnections with Greenland Ice and the Caraico Basin. Quarternary Science Reviews, v. 26, p. 98-114.

Díaz-Martínez, E., and Grahn,Y. 2007. Early Silurian glaciation along the western margin of Gondwana (Peru, Bolivia, and northern Argentina): palaeogeographic and dynamic setting. Palaeogeography, Palaeoclimatology, Palaeoecology, v. 245, p. 62-81.

Fanton, K.C., Holmden, C., Nowlan, G.S., and Haidl, F.M. 2002. $^{143}Nd/^{144}Nd$ and Sm/Nd Stratigraphy of Upper Ordovician epeiric sea carbonates. Geochimica et Cosmochimica Acta, v. 66, p. 241-255.

Finney, S.C., Cooper, J.D., and Berry, W.B.N. 1997. Late Ordovician Mass Extinction: Sedimentologic, Cyclostratigraphic, and Biostratigraphic Records from Platform and Basin Successions, Central Nevada. BYU Geology Studies, v. 42, p. 79-102.

Finney, S.C., Berry, W.B.N., Cooper, J.D., Ripperdan, R.L., Sweet, W.C., Jacobson, S.R., Soufiane, A., Achab, A., and Noble, P.J. 1999. Late Ordovician mass extinction: A new perspective from stratigraphic sections in central Nevada. Geology, v. 27, p. 215-218.

Ganeshram, R.S., Pedersen, T.F., Calvert, S.E., and Murray, J.W. 1995. Large changes in oceanic nutrient inventories from glacial to interglacial periods. Nature, v. 376, p. 755-758.

Ganeshram, R.S., Pedersen, T.F., Calvert, S.E., McNeill, G.W., and Fontugne, M.R. 2000. Glacial-interglacial variability in denitrification in the world's oceans. Causes and consequences. Paleoceanography, v. 15, p. 361-376.

Ghienne, J.-F. 2003. Late Ordovician sedimentary environments, glacial cycles, and post-glacial transgression in the Taoudeni basin, West Africa. Palaeogeography, Palaeoclimatology, Palaeoecology, v. 189, p. 117-145.

Grahn, Y., and Caputo, M.V. 1992. Early Silurian glaciations in Brazil. Palaeogeography, Palaeoclimatology, Palaeoecology, v. 99, p. 1-15.

Gruber, N. 2004. The dynamics of the marine nitrogen cycle and its influence on atmospheric CO_2 variations. NATO Advanced Study Institute on Carbon and Climate, p. 97-148.

Holmden, C., Creaser, R.A., Muehlenbachs, K., Leslie, S.A., and Bergstrom, S.M. 1998. Isotopic evidence for geochemical decoupling between ancient epeiric seas and bordering oceans: Implications for secular curves. Geology, v. 26, p. 567-570.

Joachimski, M.M., von Bitter, P.H., and Buggisch, W. 2006. Constraints on Pennsylvanian glacioeustatic sea-level changes using oxygen isotopes of conodont apatite: Geology, v. 34, p. 277-280.

Kaljo, D., Hints, L., Martma, T., Nõlvak, J., and Oraspõld, A. 2004. Late Ordovician carbon isotope trend in Estonia, its significance in stratigraphy and environmental analysis. Palaeogeography, Palaeoclimatology, Palaeoecology, v. 210, p. 165-185.

Kolodny, Y., Luz, B., and Navon, O. 1983. Oxygen isotope variations in phosphate of biogenic apatites 1. Fish bone apatite - rechecking the rules of the game. Earth and Planetary Science Letters, v. 64, p. 398-404.

Kump, L.R., Arthur, M.A., Patzkowsky, M.E., Gibbs, M.T., Pinkus, D.S., and Sheehan, P.M. 1999. A weathering hypothesis for glaciation at high atmospheric pCO2 during the Late Ordovician. Palaeogeography, Palaeoclimatology, Palaeoecology, v. 152, p. 173-187.

Lécuyer, C., Grandjean, P., and Emig, C.C. 1996. Determination of oxygen isotope fractionation between water and phosphate from living lingulids: Potential application to palaeoenvironmental studies. Palaeogeography, Palaeoclimatology, Palaeoecology, v. 126, p. 101-108.

Le Heron, D.P., Ghienne, J.-F., Houicha, M.E., Khoukhi, Y., and Rubino, J.-L. 2006. Maximum extent of ice sheets in Morocco during the Late Ordovician glaciation. Palaeogeography, Palaeoclimatology, Palaeoecology, (in press).

Lloyd, M.R. 1964. Variations in the oxygen and carbon isotope ratios of Florida Bay mollusks and their environmental significance. Journal of Geology, v. 72, p. 84-111.

Longinelli, A., and Nuti, S. 1973. Revised phosphate-water isotopic temperature scale. Earth and Planetary Science Letters, v. 19, p. 373-376.

Longinelli, A. 1984. Oxygen isotopes in mammal bone phosphate - a new tool for Paleohydrological and Paleoclimatological research. Geochimica Et Cosmochimica Acta, v. 48, p. 385-390.

Luz, B., Kolodny, Y., and Kovach, J. 1984. Oxygen isotope variations in phosphate of biogenic apatites 3. Conodonts. Earth and Planetary Science Letters, v. 69, p. 255-262.

Lyle, M., Koizumi, I., Delaney, M.L., and Barron, J.A. 2000. Sedimentary record of the California Current system, middle Miocene to Holocene. a synthesis of Leg 167 results, In: Lyle, M., Koizumi, I., Richter, C., and Moore, Jr., T.C., (Eds.), Proceeding of the Ocean Drilling Program, Scientific Results, v. 167, p. 341-376.

Melchin, M.J., and Mitchell, C.E. 1991. Late Ordovician extinction in the Graptoloidea. In: Barnes, C.R., and Williams, S.H. (Eds.), Advances in Ordovician Geology. Paper-Geological Survey of Canada, v. 90-9, p. 143-156.

Melchin, M.J., and Holmden, C. 2006a. Carbon isotope chemostratigraphy in Arctic Canada: Seal-level forcing of carbonate platform weathering and implications for Hirnantian global correlation. Palaeogeography, Palaeoclimatology, Palaeoecology, v. 234, p. 186-200.

Melchin, M.J., and Holmden, C. 2006b. Carbon isotope chemostratigraphy of the Llandovery in Arctic Canada: Implications for global correlation and sea-level change. GFF, v. 128, p. 173-180.

Munnecke, A., Samtleben, C., and Bickert, T. 2003. The Ireviken Event in the lower Silurian of Gotland, Sweden – relation to similar Palaeozoic and Proterozoic events. Palaeogeography, Palaeoclimatology, Palaeoecology, v. 195, p. 99-124.

O'Neil, J.R., Roe, L.J., Reinhard, E., and Blake, R.E. 1994. A rapid and precise method of oxygen isotope analysis of biogenic phosphate. Israel Journal of Earth-Sciences, v. 43, p. 203-212.

Panchuk, K.M., Holmden, C., and Kump, L.R. 2005. Sensitivity of the epeiric sea carbon isotope record to local-scale carbon cycle processes: Tales from the Mohawkian Sea. Palaeogeography, Palaeoclimatology, Palaeoecology, v. 228, p. 320-337.

Panchuk, K.M., Holmden, C., and Leslie, S.A. 2006. Local controls on carbon cycling in the Ordovician Midcontinent Region of North America with implications for carbon isotope secular curves. Journal of Sedimentary Research, v. 76, p. 200-211.

Patterson, W.P., and Walter, L.M. 1994. Depletion in ^{13}C in seawater ΣCO_2 on modern carbonate platforms. Significance for the carbon isotopic record of carbonates. Geology, v. 22, p. 885-888.

Saltzman, M.R. 2002. Carbon isotope ($\delta^{13}C$) stratigraphy across the Silurian-Devonian transition in North America: evidence for a perturbation of the global carbon cycle. Palaeogeography, Palaeoclimatology, Palaeoecology, v. 182, p. 83-100.

Saltzman, M.R. 2003. Late Paleozoic ice age: Oceanic gateway or pCO_2?. Geology, v. 31, p. 151-154.

Shemesh, A., Kolodny, Y., and Luz, B. 1983. Oxygen isotope variations in phosphate of biogenic apatites 2. Phosphorite rocks. Earth and Planetary Science Letters, v. 64, p. 405-416.

Sheehan, P.M. 2001. History of marine biodiversity. Geological Journal, v. 36, p. 231-249.

Sigman, D.M., and Boyle, E.A. 2000. Glacial/interglacial variations in atmospheric carbon dioxide. Nature, v. 407, p. 859-869.

Stephan, E. 2000. Oxygen isotope analysis of animal bone phosphate: Method refinement, influence of consolidants, and reconstruction of palaeotemperatures for Holocene sites. Journal of Archaeological Science, v. 27, p. 523-535.

Storch, P. 2006. Facies development, depositional settings and sequence stratigraphy across the Ordovician–Silurian boundary: a new perspective from the Barrandian area of the Czech Republic. Geological Journal, v. 41, p. 163–192.

Swart, P.K., Reijmer, J.J.G., and Otto, R. (in press), Variations in the $\delta^{13}C$, $\delta^{18}O$, and mineralogy of surface sediments on Great Bahama Bank: Implications for reading the fossil record.

Veizer, J., Ala, D., Azmy, K., Bruckshen, P., Buhl, D., Bruhn, F., Carden, G.A.F., Diener, A., Ebneth, S., Godderis, Y., Jasper, T., Korte, C., Pawellek, F., Podlaha, O.G., and

Strauss, H. 1999. $^{87}Sr/^{86}Sr$, $\delta^{13}C$ and $\delta^{18}O$ evolution of Phanerozoic seawater. Chemical Geology, v. 161, p. 59-88.

Yapps, C.J, and Poths, H. 1992. Ancient atmospheric CO_2 pressures inferred from natural goethites. Nature, v. 355, p. 342-344.

CHAPTER 2. CARBON AND NITROGEN CYCLING DURING THE HIRNANTIAN GLACIATION: IMPLICATIONS FOR EPEIRIC SEA ISOTOPE GRADIENTS, PRODUCTIVITY AND CALCITE DUST DEPOSITION

2.1 Abstract

The impact of variability in climate and ocean circulation on marine carbon and nitrogen cycling was investigated for the late Ordovician Hirnantian glaciation. Study sections from two basins in western Laurentia included two stratigraphic sections from Nevada and one from the Yukon. The opportunity to compare coupled $\delta^{13}C_{carb}$, $\delta^{13}C_{org}$ and $\delta^{13}C_{grap}$ profiles between ocean and epeiric platform settings enabled a more thorough assessment of environmental and diagenetic factors influencing the preservation of seawater $\delta^{13}C$ signals in each deposit. Using the best-preserved sedimentary components, a ~4‰ difference in peak magnitude values was found between Hirnantian $\delta^{13}C$ excursions reconstructed from shallow platform and slope deposits—with shallow platform sediment recording larger excursions. The inferred platform gradient in sedimentary $\delta^{13}C$ values is interpreted to reflect seawater $\delta^{13}C$ gradients in dissolved inorganic carbon. Gradients of similar magnitude have been reported from Hirnantian platforms in the Canadian Arctic and Baltic basins. Taking the most oceanward sections, a positive shift of just 2.6 ±0.4‰ quantifies the impact of the Hirnantian carbon cycle perturbation on the ocean carbon reservoir, significantly less than the 5–7‰ shifts recorded in epeiric platform settings.

A $\delta^{15}N$ profile through the Hirnantian glacial interval records a 2‰ positive shift in the Vinini Creek section, Nevada. Interpreted as a major Late Ordovician upwelling zone, high organic carbon (>1 wt.%) and hydrogen indices (400–600) make the Vinini Creek section a suitable candidate for the preservation of original sedimentary $\delta^{15}N$ records. To explain the results, a conceptual model of ocean nitrogen cycling is presented that highlights the dual role of cyanobacteria as primary producers and nitrogen fixers. In greenhouse climates, deepwater fixed nitrogen inventories decline due to denitrification in the ocean's expansive oxygen minimum zones. This causes algal productivity to become strongly dependent on a continuous supply of fixed nitrogen from cyanobacteria in the photic zone. Nitrogen fixation imparts low $\delta^{15}N$ values to the cyanobacterial biomass, and since they are the primary source of nitrogen, the algal biomass adopts a similarly low $\delta^{15}N$ value. The cooler climate of the Hirnantian icehouse led to

increased ocean ventilation, greater partitioning of atmospheric oxygen into downwelling surface waters, oxygen minimum zone shrinkage, and declining denitrification rates. The decrease in denitrification allowed for more upwelling of recycled nitrogen with high $\delta^{15}N$ values into the photic zone that increased the $\delta^{15}N$ value of fixed nitrogen pool in the photic zone. This in turn shifted the exported organic matter from the photic zone to higher $\delta^{15}N$ values, consistent with the observed positive shift during the Hirnantian glaciation.

No compelling evidence was found for an increase in ocean productivity as the main cause of the 2.6‰ shift in the $\delta^{13}C$ value of the Hirnantian global ocean. The shift in the $\delta^{13}C$ is attributed to increased carbonate weathering during the glacio-eustatic sea level lowstand. Increased productivity may, however, be partly responsible for the much larger shifts recorded in the epeiric seas (5-7‰). Weathering of carbonate sediment will be accompanied by nutrient release (e.g., Fe and PO_4) with some nutrients delivered by calcite dust. Because the supply of calcite dust drops off rapidly with increasing distance from the paleo-shoreline, any ^{13}C enriched DIC, or ^{13}C increase from primary productivity, will decrease towards the ocean—a pattern consistent with the orientation of the inferred seawater gradient in $\delta^{13}C$ values. The absence of vascular plants, the predictable increase in the velocity of the trade winds in icehouse climates, and the large quantities of calcite sediment exposed by the glacio-eustatic lowering of sea level, all point to a prominent role for calcite dust as a component of the early Paleozoic carbon cycle.

2.2 Introduction

The Hirnantian (latest Ordovician) glaciation occurred in the midst of a prolonged early Paleozoic greenhouse climate with atmospheric CO_2 levels 12 to 16 times higher than the present (Berner, 1990; Yapp and Poths, 1992). Such high levels of greenhouse gases would at first seem to be incompatible with the growth of continental ice sheets. But the discovery of early Silurian tillites, and sea level lowstand deposits bearing sedimentological and geochemical attributes similar to those of the Hirnantian glacio-eustatic cycle, suggests that early Paleozoic climates were more variable than previously thought (Loydell, 1998; Munnecke et al., 2003; Johnson, 2006; Long, 2007). Climate change, however, is not the only distinguishing feature of the Hirnantian Stage that lasted approximately 1.9 million years (Cooper and Sadler, 2004). Hirnantian stratigraphic sections host evidence of the second largest mass extinction event in the

Phanerozoic (Bambach et al., 2004), and a carbon cycle perturbation that dwarfs those of the Pleistocene glaciations. How the Hirnantian glaciation provoked such a dramatic response from the marine carbon cycle is one of the broader questions that motivate this work.

Herein I present $\delta^{13}C$ records of bulk organic matter, graptolite periderm, and bulk carbonate sediment in three Hirnantian sections and $\delta^{15}N$ of bulk organic matter in two sections from western Laurentia (Fig. 2.1). I studied two sections from Nevada, situated south of the paleoequator during the Hirnantian. The distal section is located along Vinini Creek, in the Roberts Mountains, whereas the proximal composite section was reconstructed from sections in the Copenhagen Canyon of the Monitor Range (Finney et al., 1999). The third study section is located along the Blackstone River in the Ogilvie Mountains, Yukon Territory and was situated north of the paleoequator during the Late Ordovician. I seek to understand the significance of shelf gradients in $\delta^{13}C$ values preserved in bulk carbonate and organic matter found in previous studies of Hirnantian epeiric platforms (Finney et al., 1999; Kaljo et al., 2004; Melchin and Holmden, 2006a), features that Melchin and Holmden (2006a) suggested reflect original seawater gradients in $\delta^{13}C_{DIC}$ values. According to the authors, declining Hirnantian sea level exposed vast areas of carbonate sediment in tropical and subtropical epeiric seas, thereby shifting the $\delta^{13}C_{DIC}$ of local carbon weathering fluxes to higher values. Epeiric seas in low latitudes received the carbonate weathering flux directly, and $\delta^{13}C_{DIC}$ values rose quickly because of the relatively small DIC pools and restricted circulation with the surface ocean. By contrast, the impact of carbonate weathering on the ocean $\delta^{13}C_{DIC}$ value was smaller because the globally weighted $\delta^{13}C_{DIC}$ value of weathered carbon to the oceans was lowered by contributions from high latitude silicate weathering. In addition, the large DIC reservoir of the ocean damped the response to carbon weathering flux changes.

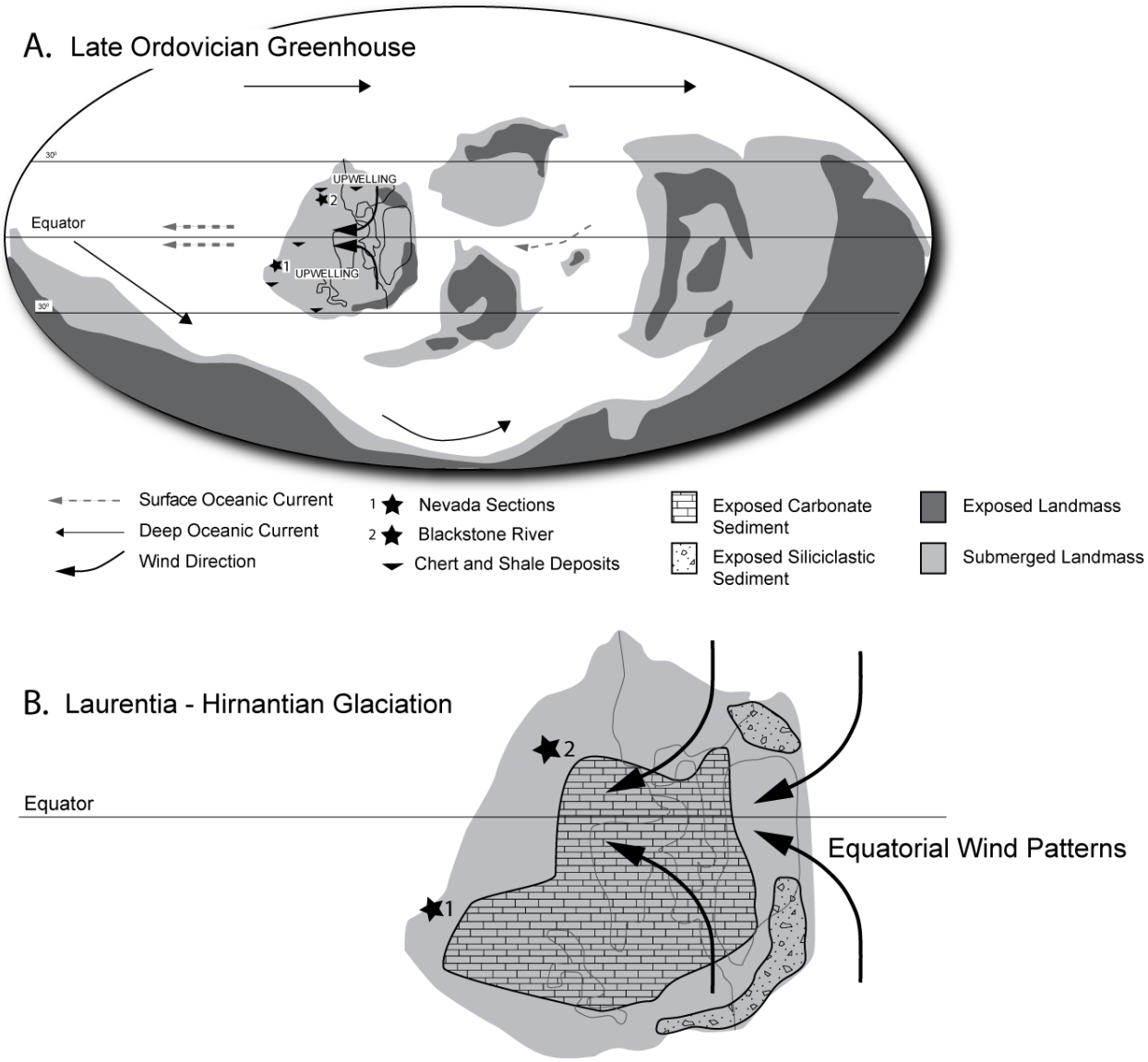

Figure 2.1 A. Late Ordovician paleogeographic map of Laurentia showing the submerged (light grey) and emergent (dark grey) areas of the Laurentian craton, and the position of the paleoequator (modified from Scotese 1997). The locations of the study areas are shown with the ★ symbol (1. Nevada; 2. Yukon). Implied Ocean currents, wind directions and location of cherty limestones; indicative of upwelling zones are modified from Pope and Steffen (2003). B. Schematic of Laurentian exposed carbonate platforms during the Hirnantian glacioeustatic sea level fall modified from Kump et al. (1999). Arrows denote equatorial wind patterns during the Hirnantian resulting from Hadley cell contraction.

A more robust test of the seawater gradient hypothesis is to demonstrate that spatial and temporal $\delta^{13}C$ trends are preserved in both the inorganic and organic carbon fractions of the sediment (Patterson and Walter, 1994a; Holmden et al., 1998; Immenhauser et al., 2003; Gischler and Lomando, 2005; Panchuk et al., 2006; Fanton and Holmden, 2007). However, because shallow water settings are typically rich in carbonate sediment but poor in organic matter, whereas deepwater settings are opposite, it is sometimes difficult to produce $\delta^{13}C$ profiles from both fractions. Because calcareous plankton had not yet evolved (cf., Munnecke et al., 2003), deepwater carbonates must be examined for evidence of transport from nearby platforms. Furthermore, organic carbon in deepwater sediment records surface water properties, not bottom waters, and proximal sediments are susceptible to mixing with terrestrially derived organic carbon that can overprint the seawater signature recorded in marine sediment.

Preservation is also a concern for sedimentary $\delta^{15}N$ records of bulk organic matter. There is a suspicion that many of the ancient records are altered by isotopic fractionation during denitrification and remobilization of nitrogen species in the sediment (Libes and Deuser, 1988; Calvert et al., 1996; Sachs and Rapeta, 1999; Lehmann et al., 2002). The alteration issue is exacerbated by the possibility that the marine nitrogen cycle operated differently in the past, and the general lack of ancient case studies from which to devise and test diagenetic screening strategies. In spite of the pitfalls, there are good reasons for pursuing the record of $\delta^{15}N$ cycling associated with the Hirnantian glaciation. Downcore records of sedimentary $\delta^{15}N$ trends beneath modern upwelling zones reveal increased water column denitrification during warm Pleistocene interglacials ($\delta^{15}N$ = 7–8‰; oxygen minimum zone expansion) and reduced denitrification during cooler glacials ($\delta^{15}N$ = 4–5‰; oxygen minimum zone shrinkage) (Altabet et al., 1995; Ganeshram et al., 1995; Lyle et al., 2000; Ganeshram et al., 2000; Herbert et al., 2001; Altabet et al., 2002; Dean, 2007). Denitrification rates are tightly coupled to ocean ventilation rate and oxygen minimum zone development. The Vinini Creek setting is interpreted as a major Late Ordovician upwelling zone (Finney et al., 2007). Sedimentary TOC values are high (1–20 wt.%), and by analogy with Pleistocene upwelling zones, the sedimentary $\delta^{15}N$ record may be well preserved in this setting. If so, a secular record of $\delta^{15}N$ spanning the climate transition from late Ordovician greenhouse to Hirnantian icehouse may provide a valuable proxy record of ocean circulation and redox changes.

2.3 Materials and Methods

Whole-rock samples from the Vinini Creek and Blackstone River sections were collected in the summers of 2005 and 2006, respectively. Samples from the Monitor Range section were collected during an earlier field season by Finney et al. (1999). All of the isotopic data presented herein are new. The sampling protocol employed at Vinini Creek and Blackstone River did not discriminate between subtle variations in the lithologies present in the section, whereas the sampling of the Monitor Range section targeted the limestone units, and avoided shale partings. The Vinini Creek and Blackstone River samples were broken into gravel sized pieces to expose fresh surfaces. Pieces contaminated by modern plant traces on fracture surfaces, or those with visible calcite veining, were carefully removed before powdering in a tungsten carbide swing-mill device. Carbon and oxygen isotope values of carbonate were derived from 50-100 μg of limestone powder using a Kiel III carbonate device directly coupled to a Thermo Finnigan MAT 253 instrument. The data are reported in the standard delta (δ) notation reflecting per mil (‰) variations in the $^{13}C/^{12}C$ ratio relative to Vienna PeeDee Belemnite (VPDB). Calibration of our reference gas to the VPDB scale was performed by repeated measurements of NIST (NBS) 19 normalized to the internationally accepted values of 1.95‰ and –2.20‰ for $\delta^{13}C$ and $\delta^{18}O$, respectively. The reproducibility of the $\delta^{13}C_{carb}$ values is based on repeated analyses of an internal carbonate standard yielding ±0.05‰ (1σ) over the course of this work.

Preparation of the bulk organic matter used for the measurements of $\delta^{13}C_{org}$ and $\delta^{15}N_{TN}$ involved accurately weighing ~2g of powdered rock, followed by digestion in HCl to remove carbonate minerals. The residue, consisting of organic matter, silicates, and oxides, was thoroughly rinsed, dried and then re-powdered to achieve sample homogeneity. Total organic carbon (TOC) was determined by comparing the sum of the ion beam voltages for the masses 44, 45, and 46 between the samples and an internal organic carbon standard with a known concentration of carbon. Samples of graptolite periderm were collected from freshly cleaved rock surfaces using a razor blade. Care was taken to avoid matrix sediment. The graptolites were treated with 6.0 N HCl prior to mass spectrometric analysis in order to remove traces of contaminant calcite. Total nitrogen contents (TN) were determined similarly to TOC using

masses 28 and 30 and the nitrogen concentration of the standard. The uncertainty in TOC and TN is ±5% and ±25% (1σ), respectively, based on replicate analyses.

$\delta^{13}C_{org}$ and $\delta^{15}N_{TN}$ analyses were performed using a Flash Elemental Analyzer (EA) coupled to a Thermo Finnigan Delta Plus XL instrument operating in continuous flow mode. The analyses are reported in the standard delta (δ) notation reflecting the per mil variation in $^{13}C/^{12}C$ and $^{15}N/^{14}N$ ratios relative to VPDB and Atmospheric N_2, respectively. The reference materials used for the $\delta^{13}C_{org}$ and $\delta^{15}N_{TN}$ measurements were calibrated against international standards: L-SVEC ($\delta^{13}C$ = –46.6‰ VPDB) and IAEA-CH6 ($\delta^{13}C$ = –10.45‰ VPDB) for $\delta^{13}C_{org}$; USGS–25 ($\delta^{15}N$ = –30.4‰ Atm. N_2) and IAEA-305A ($\delta^{15}N$ = 39.8‰ Atm. N_2) for $\delta^{15}N_{TN}$. The 1σ external precision for $\delta^{13}C_{org}$ and $\delta^{15}N_{TN}$ are, respectively, ±0.1‰ and ±0.4‰, based on repeated analyses of caffeine as an internal standard. Molar C/N ratios were calculated from TOC and TN concentrations.

Calcium, magnesium, and strontium concentrations were determined using an atomic absorption instrument with uncertainties of better than ±10% (2σ) based on replicate analyses of internal standards. Mg/Ca and Sr/Ca are reported as molar ratios.

Rock-Eval analysis was performed using a Rock-Eval VI apparatus in the Organic Geochemistry Laboratory, Geological Survey of Canada, Calgary Alberta. Approximately 70 mg of whole rock powder was heated under an inert atmosphere of N_2 to determine the quantity of free hydrocarbons (*S1*) and those that might be released after maturation (*S2*). The T_{max} value is the temperature when the *S2* peak reaches its maximum. It is used as a maturity indicator for the organic matter. Hydrogen index (HI) is an indicator of the richness of hydrogen in the organic matter compared to carbon in units of mg/g.

2.4 Graptolite Biostratigraphy

The Vinini Creek section in Nevada (Fig. 2.2) is host to a rich graptolite fauna that includes four graptolite zones. From bottom to top these are: *D. ornatus*, *P. pacificus* (including an upper *D. mirus* Subzone), *N. extraordinarius*, and *N. persculptus* (Finney et al., 1999, modified in Mitchell et al., 2007). Continuous deposition through the *D. ornatus* to the *N.*

persculptus zones is well documented at Vinini Creek (Finney et al., 1997). New graptolite collections from the 2005 expedition show *N. persculptus* in what was previously referred to as the upper *N. extraordinarius* Zone. This places the base of the *N. persculptus* Zone at 23.5 m instead of the previously published 26 m level in Finney et al. (1999).

The sparse graptolite occurrences at Monitor Range in Nevada (Fig. 2.3) make it difficult to achieve an exact biostratigraphic correlation with Vinini Creek. Graptolites representing the *P. pacificus* Zone disappear at 152 m—along with conodonts and chitinozoans—and thereafter the section is barren until the first appearance of *N. persculptus* near the top of the section at 198 m (Finney et al., 1999). A chemostratigraphic correlation using the $\delta^{13}C$ profiles would place the *D. mirus* Subzone between 144 and 152 m, and the base of the *N. persculptus* Zone at approximately 175 m (Fig. 2.3). The absence of Hirnantian graptolites in the Monitor Range section most likely reflects watermass properties unfavourable for graptolite colonization and poor taphonomic conditions for graptolite preservation, rather than the omission of Hirnantian rocks.

The Blackstone River section in the Yukon (Fig. 2.4) yielded a graptolite succession with four zones and one subzone. From bottom to top these are the *P. pacificus* (again including its upper, *D. mirus, subzone)*, *N. extraordinarius*, and *N. persculptus* zones and a combined *A. ascensus-P. acuminatus Zone*. Although the base of the *N. extraordinarius* Zone is well defined, the overlying limestone-rich interval has not produced graptolites, but instead yield common trilobites and brachiopods among other benthic fossils. I interpret these rocks to have been deposited in relatively proximal conditions during the sea level fall associated with the Hirnantian glacial maxima. Graptolites indicative of the *N. persculptus* Zone first appear at the base of the succession of black shales that overly these early Hirnantian lowstand limestones and this association suggests the base of the zone likely falls within the non-graptoliferus interval. The base of the *N. persculptus* Zone has been estimated based on a comparison of the patterns of change of the $\delta^{13}C$ profiles in the three studied sections (Fig. 2.4).

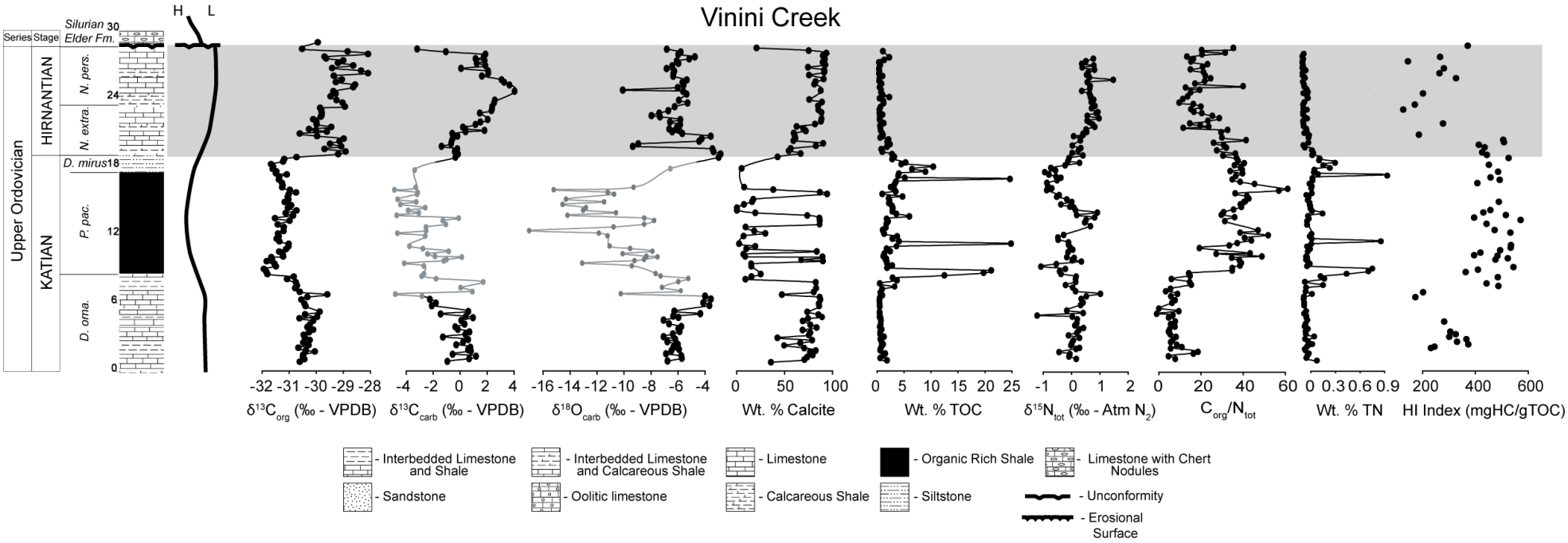

Figure 2.2. Upper Katian and Hirnantian section at Vinini Creek (Nevada) showing lithologies, graptolite zones, stratigraphic ages and sea-level curve (modified from Finney et al., 1999) compared with stratigraphic trends in carbon and nitrogen isotopes and geochemistry. The stratigraphic thickness of the Hirnantian $\delta^{13}C$ excursion is shaded grey. The end of the excursion appears to be missing, interpreted as an omission surface. The $\delta^{13}C_{carb}$ and $\delta^{18}O_{carb}$ trends are shaded grey where alteration is suspected because of the low calcite abundances and correspondingly low $\delta^{18}O_{carb}$ values. Abbreviations: *D. ornatus (D. orna.)*; *P. pacificus (P. pac.); N. extraordinarius (N. extra.)*; *N. persculptus (N. pers.); Silurian Elder Formation (Silurian Elder Fm.).*

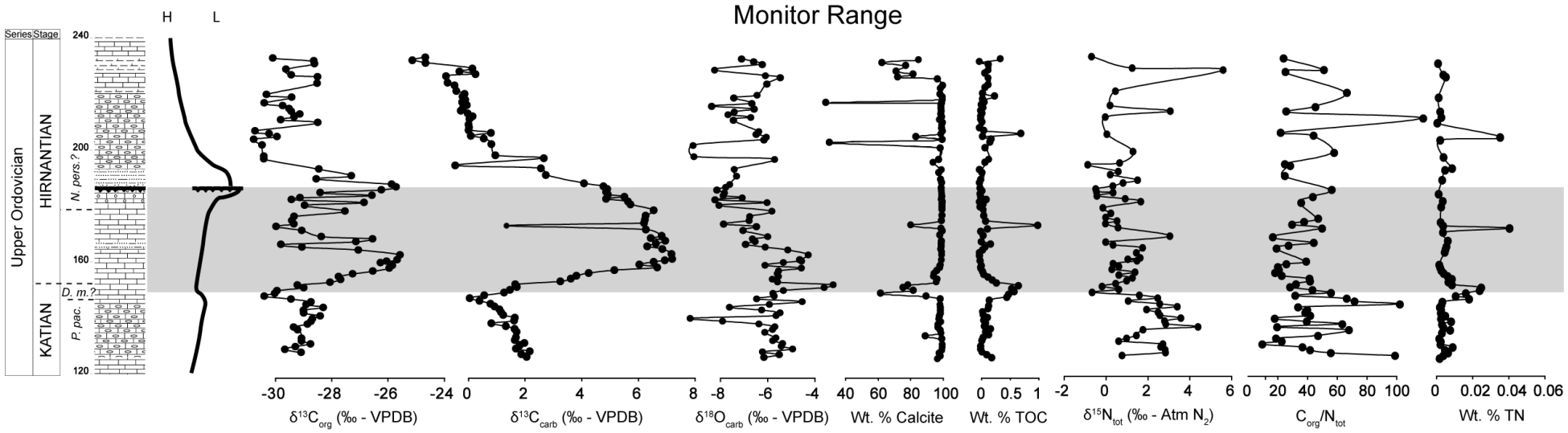

Figure 2.3. Upper Katian and Hirnantian section at Monitor Range (Nevada) showing lithologies, graptolite zones, stratigraphic ages and sea-level curve (modified from Finney et al., 1999) compared with stratigraphic trends in carbon and nitrogen isotopes and geochemistry. The Hirnantian $\delta^{13}C$ excursion is shaded grey. The approximate stratigraphic position of the *D. mirus* Subzone was determined by comparing the TOC and $\delta^{13}C$ trends between Monitor Range and Vinini Creek. The $\delta^{13}C_{carb}$ that is shaded grey represents suspected sampling of an interbedded shale. Abbreviation: *D. mirus (D. m.).*

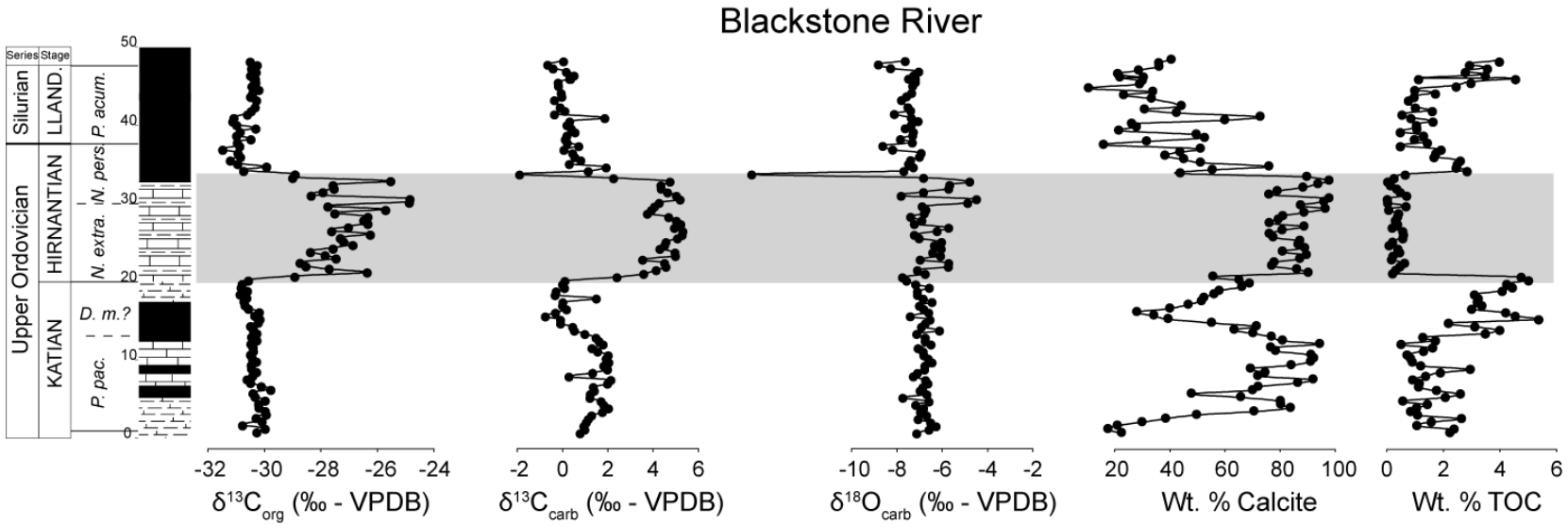

Figure 2.4. Upper Katian to lowest Silurian section at Blackstone River (Yukon) showing lithologies, graptolite zones, and stratigraphic ages compared with stratigraphic trends in carbon isotopes and geochemistry. The Hirnantian $\delta^{13}C$ excursion is shaded grey. The approximate stratigraphic position of the *D. mirus* Subzone was determined by comparing the TOC and $\delta^{13}C$ trends between Blackstone River and Vinini ICreek. Abbreviation: *A. ascensus-P. acuminatus Zone (P. acum.).*

2.5 Depositional Setting

The strata of the Vinini Formation at Vinini Creek (Fig. 2.2) were deposited in a deepwater ocean floor to continental rise setting (Finney et al., 1997; Finney et al., 2007). The *D. ornatus* Zone, comprising the bottom 8.5 m of section, consists of interbedded mudstone, lime mudstone, and shale. Calcite content reaches a maximum of 90% at 6 m, denoting a possible pre-Hirnantian shallowing during *D. ornatus* time (Finney et al., 1999; Figure 2). The lithology changes abruptly in the overlying *P. pacificus* Zone, shifting to organic-rich, laminated mudstones with subsidiary interbedded lime mudstone, phosphatized stringers, and high diversity graptolite faunas (Mitchell et al., 2007); suggesting not only deeper water conditions, but intense upwelling above a well developed oxygen minimum zone (Finney et al., 2007). An abrupt shift to an organic rich, laminated, brown, shalely siltstone is coincident with the *D. mirus* Subzone immediately below the base of the Hirnantian Stage. Finney et al. (2007) interpreted the *D. mirus* Subzone lithofacies to reflect diminished upwelling, oxygen minimum zone shrinkage, and sea level fall associated with the onset of the Hirnantian glaciation. Graptolite faunas become less diverse through this interval.

In the overlying *N. extraordinarius* Zone, the glacio-eustatic lowstand deposits feature lime mudstone and interbedded shale that persists upwards into the *N. persculptus* Zone. There is a tendency towards thickening of limestone beds in the peak interval of the Hirnantian $\delta^{13}C_{carb}$ excursion (Finney et al., 1997; 1999). The stratigraphic position of the sea level lowstand is not known with precision at Vinini Creek. The top of the section is disrupted by a disconformity surface where Hirnantian strata containing *N. persculptus* graptolites are overlain by Silurian strata of the Elder Formation (middle Llandovery). Finney et al. (1999) interpreted this disconformable contact as an omission surface recording nondeposition and submarine erosion of latest Ordovician and earliest Silurian age sediment. Goldman et al. (2007) described a similar omission surface in the Phi Kappa Formation, central Idaho, which is marked there by a 15 cm-thick quartzite bed that cuts down into probable Hirnantian carbonates and is overlain by Rhuddanian black slates of the *Coronograptus cyphus* Zone.

The Monitor Range section presented in Finney et al. (1997) is a composite re-constructed from outcrop sections: a lower one on Martin Ridge and an upper one in the

Copenhagen Canyon. In this work, only the upper 120 m of the Monitor Range composite section, that part represented by the Copenhagen Canyon section, were re-studied (Fig. 2.3). Inorganic carbon isotope data from lower in the section was published by Saltzman and Young (2005). The Monitor Range section was deposited in an outer platform environment of a vast epeiric sea, with the emergent Transcontinental Arch to the east and the Panthalassa Ocean to the west (Dunham, 1977; Finney et al., 1997; 2007). Compared to the wave agitated, coarser grained, fossiliferous sediment in the statigraphically equivalent mid-platform section at Lone Mountain (Finney et al., 1997), the Martin Ridge sediment exhibits characteristics of quieter, deepwater sedimentation, with evidence for oxygen depleted bottom waters. Dunham (1977) attributed this to the presence of a bathymetric low on the outer Nevada platform that he called the Martin Ridge Basin. He estimated the depth of the basin to have been ~100m below the level of the surrounding platform.

The lowermost 50 m of the Copenhagen Canyon section consists of thick beds of cherty lime mudstone with thin interbeds of shale and calcareous mudstone. The stratigraphic pattern of facies has been used as a sea- level indicator in this section. Where *P. pacificus* is present, water depth and lithofacies indicate deeper water. The sea level curve of Finney et al. (1999) is shown for reference in Fig. 3. A notable deepening event occurs at 148 m, immediately below the shift to shallow water facies indicative of the Hirnantian sea level fall (Finney et al., 1999; 2007). *P. pacificus* disappears at 126m, briefly reappears at ~148m, suggesting a rise in sea level before *P. pacificus* becomes extinct at 152m. An exposure surface at ~187 m overlain by well sorted, wave-rippled quartizite was interpreted by Finney et al. (1999) as the maximum sea level lowstand. Overlying strata consist of a fining upward sequence of packstone, wackestone, and lime mudstone indicative of the post-glacial rise in Hirnantian sea level (Finney et al. 1997).

The strata of the Road River Formation at the Blackstone River section (Fig. 2.4) were deposited in the Blackstone Trough. The depositional setting is interpreted as an intracratonic basin to carbonate slope environment, bounded to the south, east, and northwest by carbonate platforms, and to the northeast by the deepwater Richardson Trough (Cecile et al. 1997). Strata of the lower 19.5 m that covers the *P. pacificus* and basal *N. extraordinarius* zones, consist of interbedded calcareous, black, graptolitic shales and laminated to thinly bedded, argillaceous lime mudstones. The Hirnantian interval (*N. extraordinarius* and inferred lower part of the *P.*

persculptus zones) consists primarily of interbedded, bioturbated to finely rippled laminated lime mudstones and fossiliferous wackestones with occasional packstones. The occurrence of beds showing bioturbation, ripple cross-lamination, and significant increases in abundances of shelly fossils, suggests that these strata represent a more shallow-water environment during the Hirnantian than the underlying and overlying black shale-dominated units. One exception is the interval from 26.5-30.4 m that appears to represent a temporary deepening. The strata from 32.5 to 50.0 m (representing the upper *N. persculptus*, *A. ascensus*, and *P. acuminatus* zones) are predominantly calcareous, black, graptolitic shales with a few, thin to thick, laminated lime mudstone interbeds.

2.6 Results

2.6.1 Trends in carbon isotope profiles

All of the study sections exhibit positive $\delta^{13}C_{carb}$ and $\delta^{13}C_{org}$ excursions during the Hirnantian. At Vinini Creek and Monitor Range, the $\delta^{13}C_{carb}$ excursions trace one broad peak, whereas the $\delta^{13}C_{org}$ excursions appear to show two peaks during the same stratigraphic interval (Fig. 2.2 and 2.3). Two peaks, separated by a weak (~1.5‰) negative shift can be recognized in the $\delta^{13}C_{carb}$ excursion at Blackstone River (Fig. 2.4), but this is not evident in the corresponding $\delta^{13}C_{org}$ excursion.

Baseline $\delta^{13}C_{carb}$ and $\delta^{13}C_{org}$ trends in all sections shift to more negative values immediately preceding the Hirnantian positive excursion, but not synchronously or with the same relative magnitudes. Lithofacies shifts occur coincidentally with the $\delta^{13}C$ baseline shift, and depending on the section, TOC and silt increases, and calcite decreases.

The Hirnantian $\delta^{13}C_{carb}$ excursion at Monitor Range is the largest of the three sections, ranging between 5 and 7‰. Baseline position is critical to the calculation of peak excursion magnitudes, and the range in the above values reflects the uncertainty regarding the significance of the brief pre-Hirnantian shift in baselines to more negative $\delta^{13}C_{carb}$ values seen in all three sections. The corresponding two-peaked $\delta^{13}C_{org}$ excursion in the Monitor Range section is smaller than the $\delta^{13}C_{carb}$ excursion, reaching just 3.0 to 4.6‰ above baseline. In the Blackstone River section the inorganic and organic carbon isotope records are similar with excursions of 3.2

to 4.8‰ for $\delta^{13}C_{carb,}$ and 3.8 to 4.5‰ for $\delta^{13}C_{org}$. The Vinini Creek section records the smallest excursion of 2 to 2.8‰ for $\delta^{13}C_{org}$. The magnitude of the corresponding $\delta^{13}C_{carb}$ excursion cannot be determined because of the poorly defined baseline.

Significant differences are found in the behaviour of the inorganic and organic carbon isotope profiles within and between the sections. The Vinini Creek section displays more scatter in the $\delta^{13}C_{carb}$ profile than in the corresponding $\delta^{13}C_{org}$ profile, whereas the opposite is true in the Monitor Range and Blackstone River sections. Scatter in the $\delta^{13}C_{carb}$ and $\delta^{13}C_{org}$ profiles increases when calcite and TOC levels are low, respectively. Calcite poor intervals in the Vinini Creek section (<20 wt. %) are also correlated with low $\delta^{18}O_{carb}$ values (-13 to -17‰), indicative of late stage diagenesis. The considerable scatter found in at least one of the carbon isotope profiles from each of the two sections in Nevada imparts considerable variability to the reconstructed $\Delta^{13}C$ profiles ($\delta^{13}C_{carb} - \delta^{13}C_{org}$) (Fig. 2.5). The Blackstone River section records the least variable $\Delta^{13}C$ profile (Fig. 2.5). If attention is restricted to stratigraphic intervals of >80 wt.% calcite, the Blackstone River data yield a $\Delta^{13}C$ value of 31.7‰ ± 0.8‰ (n= 1σ).

Graptolites recovered from the Vinini Creek section place the beginning of the Hirnantian $\delta^{13}C$ excursion firmly in the upper *D. mirus* Subzone (Fig. 2.2). The first appearance of *N. extraordinarius*, which defines the base of the Hirnantian Stage, occurs precisely at the stratigraphic level where the first peak values are recorded by the Hirnantian $\delta^{13}C_{org}$ excursion. The termination of the excursion occurs within the middle of the *N. persculptus* Zone, which is best seen in the Blackstone River section (Fig. 2.4). The stratigraphic tracing of the rising and falling limbs of the Hirnantian excursion is recorded identically between the inorganic and organic carbon fractions of the sediment in the Monitor Range and Blackstone River sections. In the peak intervals, however, there are differences between the $\delta^{13}C$ profiles, most notably at Monitor Range where two positive excursions may be distinguished in the $\delta^{13}C_{org}$ profile, separated by a negative excursion back to pre-Hirnantian baseline values. The uppermost peak in the Monitor Range section is stratigraphically coincident with an oolitic dolograinstone and an irregular corroded surface that Finney et al. (1999) identified as the position of the maximum sea level lowstand of the Hirnantian glaciation.

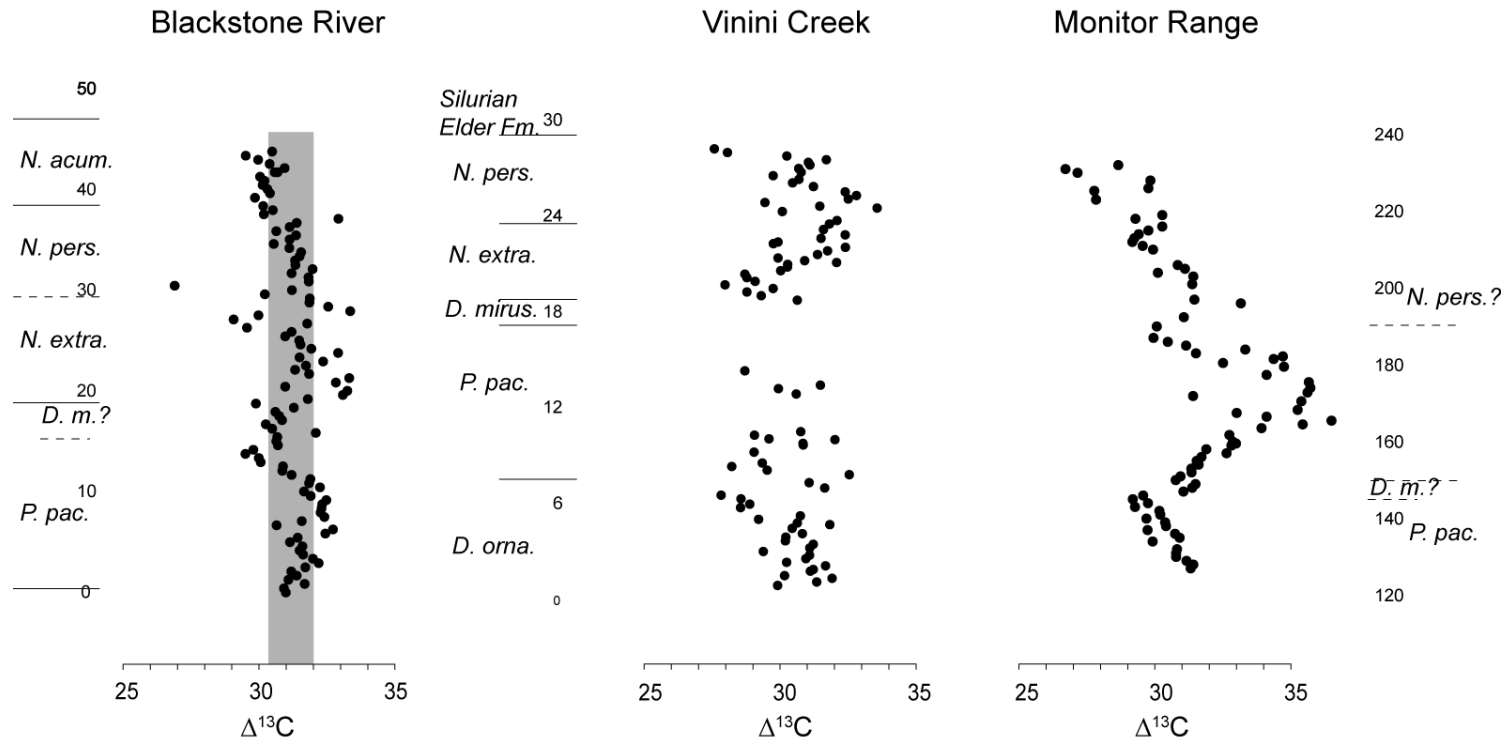

Figure 2.5. $\Delta^{13}C$ profiles for Vinini Creek, Blackstone River, and Monitor Range measured against stratigraphic thickness for each section. The average $\Delta^{13}C$ value at Blackstone River is 31.3‰ ±0.9. Sample points within the shaded band are within 1σ of the mean. The relatively invariant $\Delta^{13}C$ in the Blackstone section is evidence that both the $\delta^{13}C_{carb}$ and $\delta^{13}C_{org}$ trends faithfully reflect seawater $\delta^{13}C_{DIC}$ trends. The scatter in the $\Delta^{13}C$ trends from Nevada are interpreted as evidence that the $\delta^{13}C_{org}$ trend at Monitor is altered, and that the $\delta^{13}C_{carb}$ trend at Vinini Creek is altered.

Two positive excursions of smaller amplitude may be found below the Hirnantian Stage in the Vinini Creek section: a 1‰ excursion in the *P. pacificus* Zone, and a 1.5‰ excursion in the *D. ornatus* Zone (Fig. 2.2). Correlative excursions in the lower Monitor Range section (not sampled) may be evident in the $\delta^{13}C_{carb}$ profile in Saltzman and Young (2005), but the precise stratigraphic timing, and apparent differences in sampling resolution, hampers a definitive match.

$\delta^{13}C_{grap}$ and $\delta^{13}C_{org}$ trends correlate reasonably well through the Vinini Creek section (Fig. 2.6). In some intervals $\delta^{13}C_{grap}$ and $\delta^{13}C_{org}$ trends are identical (±0.1‰) but in others there is an approximately 1.0‰ offset between them, with $\delta^{13}C_{grap}$ values shifted to higher values. The correspondence appears to be weakest where the $\delta^{13}C_{org}$ values are lowest. The Hirnantian $\delta^{13}C_{grap}$ excursion is 2.5‰, comparing reasonably well with the 2 to 2.8‰ excursion recorded in the bulk organic matter. On the whole, graptolite $\delta^{13}C$ coverage is insufficient to test in detail whether all of the nuances in the shape of the $\delta^{13}C_{org}$ profile are in fact replicated in the $\delta^{13}C_{grap}$ profile. It is perhaps significant, however, that the $\delta^{13}C_{grap}$ value for a single sample from the 'trough' interval between the two $\delta^{13}C_{org}$ peaks failed to record this prominent feature.

2.6.2 Trends in $\delta^{15}N_{TN}$ and C_{org}/N_{TN} Data

Samples with the highest C_{org}/N_{TN} occur in the organic rich black shales of the *P. pacificus* Zone in the Vinini Creek section (Fig. 2.2), identified as an upwelling zone by Finney et al. (2007). The Vinini Creek section exhibits more smoothly varying stratigraphic trends in both $\delta^{15}N_{TN}$ and C_{org}/N_{TN} than Monitor Range (Fig. 2.2 and 2.3). There is a tendency for $\delta^{15}N_{TN}$ to vary positively with $\delta^{13}C_{org}$ in the Vinini Creek section, and negatively with C_{org}/N_{TN} and TOC.

The glacial age strata in the Vinini Creek section are associated with a 1.5‰ positive shift in $\delta^{15}N_{TN}$ beginning in the *D. mirus* Subzone. The $\delta^{15}N_{TN}$ values begin rising ~0.5m before the $\delta^{13}C_{org}$, and reach peak values at the beginning of the second $\delta^{13}C_{org}$ excursion.

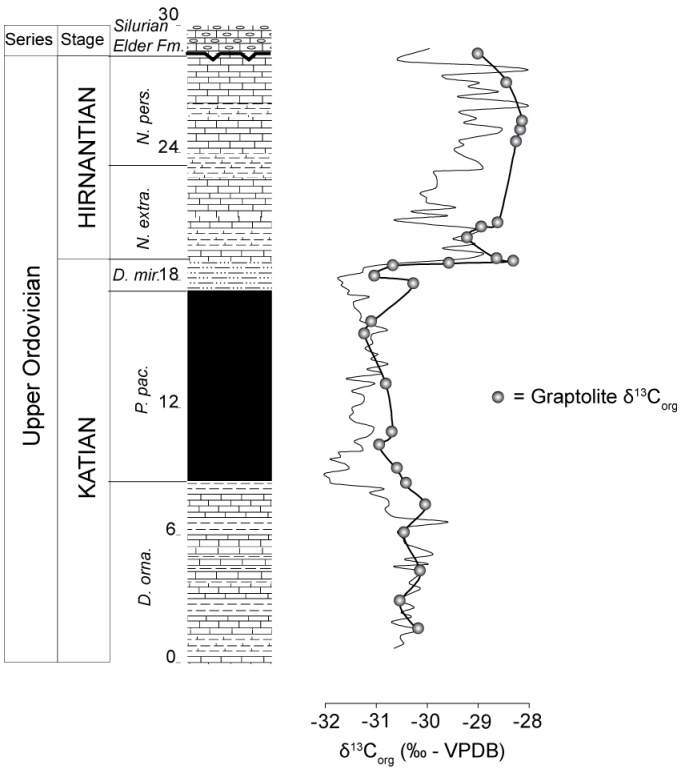

Figure 2.6. Carbon isotope trends of bulk organic matter ($\delta^{13}C_{org}$) and graptolite periderm ($\delta^{13}C_{grap)}$ are shown against stratigraphic thickness in the Vinini Creek section. The close tracking of $\delta^{13}C_{org}$ and $\delta^{13}C_{grap}$ values and the inferences regarding trophic level, suggest that in this distal environment, where the water column was likely stratified, the bulk organic matter is predominantly the remains of phytoplankton from the upper water mass.

2.6.3 Trends in Supporting Geochemical Data

Stratigraphic trends in TOC, TN, wt.% siliciclastics and wt.% calcite are shown in Figures 2.2, 2.3, and 2.4; Mg/Ca and Sr/Ca trends are shown in Fig. 2.7. Considering the fact that the lithology of the Monitor Range section is mostly calcite rich, the *D. mirus* Subzone stands out as an interval where calcite levels decline, and concomitant siliciclastic levels rise from 5 to 40 wt.%. There are also spikes in Mg/Ca ratio in this interval in both sections (Fig. 2.7). A similar pattern of decreasing calcite levels and increasing silt is observed in stratigraphically equivalent intervals in the Blackstone River section. Although siliciclastic lithologies dominate the pre-Hirnantian strata in the Vinini Creek section, the *D. mirus* Subzone is easily recognized by its brown (rather than black) colour, and its greater silt content.

Average TOC is much higher in the Vinini Creek (2.4 wt.%) and Blackstone River sections (1.8 wt.%) than in the Monitor Range section (0.15 wt.%), which is consistent with the deeper water settings of the first two. TOC spikes characterize the *D. mirus* Subzone in all sections (Fig. 2.2, 2.3, and 2.4). The lowest TOC in each section is found in sediment deposited during the Hirnantian sea level lowstand, in the peak interval of the positive $\delta^{13}C$ excursion. TOC levels increase at the end of the glaciation, as $\delta^{13}C$ values return to pre-excursion baseline values.

Finney et al. (2007) attributed high levels of sedimentary TOC, phosphate (up to 10,000 ppm), and redox sensitive trace metals in the Vinini Creek section in the *P. pacificus* Zone, (below the *D. mirus* Subzone) to upwelling above an expansive oxygen minimum zone. Towards the base of the section, in the *D. ornatus* Zone, TOC decreases to low levels, % calcite rises, and $\delta^{13}C_{org}$ values increase—a pattern reminiscent of the Hirnantian sea level lowstand.

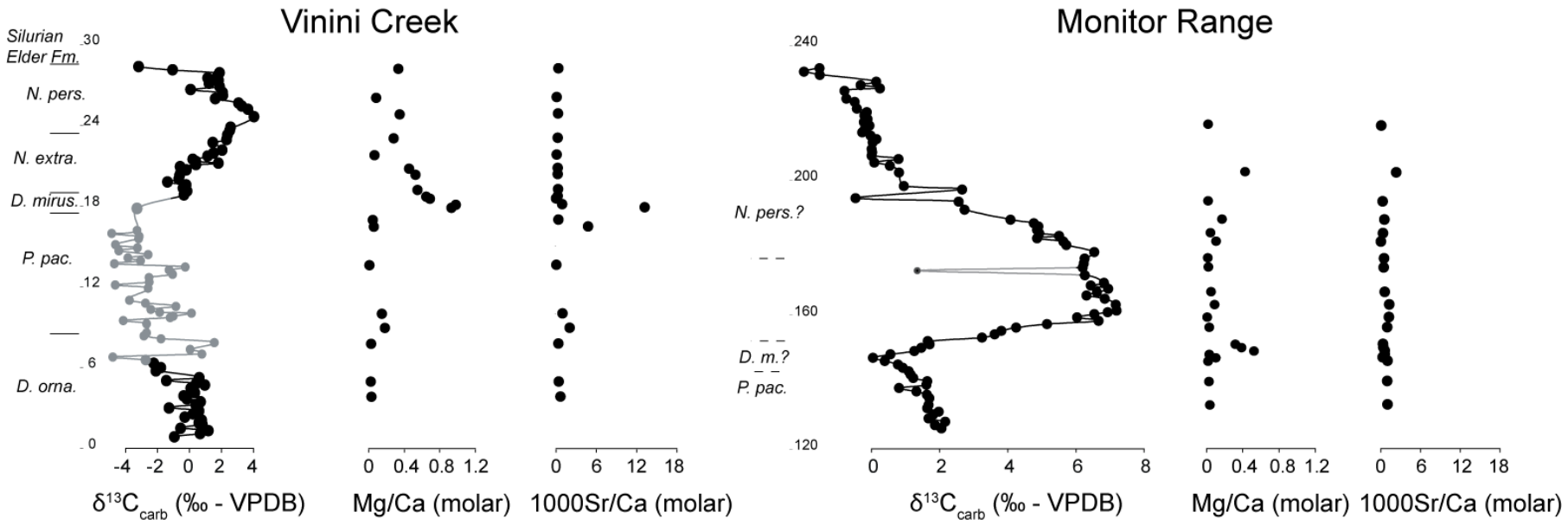

Figure 2.7. Molar Mg/Ca and 1000Sr/Ca data are shown against stratigraphic thickness for selected intervals through the Vinini Creek and Monitor Range sections. An increase in Mg/Ca during the *D. mirus* Subzone reveals the possible presence of dolomite.

The stratigraphic trend in hydrogen indices (HI) in the Vinini Creek section (Fig. 2.2) exhibits a negative relationship with $\delta^{13}C_{org}$, and a positive relationship with TOC and TN. Low HI values (140–370) characterize the *D. ornatus* and middle *N. extraordinarius* to *N. persculptus* Zones, which have relatively high $\delta^{13}C_{org}$ values. High HI values (360–570) characterize the *P. pacificus* Zone, *D. mirus* Subzone, and lower *N. extraordinarius* Zone. Stratigraphic intervals with low HI and TOC suggest that the organic matter may be more oxidized than in those intervals with high HI and TOC (Fig. 2.2). Based on the range in HI and the T*max* values, organic matter from Vinini Creek is considered immature to marginally mature. Very little or no staining by migrated hydrocarbons is evident from the Production Index ((S1/(S1+S2)), where S1= hydrocarbons evolved (distilled or thermovaporized) at 300°C, and S2 = hydrocarbons evolved during heating at 25°C /min between 300°C and 600°C) of Vinini Creek samples. Monitor Range TOC and TN abundances are too low (0 – 1%) to yield reliable HI data. Rock-Eval was not performed on the Blackstone River section.

2.7 Discussion

2.7.1 Comparisons Between Corresponding $\delta^{13}C_{carb}$, $\delta^{13}C_{org}$, and $\delta^{13}C_{grap}$ Profiles

With two secular records of $\delta^{13}C$ from each section, the preservation of one trend can be evaluated against the other using the parameter $\Delta^{13}C$. In the Blackstone River section, a $\Delta^{13}C$ value of 31.7‰ was found for intervals where the calcite content is 80 wt.% or higher. The relatively constant $\Delta^{13}C$ trend through the Hirnantian excursion interval is significant in two ways. First, it increases the likelihood that the sedimentary $\delta^{13}C_{carb}$ and $\delta^{13}C_{org}$ trends reflect variability in local seawater DIC trends during the Hirnantian glaciation event. Second, it suggests that there were no significant changes in the constitution of the phytoplankton community, even though some genera of graptolites were taxonomically devastated by extinctions (Chen et al., 2005; 2006; Finney et al., 2007). From these observations I conclude that the organic matter and the carbonate sediment must have formed from the same neritic watermass, which has implications for the degree to which the water column was vertically stratified at this location. For example, if primary organic matter production was mostly confined to warm surface waters, and carbonate production to cooler bottom waters, then any water column gradient in $\delta^{13}C_{DIC}$ could not have been greater than ~2‰ throughout the entire

Hirnantian glacio-eustatic cycle to be in agreement with the limited stratigraphic variability exhibited in $\Delta^{13}C$. This is approximately the same difference that occurs between surface and deep ocean water masses today as a consequence of biological pumping.

$\Delta^{13}C$ trends in the two Nevada sections exhibit more variability (Fig. 2.5) than in the Blackstone River section. This is evidence for alteration (or masking) of the original seawater signal in at least one of the sedimentary carbon fractions. At Monitor Range, the most likely altered profile is $\delta^{13}C_{org}$, which shows greater variability than $\delta^{13}C_{carb}$ and smaller peak magnitude shifts during the Hirnantian excursion interval. This is consistent with the findings of Kump et al. (1999) in a nearby section from Martin Ridge, metres from the one measured in this study. Their $\delta^{13}C_{org}$ profile shows no positive excursion through the Hirnantian interval. Instead, values remain between –30.0% and –32.7‰. By contrast, $\delta^{13}C_{carb}$ profiles are identical between the two sections, suggesting that the $\delta^{13}C_{org}$ profiles are altered.

The situation in the Vinini Creek section is quite different. A number of lines of evidence point to the $\delta^{13}C_{carb}$ profile as being the least reliable one. Samples with low calcite abundances in the *P. pacificus* Zone exhibit low $\delta^{18}O$ values, thus indicating calcite precipitation from hot fluids or cool meteoric waters during burial or tectonic uplift, respectively. Where this occurs, the corresponding $\delta^{13}C_{carb}$ values are unlikely to reflect seawater DIC at the time of deposition.

Samples with high calcite contents may be unreliable as well, but for a different reason. Finney et al. (1997) argued that three calcite-rich intervals in the otherwise dominantly siliciclastic strata of the *P. pacificus* Zone were transported from the platform. The same may be true for carbonates deposited during the Hirnantian. Although these were deposited during the glaciation when sea level was ~100m lower, this fall in sea level seems too small to allow for the development of a benthic carbonate factory in a deep ocean setting where none was established immediately lower in the section. Because local bottom water $\delta^{13}C_{DIC}$ values cannot be reliably inferred from transported sediment, I consider the $\delta^{13}C_{carb}$ trend to be a poor recorder of local seawater $\delta^{13}C_{DIC}$ values in this setting. Melchin and Holmden (2006a) reached a similar conclusion in their study of Hirnantian deepwater carbonate deposits of the Cape Phillips Basin.

Bulk organic matter may have been altered in the Vinini Creek section by post-depositional alteration (e.g., Lehmann et al., 2002) or mixing between isotopically distinct sources (e.g., Pancost et al., 1999). One way to evaluate this is to look for covariance between the $\delta^{13}C$ values of bulk organic matter and graptolite periderm (Fig. 2.6). Graptolites are the remains of macrozooplankton that fed on smaller plankton in the water column. Consistent with their higher trophic level, Lo Duca and Pratt (2002) showed that graptolite $\delta^{13}C$ values were 1–2‰ higher than co-existing phytoplankton. Secular $\delta^{13}C$ trends reconstructed from graptolite periderm may help to avoid some of the pitfalls of using bulk organic matter, such as source mixing and selective degradation of organic constituents.

$\delta^{13}C_{grap}$ and $\delta^{13}C_{org}$ profiles track each other closely through the Hirnantian excursion. Some sections of the $\delta^{13}C_{grap}$ curve are offset to higher values, consistent with the trophic level effect. Other sections show considerable overlap that indicates: (1) the bulk organic matter may consist predominantly of the remains of graptolites, (2) sea surface temperatures may have influenced graptolite metabolic rates with higher temperatures yielding lower $\delta^{13}C_{grap}$ values, (3) the bulk organic matter may be altered, or shifted by source mixing effects, or (4) the graptolite diet may have contained a higher proportion of chemotrophs with lower $\delta^{13}C$ values.

It has been suggested that some graptolites may have foraged for bacteria in the eutrophic waters of oxygen minimum zones (e.g., Berry et al., 1987). Organic matter produced by non-photosynthetic bacteria (chemotrophs) is lower in $\delta^{13}C$ value than primary produced organic matter (cf., Kodina et al., 1996; Hollander and Smith, 2001; Burdige, 2007). The reason has to do with local recycling of organic matter in water columns or sediment pore fluids with low dissolved oxygen levels. In these environments, ^{12}C-enriched methane and respired CO_2 contributes significantly to the DIC pool. In the Black Sea, for example, organic matter produced by chemotrophs is ~3‰ lower in $\delta^{13}C$ value than phototrophs (Kodina et al., 1996), and up to 30% of the organic matter sinking through the water column may be attributed to them (Karl, 1999). In eutrophic Lake Mendota, Wisconsin, bacterial production of organic carbon in the hypolimnion is shifted to 8‰ lower $\delta^{13}C$ values (–34‰) compared to the photosynthate in the epilimnion (–26‰) (Hollander and Smith, 2001). Because graptolites appear to have thrived in continental margin upwelling zones where oxygen minimum zones are inferred on the basis of

the organic rich facies in which they are found (Finney et al., 2007), their diet may have included these types of bacteria, thus shifting the periderm carbon in some graptolite species to lower $\delta^{13}C$ values.

2.7.2 Origin of low $\delta^{13}C_{org}$ Values in the Monitor Range Section

Kump et al. (1999) faced a similar problem explaining anomalously low $\delta^{13}C_{org}$ values in their Monitor Range section from Copenhagen Canyon, only metres away from our section. As indicated above, the $\delta^{13}C_{carb}$ profiles are virtually identical between the two sections, each displaying prominent excursions of about 5 to 7‰. The striking differences between the $\delta^{13}C_{org}$ profiles suggest, however, metre scale variability in the preservation of the seawater signature in bulk organic matter in this setting. Such a high degree of variability in $\delta^{13}C_{org}$ values is not apparent in other sections in this study. It also contrasts with the $\delta^{13}C_{org}$ profiles reconstructed from the Cape Phillips basin, where there is a 6‰ excursion in the organic carbon fraction of an inner platform section (Eleanor Lake; Melchin and Holmden, 2006a; Fig. 2) of the same magnitude as the $\delta^{13}C_{carb}$ excursion from Monitor Range. This indicates that bulk organic matter is not everywhere compromised as a reliable recorder of changes in local scale seawater $\delta^{13}C$ values during the Hirnantian glaciation.

Thermal alteration of organic matter was considered and rejected by Kump et al. (1999) as an explanation for the extreme heterogeneity in $\delta^{13}C_{org}$ values. They based their conclusion on relatively low conodont alteration indices that indicated burial temperatures between 110 and 200°C, and the fact that thermal alteration tends to elevate residual organic matter $\delta^{13}C$ values (Lewan, 1983). A more promising explanation involves selective degradation of organic components like proteins and carbohydrates that are higher in $\delta^{13}C$ value (and more easily remineralized) than lipids (e.g., Hedges et al., 1988). Remineralization under both oxic and anoxic conditions has been shown to shift the residual bulk organic matter by as much as –4‰ (Benner et al., 1987; Teece et al., 1999; Lehmann et al., 2002; Versteegh and Zonneveld 2002; Sun et al., 2004). There is no evidence, however, for negatively covarying trends between $\delta^{13}C_{org}$ and TOC values in the same section (also discussed by Kump et al., 1999), as might be expected if low TOC magnified the ^{12}C-enrichment of bulk organic matter caused by the loss of a ^{13}C

enriched component. Instead, TOC is higher in the more altered Kump et al. section (~0.4%) than the one reported in this paper (~0.15%).

Source mixing is a reasonable alternative to selective degradation of organic matter. In fact, the two processes may work together to amplify the impact of an isotopically distinct, more refractory component. A good example was described from the Midcontinent Region in samples of Upper Ordovician sediment from the Galena Group. Organic components belonging to the alga, *Gloeocapsomorpha prisca*, are enriched in ^{13}C by up to 7‰ compared to similar components from the other phytoplankton in the samples (Pancost et al., 1999). Because the cell wall belonging to *G. prisca* is relatively resistant to degradation, selective remineralization shifts the bulk organic matter to higher $\delta^{13}C_{org}$ values if *G. prisca* is present. In a core through the Galena Group, two out of five carbon isotope excursions showed larger $\delta^{13}C_{org}$ excursions than $\delta^{13}C_{carb}$ excursions. This was attributed to the presence of *G. prisca* in the bulk organic matter (Fanton and Holmden, 2007).

The Galena Group example illustrates what might have happened to the organic matter in the Monitor Range sediment. However, the inferred organism produced an organic component that was lower in $\delta^{13}C$ value (not higher) than the standing stock of late Ordovician phytoplankton. It is possible that the organism responsible may have come from the terrestrial environment. Although vascular plants had not yet evolved in the late Ordovician, Panchuk et al. (2005) suggested that bryophytes (hornworts, liverworts, and mosses), as documented from Ordovician stratigraphic sections worldwide (Shear, 1991; Strother et al., 1996; Redecker et al., 2000; Steemans, 2000; Wellman et al., 2003; Rubenstein and Vaccari, 2004), may have supplied particulate organic carbon to the Laurentian epeiric seas located east of the Transcontinental Arch, in slightly younger strata. In their model, the inferred POC flux was oxidized in the epeiric sea environment as an explanation for the low $\delta^{13}C_{carb}$ and $\delta^{13}C_{org}$ values of the Midcontinent Aquafacies (Holmden et al., 1998; Panchuk et al., 2006). However, to explain the Monitor Range results, the terrestrial POC flux would need to reach the Martin Ridge Basin before it was oxidized, where it could then be preserved in the low oxygen bottom waters (Dunham, 1977). POC delivery in the suspended load of a river is a possibility, but perhaps not likely owing to the distal shelf location of the basin. An eolian source of POC would be more likely to reach the

outer platform before being oxidized. Although modern day bryophytes have $\delta^{13}C_{org}$ values ranging from –22‰ to –29‰ (Taylor et al., 2003), higher P_{CO2} levels in the Ordovician may have supported much lower values similar to a study of Devonian bryophytes that show $\delta^{13}C_{org}$ values as low as –40‰ (Jahren et al., 2003).

Although the terrestrial contaminant hypothesis has merits, a marine source of organic matter can also explain the data. The low oxygen bottom waters of the Martin Ridge Basin may have hosted a community of chemosynthetic bacteria. The low $\delta^{13}C$ value organic matter produced by the chemotrophs (e.g., Hollander and Smith, 2001; Burdige, 2007), if mixed with the algal photosynthate, would lower bulk organic matter $\delta^{13}C_{org}$ values below the $\delta^{13}C_{carb}$ values of the laminated host carbonates—which were themselves transported to the Martin Ridge Basin from carbonate factories surrounding the periphery of the basin. This process has been noted in the Santa Monica Basin where Gong and Hollander (1997) described a depression in the seafloor 60m deeper than the surrounding seafloor. The difference in depth is sufficient to restrict ventilation and promote the development of anoxic bottom waters in the depocenter of this depression. A 1,550-year record of laminated sediment shows TOC and fatty acid concentrations increasing upwards towards the sediment–water interface. Bulk $\delta^{13}C_{org}$ values decrease over the same interval by –0.5‰ to –1.0‰ (Figure 7; Gong and Hollander, 1997). The authors attribute this trend to increasing anoxia, bacterial chemotrophy, and microbial re-packaging of the algal photosynthate at the sediment-water interface, or just below. No change in bulk $\delta^{13}C_{org}$ values was observed over the same interval in a core taken from the rim of the basin, in sediment overlain by bottom waters with normal oxygen levels.

Although it is difficult to rule out the terrestrial source hypothesis completely, two observations favour the microbial re-packaging hypothesis. First, overprinting is highly variable between the two sets of Monitor Range samples (this study and Kump et al., 1999), which suggests that source mixing alone is not the explanation. Second, a lipid-rich biomass that is more resistant to oxic degradation fits with the observation that the section measured by Kump et al. (1999) has higher TOC, and yet records greater variability in $\delta^{13}C_{org}$ values than the Martin Ridge section from this study. A biomarker study could shed further light on the organic carbon source-mixing hypothesis.

2.7.3 Secular Changes in $\delta^{15}N_{TN}$ and its Relation to Ocean Redox Changes

A substantial body of work on nitrogen cycling in Quaternary marine sediment has shown that changes in sedimentary $\delta^{15}N_{TN}$ values accompany glacial–interglacial climate changes (cf., Graneshram et al., 2001; Meissner et al., 2005). The most common explanation relates to the impact of climate cooling on ocean ventilation, oxygenation, and contraction of oxygen minimum zones in areas of significant oceanic upwelling (Altabet et al., 1995; Ganeshram et al., 1995; Lyle et al., 2000; Graneshram et al., 2001; Herbert et al., 2001; Altabet et al., 2002; Dean, 2007). These studies are relevant to the interpretation of the $\delta^{15}N_{TN}$ record in the Vinini Creek section because, as pointed out by Finney et al. (2007), the depositional environment in the *P. pacificus* Zone preserves many of the sedimentary characteristics expected of a major Ordovician upwelling system, including high graptolite diversity, TOC, phosphate, and redox sensitive trace metals. Downcore trends in sedimentary $\delta^{15}N$ values beneath modern upwelling zones reveal increased water column denitrification during warm interglacials ($\delta^{15}N$ = 7–8‰) driven by oxygen minimum zone expansion, and a corresponding opposite shift ($\delta^{15}N$ = 4–5‰) during cooler glacials. Denitrification converts fixed nitrogen into nitrogen gas, a process favouring the lighter isotope, leaving the residual fixed nitrogen pool higher in $\delta^{15}N$ value.

Although it is reasonable to presume that the climate-driven ocean circulation effects, and the changes in ocean redox state, documented for the Pleistocene glaciations should have affected the Hirnantian ocean in a similar way, sedimentary $\delta^{15}N_{TN}$ values measured at Vinini Creek exhibit an isotopic shift opposite to that expected (Fig. 2.2). It is possible that the impact of glaciation on the Hirnantian nitrogen cycle was dramatically different than in recent glaciations, or it may be that the $\delta^{15}N_{TN}$ record in the Vinini Creek section is altered. Unfortunately, the $\delta^{15}N_{TN}$ record in the Monitor Range record is of little use in addressing this question owing to the circumstances of its depositional environment, and the source/alteration of its organic matter deduced from carbon isotopes (Fig. 2.3). Modern studies are also mostly unhelpful in this regard, giving little sense of a consistent alteration trend against which to evaluate $\delta^{15}N_{TN}$ preservation in ancient samples (Libes and Deuser, 1988; Holmes et al., 1999; Sachs and Repeta, 1999; Lehmann et al., 2002). Two observations in particular support the preservation of original $\delta^{15}N_{TN}$ records in the Vinini Creek section: (1) organic rich sediment in

modern upwelling zones appear to be excellent environments for the preservation of original sedimentary $\delta^{15}N_{TN}$ values (Altabet and Francois, 1994; Altabet et al., 1999; Voss et al., 2001), and (2) sediment hosting the positive Hirnantian shift in $\delta^{15}N_{TN}$ values (uppermost *P. pacificus* to lowermost *N. extraordinarious* Zones) record similarly high TOC and HI indices, thus, making it unlikely that the shift itself is a function of glacial age switching of the organic matter source or the alteration regime. These considerations suggest that the $\delta^{15}N_{TN}$ response to Pleistocene climate and ocean circulation changes is a poor analogue for changes in nitrogen cycling that occurred during the Hirnantian glaciation.

A more representative analogue may be found in the oceanic conditions of the Cretaceous, which led to the deposition of organic rich sediment during the Cretaceous Oceanic Anoxic Events (OAE), and the Pleistocene age Mediterranean sapropels. The average TOC of 2.5% in *P. pacificus* sediment in the Vinini Creek section—with HI indices between 400 and 600, and C_{org}/N_{TN} between 20 and 40—compares reasonably well with Cretaceous OAE II yielding HI >450 and C/N between 25 and 50 (Junium and Arthur, 2007) and Mediterranean sapropels yielding TOC of ~4% and C/N of 20 (Meyers and Bernasconi, 2005). In both examples, sedimentary $\delta^{15}N_{TN}$ values are just as low as those found in the Vinini Creek section: –3.9 to +1.2‰ for OAE, and –2‰ for Mediterranean sapropels. In addition, the laminated organic rich sediment of the Late Devonian New Albany shale also yield low $\delta^{15}N_{TN}$ values of 0 to 2‰ (Calvert et al., 1996).

The low $\delta^{15}N$ values in sapropels have been attributed to nitrogen replete conditions in Mediterranean surface waters (Calvert et al., 1992) and, more recently, significant biomass contributions from cyanobacteria (Meyers and Bernasconi, 2005; Borgendahl and Westman, 2007). Cyanobacteria directly assimilate atmospheric nitrogen dissolved in seawater while photosynthetic algae require a steady supply of (recycled) fixed nitrogen through upwelling or continental weathering to sustain productivity. Because there is only a small isotopic fractionation effect associated with nitrogen fixation, cyanobacteria such as *Trichodesmium*, produce organic matter with $\delta^{15}N$ values between 0 and –2‰ (Altabet, 2007; and references therein), similar to the atmospheric source (0‰). Algae that are dependent on recycled nitrogen from upwelling zones have higher $\delta^{15}N$ values, due to partial denitrification of remineralized

organic matter in the ocean's depths. In addition, surface waters with very low fixed nitrogen inventories are characterized by high $\delta^{15}N$ values because algal assimilation of nitrogen favours the light isotope, thus leaving the residual fixed nitrogen pool higher in $\delta^{15}N$ value (Altabet and Francois, 1994; Altabet et al., 1999; Voss et al., 2001).

Low oceanic inventories of recycled nitrogen may have been more common in the Earth's warmer past than today. Greenhouse climates were characterized by reduced equator to poleward temperature gradients, reduced ocean ventilation rates, reduced partitioning of atmospheric oxygen into seawater, and expansion of oxygen minimum zones; precisely the conditions that favour increased denitrification in the water column, and low return rates of fixed nitrogen to the photic zone (e.g., Altabet, 2007). These conditions favour cyanobacterial productivity when nitrogen release from decaying cells would be available to support algal productivity. Because there is little opportunity for recycling of fixed nitrogen in the relatively thin layer of the photic zone (Fig. 2.8), a continuous supply of this fixed nitrogen is required. Because this scenario affords no opportunity for the algae to overproduce and draw down the level of the fixed nitrogen pool, the $\delta^{15}N$ values of the algae will be similar to, or lower than, the $\delta^{15}N$ values of the cyanobacteria.

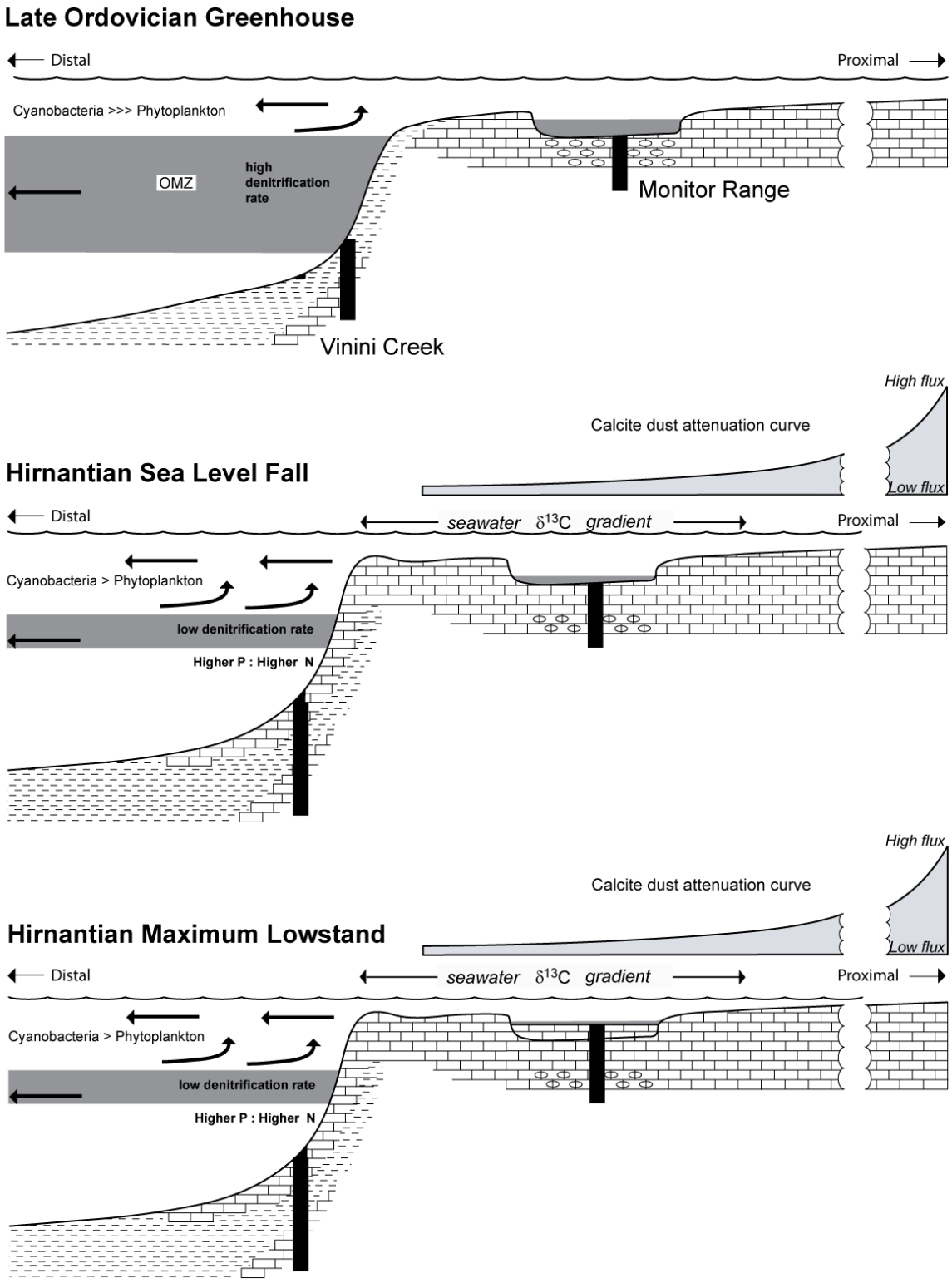

Figure 2.8. A conceptual model relating ocean OMZ, platform bottom water oxygenation, and productivity along a transect of the Nevada shelf and basin to pre-Hirnantian (greenhouse) and Hirnantian sea level fall and lowstand climate and sea-level. For detailed discussion of model, see text.

The +2‰ shift in sedimentary $\delta^{15}N$ values during the Hirnantian glaciation can now be explained. If the above conceptual model of greenhouse nitrogen cycling is correct, glacial age cooling increased ocean ventilation and oxygenation, caused shrinkage of the oxygen minimum zones, and decreased rates of denitrification (Fig. 2.8). This in turn increased the ^{15}N enriched upwelling flux of remineralized fixed nitrogen to the photic zone and algal productivity became less dependent on cyanobacterial productivity for fixed nitrogen. This is reflected in the higher $\delta^{15}N$ values of the organic matter exported from the photic zone and preserved in the sediment of the Vinini Creek Formation (Fig. 2.2), during the Hirnantian glaciation. As a test of this hypothesis, a biomarker study such as the one undertaken by Kuypers et al. (2004) on Cretaceous OAE could be performed to see whether cyanobacterial productivity increases relative to algal productivity during greenhouse climates, and decreases during icehouse climates. The model fits the prevailing view of the factors controlling cyanobacterial productivity. Specifically, that low growth rates and high energy demand for assimilating atmospheric nitrogen puts cyanobacteria at a competitive disadvantage to phosynthetic algae when recycled nitrogen inventories are high. The production advantage shifts to cyanobacteria only when recycled nitrogen inventories are low (Tyrrell 1999).

The Hirnantian $\delta^{15}N$ value of +1‰ is still low compared to the +5‰ value of fixed nitrogen in the oceans today (Altabet et al., 2007). This could reflect three things: (1) the $\delta^{15}N$ value of atmospheric N_2 was lower, (2) the stratigraphic variations in $\delta^{15}N$ were homogenized by diagenesis, but not completely overprinted, and (3) the oxygen minimum zones shrunk during glaciation, as suggested, but still covered a greater area in the Hirnantian ocean than they do at the present day. This means that denitrification rates would have to be higher in the Hirnantian than at the present day, and cyanobacterial productivity would remain higher as well. This is consistent with the idea that, although CO_2 levels dropped during the Hirnantian glaciation event, they were still high compared to the present day, perhaps ten times higher according to the modeling of Hirnantian atmospheric pCO_2 levels by Kump et al. (1999).

2.7.4 Hirnantian Shelf Gradient in $\delta^{13}C$ and its Relation to Seawater

One of the main objectives of this study was to determine whether Hirnantian shelf gradients in $\delta^{13}C$ values could be documented in both the inorganic and organic carbon fractions of the sediment from the same basin. Previous work in the Cape Phillips Basin found a 4.2‰ gradient in the sedimentary organic carbon fraction (Melchin and Holmden, 2006a), but the inorganic carbon fraction was considered altered. In the Baltic Basin, a 3.0‰ gradient is evident in the inorganic carbon fraction, but the $\delta^{13}C$ value of the organic carbon fraction was not measured (Kaljo et al., 2004). In Nevada, the isotopic variability in the organic matter fraction at Monitor Range—regardless of its ultimate origin and relationship to the unique depositional environment of the Martin Ridge Basin—means that $\delta^{13}C_{org}$ values by themselves cannot be used to determine the magnitude of the gradient. And neither is the carbonate carbon fraction, alone, suitable to this task because of the presumably allochthonous nature of the carbonate sediment in the Vinini Creek section. Instead the size of the gradient between the Nevada platform and the surface ocean is estimated using only the best-preserved records from each section—$\delta^{13}C_{org}$ and $\delta^{13}C_{grap}$ profiles from Vinini Creek, and the $\delta^{13}C_{carb}$ profile from Monitor Range. Taking this approach, a gradient of ~4.0‰ is calculated, depending on where baselines are taken. Fortunately, it makes little difference to the calculation of the gradient that the $\delta^{13}C_{org}$ profile from one section is being compared to the $\delta^{13}C_{carb}$ profile from the other, as long as each profile faithfully records local changes in seawater $\delta^{13}C_{DIC}$ values. And of course only differences in magnitude are being compared between sections and not absolute values.

It is believed that the sedimentary shelf gradients reflect original seawater shelf gradients in $\delta^{13}C_{DIC}$. Based on their orientation, seawater $\delta^{13}C$ values were higher in proximal settings than distal, and this is the case for all Hirnantian basins studied thus far, where $\delta^{13}C$ excursions between proximal and distal sections may be compared: (1) Nevada, (2) Arctic Canada (Melchin and Holmden , 2006a), and (3) Baltica, (Kaljo et al., 2004). Considering the most distal sections from these three basins to be the ones most likely to record the shift in $\delta^{13}C$ of the Hirnantian glacial ocean, a value of 2.6 ±0.4‰ is calculated. Using the $\Delta^{13}C$ value of 31.7‰ determined from the Blackstone River section, and the $\delta^{13}C_{org}$ data from the Vinini

Creek section, this corresponds to a pre-Hirnantian surface ocean $\delta^{13}C_{DIC}$ value of +0.2‰, and a Hirnantian glacial ocean value of 2.8‰.

The possibility that the Hirnantian $\delta^{13}C$ gradient is controlled by sediment mixing and dispersal patterns like those off Heron Island in the Great Barrier Reef (Weber and Woodhead, 1969), Enewetok Atoll in the Pacific (Weber and Schmalz, 1968), the coast of Kuwait in the Persian Gulf (Gischler and Lomando, 2005), or the peri-platform environment of the Grand Bahama Bank in the Caribbean (Swart and Eberli, 2005; Swart et al., in press) cannot be entirely ruled out. $\delta^{13}C$ gradients in sediment from these modern settings reflect depth dependent changes in carbonate mineral facies: ^{13}C-enriched aragonite from chlorophyte algal sources such as *Halimeda* sp. and *Penicillus* sp. characterize sediment production in shallow water settings, and less ^{13}C-enriched biogenic calcite from coralline rhodophyte algae and other sources, or aragonite from scleractinian corals, dominate the sediment production in deeper waters. Sedimentary gradients of ~2‰ are consistent with laboratory experiments showing a difference of ~1.8‰ in the equilibrium partitioning of carbon isotopes between aragonite and calcite under abiotic conditions (Rubinson and Clayton, 1969). Gradients larger than this may reflect kinetic isotope effects associated with biologically precipitated carbonates or local scale changes in seawater $\delta^{13}C$ values.

Aragonite, or its pseudomorphs, is not present in the Hirnantian deposits at Monitor Range, nor is there any stratigraphic change in Sr/Ca ratios from which to infer that aragonite was originally present in the Nevada platform sediment. If the Hirnantian shelf gradients are sedimentological artefacts, then their creation involves a complex and interdependent pattern of kinetic, equilibrium, and diagenetic effects that is at best non-intuitive. The carbonate mineral facies explanation does not explain the fact that the organic carbon fraction of the Hirnantian sediment studied thus far also records identically oriented isotopic platform gradients. In the Cape Phillips Basin, a ~4‰ gradient in $\delta^{13}C_{org}$ values rivals the magnitude of the $\delta^{13}C_{carb}$ gradient in the Baltic Basin (Kaljo et al., 2001).

Studies of seawater in modern peri-platform environments like Florida Bay and the Bahamas have shown that $\delta^{13}C_{DIC}$ values may be lower (Patterson and Walter, 1994) or

higher (Swart and Eberli, 2005; Swart et al., in press) than surface ocean values—the direction depending on the isotope balance of the competing carbon fluxes (cf. Panchuk et al., 2005). Import fluxes of organic carbon to platform waters, and its oxidization locally, decreases seawater $\delta^{13}C_{DIC}$ values (Patterson and Walter, 1994), whereas export of *in situ* produced organic carbon *via* photosynthesis increases seawater $\delta^{13}C_{DIC}$ values (Swart et al., in press). The authors suggest local scale productivity as the reason for the elevated $\delta^{13}C_{DIC}$ values measured in the restricted waters of the Grand Bahama Bank, which ranges up to +2.5‰ compared to +1.5‰ in the western Atlantic (Kroopnick, 1985) and 1.88‰ in the Florida Straits (Patterson and Walter, 1994). The authors suggest that where higher $\delta^{13}C_{DIC}$ values are recorded in the Bahama Bank waters, these values result from the aragonite produced and fractionation during productivity by benthic algae, seagrass, and cyanobacteria.

Epeiric sea productivity is rarely discussed in the literature on ancient carbon cycling, with a couple of exceptions (Panchuk et al., 2005; Fanton and Holmden, 2007). The main conceptual obstacle is the assumed close linkage between productivity, remineralization, and sedimentary TOC over the relatively long timescales relevant to the modern ocean carbon cycle (with a residence time of 10^5 years). Traditional models dictate that a productivity driven increase in the $\delta^{13}C$ value of seawater in a shallow, nonstratified water body would be effectively cancelled through its subsequent remineralization on geological timescales. Because shallow water deposits typically contain small amounts of preserved organic matter, the assumption of complete remineralization is reinforced.

One solution to the conundrum is premised on the work of Swart et al. (in press) in the Bahamas, and mentioned in Swart and Eberli (2005), involving sea grass productivity on the Bahama Bank. At steady state, sea grass is neither increasing in total biomass nor decreasing, and the annualized production of new sea grass is balanced by its export from the system. But a standing stock of sea grass is always present, and its biomass, enriched in ^{12}C, may be enough to drive seawater DIC values in small carbon pools to higher $\delta^{13}C$ values than is found in the adjacent surface ocean. In this way, the sea grass analogy is relevant to the Ordovician, and the Hirnantian sea level lowstand, in particular. Local scale productivity may have increased on the epeiric platforms during the Hirnantian sea level lowstand, which helped to elevate shelf seawater $\delta^{13}C_{DIC}$ values higher than Hirnantian ocean $\delta^{13}C_{DIC}$ values.

2.7.5 Productivity and the Hirnantian Calcite Dust Flux Hypothesis

Sedimentological attributes discussed by Finney et al. (2007), together with the interpretation of the $\delta^{15}N$ record, put the late Ordovician greenhouse to Hirnantian icehouse transition within the uppermost *P. pacificus* Zone (perhaps starting prior to the base of the *D. mirus* Subzone) in the Vinini Creek section. Similar sediment-based features are found in stratigraphically equivalent intervals of the Monitor Range and Blackstone River sections – most notable of these is the spike in TOC. Records of TOC in all three sections, and those reported from the Cape Phillips Basin (Melchin and Holmden, 2006a), suggest pulses of additional primary productivity in the epeiric seas during this transitional period. The presence of silt and dolomite grains (inferred from Mg/Ca ratios) points to increased trade wind velocity from Hadley cell contraction, an expected consequence of climate cooling (cf., Little et al., 1997; Shi et al., 2001). Higher winds generated increased coastal upwelling, which helped to clear the ocean's Intermediate waters of enriched ^{12}C DIC and nutrients. The result was a brief interval of elevated primary production and improved conditions for organic carbon burial on the shelf, while the ocean's low oxygen containing Intermediate waters were displaced and ultimately upwelled by greater rates of downwelling in high latitudes. The fact that $\delta^{13}C$ values decline in spite of the hypothesized increase in productivity indicates that the input flux of low $\delta^{13}C$ from upwelling was larger than $\delta^{13}C$ export flux from productivity.

The extent to which this nutrient pulse from upwelling could affect productivity on the epeiric platform depends on platform position and water column depth. The amount of restriction between open ocean and epeiric sea will determine seawater exchange between the platform and ocean, and a relatively deep water-column might explain the presence of the TOC spike in the Monitor Range section, located on the platform. On the other hand, if the Martin Ridge Basin were a trough with a connection to the open ocean, then the watermass properties of the Vinini Creek setting would have a conduit by which to gain access to the platform and influence the chemistry of the Monitor Range depositional waters. It is perhaps not a coincidence that the depositional setting of the Yukon's Blackstone River area is also described as consisting of shallow platforms separated by deeper troughs (McCracken and Lenz, 1987), as this may have been a characteristic feature of the distal platform architecture.

A trough connection to the ocean would help to explain the reappearance of *P. pacificus* graptolites in the *D. mirus* equivalent strata in the Monitor Range section, coincident with the TOC spike. A shift in watermass properties and food distribution may have allowed for migration of these graptolites back into the Martin Ridge Basin before the Hirnantian sea level drop, and their subsequent extinction. Alternatively, it has been argued on sedimentological grounds that a brief sea level rise occurred just ahead of the Hirnantian sea level fall, and a deeper water column allowed *P. pacificus* graptolites to migrate inboard to the distal platform setting of the Monitor Range section (Finney et al., 2007). The shoreward shift of a eutrophic watermass, aided by the deeper water column, might also explain the presence of the TOC spike in the Monitor Range section. In this case, sea level rise increased local scale productivity and/or organic carbon burial. The Blackstone River section in the Yukon, which also records a TOC spike in the same stratigraphic interval (Fig. 2.4), shows no sediment-based evidence for a sea level rise before the Hirnantian sea level fall, and neither do the sections from the Cape Phillips Basin (Melchin and Holmden, 2006a). Either the evidence for a sea level rise has been overlooked in these sections, or the sedimentological evidence for sea level rise in the Monitor Range section is local in scale, related perhaps to the structurally controlled subsidence of the Martin Ridge Basin (or trough).

The global scale decrease in sedimentary TOC levels during the Hirnantian glaciation has led some authors to reject the productivity hypothesis in favour of the carbonate-weathering hypothesis (Kump et al., 1999; Melchin and Holmden, 2006a) as the explanation for the Hirnantian positive $\delta^{13}C$ excursion. The carbonate weathering hypothesis predicts that the $\delta^{13}C$ excursion should track glacio-eustacy because sea level controls the area of carbonate sediment exposed to weathering (Kump et al., 1999; Noble et al., 2005; Melchin and Holmden, 2006a; 2006b). Specifically, the rising limb of the $\delta^{13}C$ excursion should track the glacio-eustatic lowering of sea level, the peak interval of the excursion should correspond to the lowest sea level obtained, and the falling limb should track the post-glacial rise in sea level. The extent to which the shape of the $\delta^{13}C$ profile might genuinely behave as a proxy for relative sea level depends on the balance of the competing carbon inputs, the most important being the local productivity and mixing between isotopically distinct watermasses,

which are also susceptible to adjustments through sea level changes (e.g., Holmden et al., 1998; Panchuk et al., 2006; Fanton and Holmden, 2007). The apparent decrease in Hirnantian ocean productivity presents a bit of a conundrum in light of the fact that even more intense equatorial and coastal upwelling is predicted for the cooler glacial climate, owing to the increased trade wind velocities in a cooler climate (Berger and Wefer, 1991; Payton et al., 1996; Little et al., 1997; Jahn et al., 2003). Once again, the solution probably lies in the balance between changes in ocean productivity and changes in rates of remineralization.

One place where an increase in primary productivity could make a difference, and at the same time go relatively undetected in terms of sedimentary TOC records, is in the epeiric seas. Up to this point only the impact of increased trade wind velocity on intensification of oceanic upwelling has been considered. Trade winds as agents of nutrient dust fertilization of epeiric sea productivity may also occur. The vast landmass east of the Nevada platform that became exposed during the Hirnantian glacio-eustatic lowstand was both free of vascular plants and rich in calcite sediment. Because a vast epeiric sea still separated the western Laurentian shoreline from the Panthalasssa Ocean (Fig. 2.1b), much of the airborne supply of soluble calcite dust and nutrients may have settled into the intervening epeiric sea.

In a study of the impact of calcite dust on the Nd isotope budget of the Japan Sea, Jacobson and Holmden (2007) presented an atmospheric transport model in which calcite dust is progressively dissolved by atmospheric moisture (with a pH of ~5.7), and the aerosols scavenged from the atmosphere by rainwater falling into seawater. Because of its inherent solubility, the rate of removal of calcite dust from the atmosphere is faster than silicate dust by a factor of ten. Model runs simulating the loss of the calcite component of Asian loess over the Japan Sea shows that 80% of the calcite is lost after a distance of only 600 km from the shoreline. In the higher CO_2 atmosphere of the Hirnantian, the loss rate would likely be greater due to greater rainwater acidity.

The transport modeling predicts that the calcite dust flux will drop off exponentially from the shoreline. Accordingly, any nutrients delivered to the epeiric sea by the calcite dust flux will also drop off exponentially, as will primary productivity, and seawater $\delta^{13}C$ values (Fig. 2.8). In addition, the calcite dust flux provides another way for the carbonate weathering

flux to reach the epeiric seas—as alkalinity delivered in precipitation. The biggest flux of ^{13}C-enriched alkalinity would occur nearest to the shoreline, dropping off with distance towards the ocean as calcite is dissolved by atmospheric moisture.

In summary, the absence of vascular plants, the predictable increase in the velocity of the trade winds in icehouse climates, and the large quantities of calcite sediment exposed by the glacio-eustatic lowering of sea level, all point to a prominent role for calcite dust as a component of the early Paleozoic carbon cycle.

2.8 Conclusions

Comparisons between coupled $\delta^{13}C_{carb}$ and $\delta^{13}C_{org}$ profiles from Hirnantian platform and ocean slope settings in Nevada confirm earlier reports of Hirnantian shelf gradients in sedimentary $\delta^{13}C$ values from Arctic Canada (Melchin and Holmden, 2006a) and Baltica (Kaljo et al., 2004). These gradients are interpreted as genuine features of seawater DIC that developed during the glacio-eustatic lowstand, with proximal settings reaching higher $\delta^{13}C_{DIC}$ values than distal ones at the height of the Hirnantian glaciation. Considering the secular records from the most distal settings (this study; Kaljo et al., 2004; Melchin and Holmden, 2006a), a shift of just 2.6 ±0.4‰ is calculated for the ocean atmosphere system during the Hirnantian glaciation event—much smaller than the shifts recorded on platforms in proximal settings.

In the Monitor Range and Blackstone River sections, the stratigraphic timing of the Hirnantian $\delta^{13}C_{carb}$ and $\delta^{13}C_{org}$ shifts is synchronous. The excellent graptolite control in the Vinini Creek section puts the rise in Hirnantian $\delta^{13}C$ values in the uppermost part of the *D. mirus* Subzone, and the first attainment of peak values at the base of the *N. extraordinarius* Zone. The fall in $\delta^{13}C$ values, signalling the end of the Hirnantian glaciation, occurs in the upper *N. persculptus* Zone, as documented in the Blackstone River section. Graptolite periderm is a promising material for reconstructing secular changes in seawater $\delta^{13}C$ values in distal environments. Graptolite $\delta^{13}C$ profiles provide an alternative perspective on source mixing and alteration effects that can compromise bulk organic matter as recorders of

seawater $\delta^{13}C$ values, and with additional study, new insights into food web dynamics in upwelling zone and graptolite diets.

Hirnantian $\delta^{13}C_{carb}$ and $\delta^{13}C_{org}$ profiles in the Blackstone River section exhibit nearly identical excursions, characterized by a $\Delta^{13}C$ value of 31.7‰. This is not the case in the Monitor Range section where the $\delta^{13}C_{org}$ profile exhibits considerably more variability—two peaks separated by a deep trough—with lower peak magnitudes than the corresponding single peak of the $\delta^{13}C_{carb}$ excursion. The behaviour of the $\delta^{13}C_{org}$ profile is attributed to source mixing and/or selective preservation of organic matter in the context of the unusual depositional environment of the Martin Ridge Basin, first identified by Dunham (1977). A ^{12}C-enriched particulate source of terrestrial organic carbon (bryophytes) may have been carried to this setting as part of an eolian dust component where it was then mixed with locally produced marine organic matter. Alternatively, chemotrophic bacteria, thriving in the anoxic bottom waters of the Martin Ridge Basin, may be the source of organic matter with low $\delta^{13}C$ values. Processes such as selective degradation of organic constituents, bacterial chemotrophy driven by bottom water redox shifts, and, in some instances, even the complete microbial 'repackaging' of the primary produced organic matter, may have worked together produce the high degree of variability in $\delta^{13}C_{org}$ values documented in the Monitor Range sections.

In common with the Pleistocene glaciations, secular changes in sedimentary $\delta^{15}N_{TN}$ values appear to be responding to a changing ocean redox state. However, the isotopic shift recorded in the upwelling influenced deposits of the Vinini Creek section is in the opposite direction, however. One clue to the origin of this behaviour is the low and restricted range in sedimentary $\delta^{15}N_{TN}$ values (–1 to +1‰) compared to downcore sedimentary records in Pleistocene upwelling zones. The $\delta^{15}N_{TN}$ records are reconciled through a hypothesis that relates secular changes in Hirnantian sedimentary $\delta^{15}N_{TN}$ values to ocean redox driven changes in fixed nitrogen sources. In greenhouse climates, the flux of recycled ^{15}N enriched nitrogen upwelled from the ocean depths is so low as to be negligible. Because cyanobacteria fix their own nitrogen from the large atmospheric pool, they are favoured under these conditions, and recycling of fixed nitrogen is limited to the photic zone. Cyanobacteria

produce fixed nitrogen with characteristically low $\delta^{15}N$ values of between 0 and –2‰ (overlapping the range of sedimentary $\delta^{15}N$ values in the *P. pacificus* Zone) in the Vinini Creek section. The 2‰ shift to more positive sedimentary $\delta^{15}N_{TN}$ values during the Hirnantian glaciation is interpreted to reflect an additional input of fixed nitrogen to the photic zone from upwelling of ^{15}N enriched recycled nitrogen from the ocean's depths. Climate cooling and increased oxygenation of the oceans during icehouse climates caused oxygen minimum zones to shrink, and denitrification efficiency to decrease below 100%. This allowed some remineralized organic bound nitrogen to escape denitrification in the ocean's depths, and be returned to the photic zone in upwelling currents where it then shifted the surface water pool of fixed nitrogen in the photic zone to higher $\delta^{15}N_{TN}$ values. The positive shift may have been enhanced further by a decrease in cyanobacterial productivity and a corresponding increase in algal productivity, according to the principle of competitive advantage.

All of the shelf distal and slope sections studied, thus far, record lower TOC in the glacial age deposits than in the pre- or post-glacial deposits of the same sections. This suggests that global ocean's organic carbon remineralization rate increased more than the productivity rate during the Hirnantian glacial period. By contrast, the interplay between TOC, productivity, and remineralization on the epeiric platforms is less straightforward owing to the small DIC pools and short carbon residence times. It is proposed that calcite dust may have played a significant role in generating the inferred gradient in seawater $\delta^{13}C$ values across the Nevada platform by stimulating local scale productivity, and mixing in ^{13}C-enriched alkalinity. Calcite dust drops out of the atmosphere rapidly with increasing distance from the shorelines owing to its inherent solubility in low pH rainwater. Consequently, any productivity sustained by the nutrients delivered in dust will likewise be expected to drop off with increasing distance from the shoreline, as will the ^{13}C enriched alkalinity addition from calcite dissolution. The orientation of the Hirnantian seawater gradient, with higher values in proximal regions, has previously been attributed to local scale carbonate weathering influences (Melchin and Holmden, 2006a). The calcite dust flux hypothesis is a slightly different take on the carbonate weathering hypothesis—with the addition of local scale productivity effects—where gradients in seawater $\delta^{13}C$ values during the Hirnantian sea level

lowstand are linked to the transport properties of calcite dust in the atmosphere, in addition to the riverine additions of ^{13}C enriched DIC and nutrients.

The model of C and N cycling developed for the Hirnantian sea level lowstand (Fig. 2.8) is relevant to the origin of positive $\delta^{13}C$ excursions in other periods in Earth history, particularly in the Silurian, where similarly oriented carbon isotope shelf gradients have been documented (Noble et al., 2005) during regressions, and in some cases linked with glaciation in Gondwanaland (Kump et al., 1999; Munnecke et al., 2003; Loydell, 2007). Even our understanding of the very large $\delta^{13}C$ excursions in the Proterozoic Eon may be improved by re-examining them in terms of local scale carbon cycling processes on epeiric shelves (Giddings and Wallace, 2007).

2.9 Acknowledgements

Tim Prokopiuk is thanked for invaluable technical support in the Saskatchewan Isotope Laboratory and training on the instruments provided to D.L. This work forms part of the requirements for the M.Sc. degree to D.L. Funding from NSF (EAR 0418790) and NSERC is gratefully acknowledged. A. Atkinson is thanked for providing field assistance during collection of the Blackstone River section.

2.10 References

Allison, N. 1996. Factors influencing the stable carbon and oxygen isotopic composition of Porites lutea coral skeletons from Phuket, South Thailand. Coral Reefs, v. 15, p. 43-57.

Altabet, M.A. and Francois, R. 1994. Sedimentary nitrogen isotopic ratio as a recorder for surface ocean nitrate utilization. Global Biogeochemical Cycles, v. 8, p. 103-116.

Altabet, M.A., Francois, R., Murray, D.W., and Prell, W.L. 1995. Climate-related variations in denitrification in the Arabian Sea from sediment $^{15}N/^{14}N$ ratios. Nature, v. 373, p. 506-509.

Altabet, M.A., Pilskaln, C., Thunell, R., Pride, C., Sigman, D., Chavez, F., and Francois, R. 1999. The nitrogen isotope biogeochemistry of sinking particles from the margin of the Eastern North Pacific. Deep Sea Research Part I, v. 46, p. 655-679.

Altabet M.A., Higginson, M.J. and Murray, D.W. 2002. The effect of millennial-scale changes in Arabian Sea denitrification on atmospheric CO_2. Nature, v. 415, p. 159-162.

Altabet, M.A. 2007. Constraints on oceanic N balance/imbalance from sedimentary N-15 records. Biogeosciences, v. 4, p. 75-86.

Andrew, A.S., Hamilton, P.J., Mawson, R., Talent, J.A., and Whitford, D.J. 1994. Isotopic correlation tools in the Middle Palaeozoic and their relation to extinction events. APEA, v. 34, p 268-277.

Bambach, R.K., Knoll, A.H., and Wang, S.C. 2004. Origination, extinction, and mass depletions of marine diversity. Paleobiology, v. 30, p. 522-542.

Benner, R., Fogel, M.L., Sprague, E.K., and Hodson, R.E. 1987. Depletion of ^{13}C in lignin and its implications for stable carbon isotope studies. Nature, v. 329, p. 708-710.

Berger, W.H., and Wefer, G. 1991. Productivity of the glacial ocean: Discussion of the iron hypothesis. Limnology and Oceanograhpy, v. 36, p. 1899-1918.

Berner, R.A. 1990. Atmospheric carbon dioxide levels over Phanerozoic time. Science, v. 249, p. 1382-1386.

Berry, W.B.N., Wilde, P., and Quinby-Hunt, M.S. 1987. The oceanic non sulfidic oxygen minimum zone: a habitat for graptolites? Geological Society of Denmark Bulletin, v 35, p. 103.

Bickert, T., Pätzold, J., Samtleben, C., and Munnecke, A. 1997. Paleoenvironmental changes in the Silurian indicated by stable isotopes in brachiopod shells from Gotland, Sweden. Geochimica et Cosmochimica Acta, v. 61, p. 2717-2730.

Blakey, R.C. 2003. Detailed Paleogeography Maps. online resource available at the University of Arizona Department of Geology, URL. http.//jan.ucc.nau.edu/~rcb7/globaltext2.html.

Borgendahl, J., and Westman, P. 2007. Cyanobacteria as a trigger for increased primary productivity during sapropel formation in the Baltic Sea—a study of the Ancylus/Litorina transition. Journal of Paleolimnology, v. 38, p. 1-12.

Burdige, D.J. 2007. Preservation of organic matter in marine sediments: controls, mechanisms, and an imbalance in sediment organic carbon budgets. Chemical Review, v. 107, p. 467-485.

Calvert, S.E., Nielsen, B., and Fontugne, M.R. 1992. Evidence from nitrogen isotope ratios for enhanced productivity during the formation of eastern Mediterranean sapropels. Nature, v. 259, p. 223-225.

Calvert, S.E., Bustin, R.M., and Ingall, E.D. 1996. Influence of water column anoxia and sediment supply on the burial and preservation of organic carbon in marine shales. Geochimica et Cosmochimica Acta, v. 60, p. 1577-1593.

Cecile, M.P., Morrow, D.W., and Williams, G.K. 1997. Early Paleozoic (Cambrian to Early Devonian) tectonic framework, Canadian Cordillera. Bulletin of Canadian Petroleum Geology, v. 45, p. 54-74.

Chen, X., Rong, J.Y., Fan, J.X., Zhan, R.B., Mitchell, C.E., Harper, D.A.T., Melchin, M.J., Peng, P., Finney, S.C., and Wang, X.F. 2006. The Global boundary Stratotype Section and Point (GSSP) for the base of the Hirnantian Stage (the uppermost of the Ordovician System). Episodes, v. 29, p. 183-196.

Cooper, R.A., and Sadler, P.M. 2004. The Ordovician Period, *in* Gradstein, F.M., Ogg, J.G., and Smith, A.G., (Eds.), A Geologic Time Scale 2004. Cambridge University Press, p. 165-187.

Dean,W.E. 2007. Sediment geochemical records of productivity and oxygen depletion along the margin of western North America during the past 60,000 years. teleconnections with Greenland Ice and the Caraico Basin. Quarternary Science Reviews, v. 26, p. 98-114.

Dierssen, H.M., and Zimmerman, R.C., in submission, Benthic ecology from space: seagrass net primary production across the Bahamas Banks. Limnology and Oceanography.

Dunham, J.B. 1977. Depositional environments and paleogeography of the Upper Ordovician, Lower Silurian carbonate platform of central Nevada, In: Stewart, J.H., Stevens, C.H., and Fritsche, A.E., (Eds.), Paleozoic Paleogeography of the Western United States-I. Pacific Section. Society of Economic Paleontologists and Mineralogists, Book 7, p. 157-164.

Fanton, K.C., and Holmden, C. 2007. Sea level forcing of carbon isotope excursions in epeiric seas: implications for carbon isotope chemostratigraphy. Canadian Journal of Earth Science, v. 44, p. 807-818.

Finney, S.C., Cooper, J.D., and Berry, W.B.N. 1997. Late Ordovician mass extinction: sedimentologic, cyclostratigraphic, and biostratigraphic records from platform and basin successions, central Nevada. BYU Geology Studies, v. 42, p. 79-102.

Finney, S.C., Berry, W.B.N., Cooper, J.D., Ripperdan, R.L., Sweet, W.C., Jacobson, S.R., Soufiane, A., Achab, A., and Noble, P.J. 1999. Late Ordovician mass extinction: A new perspective from stratigraphic sections in central Nevada. Geology, v. 27, p. 215-218.

Finney, S.C., Berry, W.B.N., and Cooper, J.D. 2007. The influence of denitrifying seawater on graptolite extinction and diversification during the Hirnantian (latest Ordovician) mass extinction event. Lethaia, v. 40, p. 281-291.

Giddings, J., and Wallace, M.W. 2007. A $\delta^{13}C$ depth gradient from a mid-Cryogenian platform margin. Evidence for Neoproterozoic ocean stratification. Geochmica et Cosmochimica Acta, A321-A321 suppl. S, AUG-SEP 2007.

Gischler, E., and Lomando, A.J. 2005. Offshore sedimentary facies of a modern carbonate ramp, Kuwait, northwestern Arabian-Persian Gulf. Facies, v. 50, p. 443-462.

Ganeshram, R.S., Pedersen, T.F., Calvert, S.E., and Murray, J.W. 1995. Large changes in oceanic nutrient inventories from glacial to interglacial periods. Nature, v. 376, p. 755-758.

Ganeshram, R.S., Pedersen, T.F., Calvert, S.E., McNeill, G.W., and Fontugne, M.R. 2000. Glacial-interglacial variability in denitrification in the world's oceans: Causes and consequences. Paleoceanography, v. 15, p. 361-376.

Gong, C.R., and Hollander, D.J. 1997. Differential contribution of bacteria of sedimentary organic matter in oxic and anoxic environments, Santa Monica Basin, California. Organic Geochemistry, v. 26, p. 545-563.

Hedges, J.I., Clark, W.A., and Cowie, G.L. 1988. Fluxes and reactivities of organic-matter in a coastal marine bay. Limnology and Oceanography, v. 33, p. 1137-1152.

Hollander D.J., and Smith M.A. 2001. Microbially mediated carbon cycling as a control on the $\delta^{13}C$ of sedimentary carbon in eutrophic Lake Mendota (USA). New models for interpreting isotopic excursions in the sedimentary record. Geochimica et Cosmochimica Acta, v. 65, p. 4321-4337.

Holmden, C., Creaser, R.A., Muehlenbachs, K., Leslie, S.A., and Bergstrom, S.M. 1998. Isotopic evidence for geochemical decoupling between ancient epeiric seas and bordering oceans. Implications for secular curves. Geology, v. 26, p. 567-570.

Holmes, M.E., Eichner, C., Struck, U., and Wefer, G. 1999. Reconstruction of surface ocean nitrate utilization using stable nitrogen isotopes in sinking particles and sediments, In: Use of proxies in paleoceanography: examples from the South Atlantic, G., Fischer, and G., Wefer, (Eds.), pp. 447-468. Springer.

Immenhauser, A., Della Porta, G., Kenter, J.A.M., and Bahamonde, J.R. 2003. An alternative model for positive shifts in shallow-marine carbonate $\delta^{13}C$ and $\delta^{18}O$. Sedimentology, v. 50, p. 953-959.

Ingall, E., and Jahnke, R. 1997. Influence of water-column anoxia on the elemental fractionation of carbon and phosphorous during sediment diagenesis. Marine Geology, v. 139, p. 219-229.

Jacobsen, A.D., and Holmden, C., 2006. Calcite dust and the atmospheric supply of Nd to the Japan Sea. Earth and Planetary Science Letters, v. 244, p. 418-430.

Jahren, A.H., Porter, S., and Kuglitsch, J.J. 2003. Lichen metabolism identified in Early Devonian terrestrial organisms. Geology, v. 31, p. 99-102.

Jeppsson, L. 1990. An oceanic model for lithological and faunal changes tested on the Silurian record. Journal of Geological Society of London, v. 147, p. 663-674.

Johnson, M.E. 2006. Relationship of Silurian sea-level fluctuations to oceanic episodes and events. GFF, v. 128, p. 115-121.

Junium, C.K., and Arthur, M.A. 2007. Nitrogen cycling during the Cretaceous, Cenomanian – Turonian Oceanic Anoxic Event II. Geochemistry, Geophysics, Geosystems, v. 8, p. 1-18.

Kaljo, D., Hints, L., Martma, T., Nõlvak, J., and Oraspõld, A. 2004. Late Ordovician carbon isotope trend in Estonia, its significance in stratigraphy and environmental analysis. Palaeogeography, Palaeoclimatology, Palaeoecology, v. 210, p. 165-185.

Karl, D.M. 1999. A sea of change: Biogeochemical variability in the North Pacific Subtropical Gyre. Ecosystems, v. 2, p. 181-214.

Kodina, L.A., Bogacheva, M.P., and Lyutsarev, S.V. 1996. Particulate organic carbon in the Black sea: Isotopic composition and origin. Geokhimiya, p. 884-890.

Kump, L.R., Arthur, M.A., Patzkowsky, M.E., Gibbs, M.T., Pinkus, D.S., and Sheehan, P.M. 1999. A weathering hypothesis for glaciation at high atmospheric pCO_2 during the Late Ordovician. Palaeogeography, Palaeoclimatology, Palaeoecology, v. 152, p. 173-187.

Lehmann, M.F., Bernasconi, S.M., Barbieri, A., and McKenzie, J.A. 2002. Preservation of organic matter and alteration of its carbon and nitrogen isotope composition during simulated and in situ early sedimentary diagenesis. Geochimica et Cosmochimica Acta, v. 66, p. 3573-3584.

Lenz, A.C., and McCracken, A.D. 1987. The Ordovician Silurian boundary, Northern Canadian Cordillera – Graptolite and conodont correlation. Canadian Journal of Earth Sciences, v. 24, p. 640-652.

Lewan, M.D. 1983. Effects of thermal maturation on stable organic-carbon isotopes as determined by hydrous pyrolysis of Woodford shale. Geochimica et Cosmochimica Acta, v. 47, p. 1471-1479.

Libes, S.M., and Deuser, W.G. 1988. The isotope geochemistry of particulate nitrogen in the Peru upwelling area and the Gulf of Maine. Deep-Sea Research Part A-Oceanographic Research Papers, v. 35, p. 517-533.

Little, M.G., Schneider, R.R., Kroon, D., Price, B., Summerhayes, C.P., and Segl, M. 1997. Trade wind forcing of upwelling, seasonality, and Heinrich events as a response to sub-Milankovitch climate variability. Paleoceanography, v. 12, p. 568-576.

Lo Duca, S.T., and Pratt, L.M. 2002. Stable carbon-isotope composition of compression fossils from Lower Paleozoic konservat-lagerstätten. Palaios, v. 17, p. 287-291.

Long, D.G.F. 2007. Tempestite frequency curves, a key to Late Ordovician and Early Silurian subsidence, sea-level change, and orbital forcing in the Anticosti foreland basin, Quebec, Canada. Canadian Journal of Earth Sciences, v. 44, p. 413-431.

Loydell, D.K. 1998. Early Silurian sea-level changes. Geological Magazine, v. 135, p. 447-471.

Loydell, D.K. 2007. Early Silurian positive $\delta^{13}C$ excursions and their relationship to glaciations, sea-level changes and extinction events. Geological Journal, v. 42, p. 531-546.

Lyle, M., Koizumi, I., Delaney, M.L., and Barron, J.A. 2000. Sedimentary record of the California Current system, middle Miocene to Holocene. a synthesis of Leg 167 results, In: Lyle, M., Koizumi, I., Richter, C., Moore, Jr., T.C., (Eds.), Proceeding of the Ocean Drilling Program, Scientific Results, v. 167, p. 341-376.

Melchin, M.J., and Holmden, C. 2006a. Carbon isotope chemostratigraphy in Arctic Canada. Seal-level forcing of carbonate platform weathering and implications for Hirnantian global correlation. Palaeogeography, Palaeoclimatology, Palaeoecology, v. 234, p. 186-200.

Melchin, M.J., and Holmden, C. 2006b. Carbon isotope chemostratigraphy of the Llandovery in Arctic Canada. Implications for global correlation and sea-level change. GFF, v. 128, p. 173-180.

Meyers, P.A., and Bernasconi, S.M. 2005. Carbon and nitrogen isotope excursions in mid-Pleistocene sapropels from the Tyrrhenian Basin. Evidence from climate-induced increase in microbial primary productivity. Marine Geology, v. 220, p. 41-58.

Munnecke, A., Samtleben, C., and Bickert, T. 2003. The Ireviken Event in the lower Silurian of Gotland, Sweden – relation to similar Palaeozoic and Proterozoic events. Palaeogeography, Palaeoclimatology, Palaeoecology, v. 195, p. 99-124.

Noble, P.J., Zimmerman, M.K., Holmden, C., and Lenz, A.C. 2005. Early Silurian (Wenlockian) $\delta^{13}C$ profiles from the Cape Phillips Formation, Arctic Canada and their relation to biotic events. Canadian Journal of Earth Sciences, v. 42, p. 1419-1430.

Oppo, D.W., Raymo, M.E., Lohmann, G.P., Mix, A.C., Wright, J.D., and Prell, W.L. 1995. A $\delta^{13}C$ record of upper North-Atlantic deep-water during the past 2.6 million years. Paleoceanography, v. 10, p. 373-394.

Panchuk, K.M., Holmden, C., and Kump, L.R. 2005. Sensitivity of the epeiric sea carbon isotope record to local-scale carbon cycle processes. Tales from the Mohawkian Sea. Palaeogeography, Palaeoclimatology, Palaeoecology, v. 228, p. 320-337.

Panchuk, K.M., Holmden, C., and Leslie, S.A. 2006. Local controls on carbon cycling in the Ordovician Midcontinent Region of North America with implications for carbon isotope secular curves. Journal of Sedimentary Research, v. 76, p. 200-211.

Pancost, R.D., Freeman, K.H., and Patzkowsky, M.E. 1999. Organic-matter source variation and the expression of a late Middle Ordovician carbon isotope excursion. Geology, v. 27, p. 1015-1018.

Patterson, W.P., and Walter, L.M. 1994. Depletion in ^{13}C in seawater ΣCO_2 on modern carbonate platforms. Significance for the carbon isotopic record of carbonates. Geology, v. 22, p. 885-888.

Payton, A., Kastner, M., and Chaver, F.P. 1998. Glacial to Interglacial fluctuations in productivity in the Equatorial Pacific as indicated by marine barite. Nature, v. 274, p. 1355-1357.

Qing, H., and Veizer, J. 1994. Oxygen and carbon isotopic composition of Ordovician brachiopods: implications for coeval seawater. Geochimica et Cosmochimica Acta, v. 58, p. 4429-4442.

Redecker, D., Kodner, R., and Graham, L.E. 2000. Glomalean fungi from the Ordovician. Science, v. 289, p. 1920-1921.

Rubenstein, C.V., and Vaccari, N.E. 2004. Cryptospore assemblages from the Ordovician/Silurian boundary in the Puna region, north-west Argentina. Palaeontology, v. 47, p. 1037-1061.

Rubinson, M., and Clayton, R.N. 1969. Carbon-13 fractionation between aragonite and calcite. Geochimica et Cosmochimica Acta, v. 33, p. 997-1002.

Sachs, J.P., and Repeta, D.J. 1999. Oligotrophy and nitrogen fixation during eastern Mediterranean sapropel events. Science, v. 286, p. 2485-2488.

Saltzman, M.R., and Young, S.A. 2005. Long-lived glaciation in the Late Ordovician? Isotopic and sequence-stratigraphic evidence from western Laurentia. Geology, v. 33, p. 109-112.

Shi, N., Schneider, R., Beug, H.J., and Dupont, L.M. 2001. Southeast trade wind variations during the last 135 kyr: evidence from pollen sectra in eastern South Atlantic sediments. Earth and Planetary Science Letters, v. 187, p. 311-321.

Shear, W.A. 1991. The early development of terrestrial ecosystems. Nature, v. 351, p. 283-289.

Sigman, D.M., and Boyle, E.A. 2000. Glacial/interglacial variations in atmospheric carbon dioxide. Nature, v. 407, p. 859-869.

Sigman D.M., Altabet, M.A., McCorkle, D.C., Francois, R., and Fischer, G. 2000. The $\delta^{15}N$ of nitrate in the Southern Ocean. nitrogen cycling and circulation in the oceanic interior. Journal of Geophysical Research, v. 105, 19,599-19,614.

Steemans, P. 2000. Miospore evolution from the Ordovician to the Silurian. Review of Palaeobotany and Palynology, v. 113, p. 189-196.

Storch, P. 2006. Facies development, depositional settings and sequence stratigraphy across the Ordovician–Silurian boundary: a new perspective from the Barrandian area of the Czech Republic. Geological Journal, v. 41, p. 163–192.

Strother, P.K., Al-Hajri, S., and Traverse, A. 1996. New evidence for land plants from the lower Middle Ordovician of Saudi Arabia. Geology, v. 24, p. 55-58.

Sun, M.-Y., Zou, L., Dai, J., Ding, H., Culp, R.A., and Scranton, M.I. 2004. Molecular carbon isotopic fractionation of algal lipids during decomposition in natural oxic and anoxic seawaters. Organic Geochemistry, v. 35, p. 895-908.

Swart, P.K., and Eberli, G. 2005. The nature of the delta C-13 of periplatform sediments: Implications for stratigraphy and the global carbon cycle. Sedimentary Geology, v. 175, p. 115-129.

Swart, P.K., and Reijmer, J.J.G., and Otto, R. (in press), Variations in the $\delta^{13}C$, $\delta^{18}O$, and mineralogy of surface sediments on Great Bahama Bank: Implications for reading the fossil record. International Association of Sedimentologist.

Taylor, A.F.S., Fransson, P.M., Högberg, P., Högberg, M.N., and Plamboeck, A.H. 2003. Species level patterns in ^{13}C and ^{15}N abundance of ectomycorrhizal and saprotrophic fungal sporocarps. New Phytologist, v. 159, p. 757-774.

Teece, M.A., Fogel, M.L., Dollhopf, M.E., and Nealson, K.H. 1999. Isotopic fractionation associated with biosynthesis of fatty acids by a marine bacterium under oxic and anoxic conditions. Organic Geochemistry, v. 30, p. 1571-1579.

Tyrrell, T. 1999. The relative influences of nitrogen and phosphorus on oceanic primary production. Nature, v. 400, p. 525-531.

Versteegh, G.J.M., and Zonneveld, K.A.F. 2002. Use of Selective degradation to separate preservation from productivity. Geology, v. 30, p. 615-618.

Voss, M., Dippner, J.W., and Montoya, J.P. 2001. Nitrogen isotope patterns in the oxygen-deficient waters of the Eastern Tropical North Pacific Ocean. Deep Sea Research Part I. Oceanographic Research Papers, v. 48, p. 1905-1921.

Weber, J.N., and Woodhead, P.M. 1969. Factors affecting carbon and oxygen isotopic composition of marine carbonate sediments. 2. Heron Island Great Barrier Reef, Australia. Geochimica et Cosmochimica Acta, v. 33, p. 19-38.

Weber, J.N., and Schmalz, R.F. 1968. Factors affecting carbon and oxygen isotopic composition of marine carbonate sediments. 3. Eniwetok Atoll. Journal of Sedimentary Petrology, v. 38, p. 1270.

Wellman, C.H., Osterloff, P.L., and Mohiuddin, U. 2003. Fragments of the earliest land plants. Nature, v. 425, p. 282-285.

Wigforss-Lange, J. 1999. Carbon isotope ^{13}C enrichment in Upper Silurian (Whicliffian) marine calcareous rocks in Scania, Sweden. GFF, v. 121, p. 273-279.

Witzke, B.J. 1987. Models for circulation patterns in epicontinental seas applied to Paleozoic facies of the North America craton. Paleoceanography, v. 2, p. 229-248.

Yapps, C.J, and Poths, H. 1992. Ancient atmospheric CO_2 pressures inferred from natural goethites. Nature, v. 355, p. 342-344.

2.11 Relevance of Manuscript to Thesis

This chapter presents a conceptual model that attempts to explain changes in carbon and nitrogen cycling as it relates to the shift from greenhouse to icehouse climate during the Hirnantian. The results discussed support the carbonate weathering hypothesis as the main source for the observed $\delta^{13}C$ gradient where larger $\delta^{13}C$ excursions are seen in proximal settings compared to proximal settings.

CHAPTER 3. OXYGEN ISOTOPE ANALYSIS OF PHOSPHATE: IMPROVED PRECISION USING TC/EA CF-IRMS

3.1 Abstract

Oxygen isotope values of biogenic apatite have long demonstrated considerable promise for paleothermometry potential because of the abundance of material in the fossil record, and because of the greater resistance of apatite to diagenesis compared to carbonate. Unfortunately, this promise has not been fully realized because of the relatively poor precision of isotopic measurements, and the exceedingly small size of some of the more interesting substrates for analysis—conodont microfossils, and micromilled tooth enamel. Building on previous work, I demonstrate that it is possible to improve the precision of $\delta^{18}O_{PO4}$ measurements using a 'reverse plumbed' thermal conversion elemental analyzer (TC/EA) coupled to a CF-IRMS isotope ratio mass spectrometer via a helium stream. This modification to the flow of helium carrier gas through the TC/EA, and the careful location of the packing of glassy carbon fragments relative to the hot spot in the reactor, leads to narrower, more symmetrically distributed CO elution peaks with diminished tailing. In addition, I describe the apatite purification chemistry that uses nitric acid and cation exchange resin for the purpose of separating PO_4^{-3} from matrix cations such as Ca, Sr, and REE, followed by precipitation as Ag_3PO_4 for isotopic analysis. Purification chemistry is optimized for processing small samples, minimizing potential for isotopic fractionation of PO_4^{-3} isotopomers, and permitting Ca, Sr, and Nd retained on the resin to be eluted and purified further for the measurement of $\delta^{44}Ca$ and $^{87}Sr/^{86}Sr$ in modern biogenic apatite, as well as $^{143}Nd/^{144}Nd$ in fossil apatite. Our methodology yields an external precision of ±0.15‰ (1σ) for $\delta^{18}O_{PO4}$ on as little as 200 µg of apatite. The uncertainty is related to the preparation of the Ag_3PO_4 salt, conversion to CO gas in a reversed–plumbed TC/EA, mass spectrometric analysis of oxygen isotopes using a CF-IRMS instrument, and uncertainty in constructing calibration lines that convert raw $\delta^{18}O$ data to the VSMOW scale. Matrix matching of samples and standards for the purpose of calibration to the VSMOW scale was determined to be unnecessary. Additionally, special equipment (e.g. a fluorination line and a dual inlet mass spectrometer) is not required for the preparation of in-house isotopic standards. Our method requires only slightly modified equipment that is widely available. This fact, and the

demonstrated improvement in precision, should help to make apatite paleothermometry far more accessible to paleoclimate researchers.

3.2 Introduction

Considerable effort has been directed over the past decade towards improving the precision of oxygen isotope measurements of biogenic apatite [$Ca_5(PO_4)_3(OH,F,Cl)$], whose $\delta^{18}O$ values provide an alternative to biogenic carbonates for tracking changes in the earth's climate and environment through time. As with $\delta^{18}O$ values of calcite, $\delta^{18}O$ values of biogenic apatite record the temperature and $\delta^{18}O$ value of the water from which the mineral was precipitated. $\delta^{18}O$ values in apatite exhibit a smaller temperature fractionation relationship of ~0.23‰/^{o}C, compared to ~0.28‰/^{o}C for calcite. For this reason alone, studies utilizing $\delta^{18}O$ values in biogenic apatites could benefit from improved measurement precision, especially for sub-milligram sized samples of apatite, where the conventional techniques have failed. In contrast, it has been possible for a decade to achieve an external precision (reproducibility) of ±0.1‰ (1σ) for $\delta^{18}O$ data on calcite samples as small as 10μg. Calcite is converted to CO_2 gas using phosphoric acid administered by an automated peripheral device (e.g. Kiel IV carbonate preparation device) that is itself coupled to a dual inlet gas isotope ratio mass spectrometer (GIRMS) configured for isotopic analysis of CO_2^+ ions. Comparable precision for $\delta^{18}O_{PO4}$ measurements has only been possible for much larger samples in the range of 10–30 mg, using nickel bomb fluorination (Crowson et al., 1991), and offline quartz-tube graphite reduction (O'Neil et al., 1994) for converting phosphate oxygen to CO_2 gas prior to mass spectrometric analysis.

The large apatite samples required by conventional techniques prohibit determination of $\delta^{18}O_{PO4}$ values of small numbers of conodonts. These small, tooth-like microfossils weigh between 5 and 100 μg each; thus, hundreds to thousands of individuals were required for a single analysis. Long regarded as potentially important fossils for paleotemperature studies (Luz et al. 1984), conodonts are found in marine limestones ranging in age from late Cambrian to early Triassic. Life history studies using $\delta^{18}O_{PO4}$ time-series reconstructions from mammalian or reptilian teeth are another application that has been hampered by sample

size constraints. Sample size reduction permits recovery of more detailed records, while improved measurement precision increases confidence in any variability observed. Although a negative thermal ionization mass spectrometry (N-TIMS) technique measuring PO_3^- ions was shown to be exceedingly sensitive—requiring just one microgram of PO_4^{-3} for analysis—the relatively poor external precision of ±0.5‰ (1σ) limits its usefulness as a paleothermometer (Holmden et al., 1997).

In the late 1990s, a device became commercially available that allowed the oxygen in compounds such as NO_3^-, SO_4^{-2}, and PO_4^{-3} to be released and converted to CO by reduction with graphite (pyrolysis) in a high temperature furnace – referred to by one of the manufacturers as a Thermal Conversion Elemental Analyzer (TC/EA). The CO gas produced by the TC/EA is introduced directly to the mass spectrometer for oxygen isotope analysis of CO^+ ions. Before the pyrolysis step, the apatite sample is first converted, quantitatively, to the non-hygroscopic Ag_3PO_4 salt (Firsching, 1961). This conversion is a common preparation step for both conventional offline fluorination and silica-tube carbon reduction techniques. Its purpose is to remove sources of contaminant oxygen in compounds such as CO_3^{-2}, which replaces PO_4^{-3} in apatite, especially biogenic apatite like bone and dentine. It also removes the hydroxyl-bound oxygen in hydroxyl-apatite, the principal form of biological apatite in vertebrates. The TC/EA allows for automated measurements of $\delta^{18}O$, reducing time of sample throughput and reducing sample size by two orders of magnitude to *ca.* 200 μg of hydroxyapatite, yielding ~500 μg of Ag_3PO_4 (conversion factor of 2.5). The main drawback of the TC/EA– CF-IRMS technique has been the relatively poor external precision of $\delta^{18}O$ measurements, leading to a strategy of averaging the results of multiple analyses of large samples to improve the precision of the mean. Standard deviations of these multiple runs (1σ) range from as low as ±0.1‰, to as high as ±0.6‰, even from the same laboratory (cf., Vennemann et al., 2002).

Building on previous pyrolysis work by Kornexl et al. (1999), Venneman et al. (2002), and Lécuyer et al. (2007), I report on a two-fold improvement in the precision of $\delta^{18}O$ measurements of phosphate oxygen using a reverse-plumbed TC/EA (Gehre et al., 2004) coupled to an isotope ratio mass spectrometer via a continuous flow of helium. the improved

precision is primarily attributed to narrower CO elution peaks from the TC/EA, which makes the isotope ratio determination—calculated as the ratio of the peak areas of the transient $^{12}C^{18}O^{+}$ and $^{12}C^{16}O^{+}$ signals in the mass spectrometer—more reproducible. I also describe enhancements in preparation of Ag_3PO_4 salt that minimize potential isotopic fractionation among PO_4^{-3} isotopomers during purification and crystallization steps. Because I use cation exchange resin for this purpose, Ca, Sr, and Nd ions that were initially retained by the resin can be recovered, following the elution of the PO_4^{-3} ions, in order to support multi-isotope investigations such as $\delta^{44}Ca$, $^{87}Sr/^{86}Sr$, and $^{143}Nd/^{144}Nd$. Using the standard operating procedure (SOP) described herein, an external precision of ±0.15‰ (1σ) is achieved on samples sizes as small 200 µg of apatite. As expected, no improvement in the standard deviation, as a measure of external precision, was observed by running a single sample multiple times.

3.3 Experimental

3.3.1 Standards

All standards and samples were processed in the clean lab of the Saskatchewan Isotope Laboratory (SIL), University of Saskatchewan. This level of isolation from potential contaminants is required only if Ca, Sr, and Nd isotopes are to be analyzed in addition to phosphate oxygen. Four standard materials were used for this work. First, a commercially prepared Johnson and Matthey Alfa Aesar Ag_3PO_4, (Lot # D2AF19) was used to optimize both the pyrolysis of the Ag_3PO_4 salt to CO gas, and the measurement of $^{18}O/^{16}O$ ratios of CO^{+} gas by CF-IRMS. Second, an in-house phosphoric acid standard (SIL-P) was used to investigate potential sources of oxygen isotope fractionation during preparation of Ag_3PO_4. Third, NIST (NBS) 120c (Florida phosphate rock) was analyzed because numerous laboratories have reported $\delta^{18}O$ values for this standard, available from the National Institute for Standards and Technology (NIST) in the United States. Originally prepared for assay purposes, NIST 120c may contain different forms of phosphate, in addition to organic matter and siliciclastics. Fourth, an internal igneous apatite standard (SP-3) was prepared from apatite phenocrysts selected from an anorthosite that was previously the subject of a high

temperature oxygen isotope thermometry study by Farquhar et al. (1993) using conventional fluorination and CO_2^+ as the analyte gas.

3.3.2 Preparation of Ag_3PO_4 from natural apatite

Accurately massed aliquots of apatite standards NIST 120c and SP-3 ranging from 0.10 to 0.45 mg (approximately 0.7 to 3.0 µmoles of PO_4^{-3}) were dissolved in 0.4 mL of 0.5 M HNO_3. A tooth extracted from a monkfish taken from coastal Pacific waters by fishers operating out of the Seattle Fish Market, Pennsylvanian conodonts (*Streptognathodus sp.*) from a Kansas cyclothem, and late Ordovician conodonts from Nevada and Arctic Canada were also analyzed (0.2 – 0.4 mg of apatite). Sample dissolutions were performed at either 19°C or 70°C on a hot plate. Care was taken to minimize the potential for oxygen isotope exchange between H_3PO_4 and H_2O by not heating the samples in excess of 70°C at any point during the dissolution procedure. Studies have shown that at low pH values, oxygen isotopic exchange between PO_4^{-3} and solvent water occurs only after ~70 days at temperatures slightly exceeding 70°C (O'Neil et al., 2003). The progress of the dissolution was checked once a day using a binocular microscope. At 20°C, complete dissolution was achieved after 14 days, while at 70°C samples dissolved in two to seven days. Dissolved apatite samples were transferred to 1.5 mL centrifuge tubes and centrifuged at 10,000 rpm for seven minutes to segregate organic residue left after the dissolution of biogenic apatite, and organic matter and siliciclastic residues from NIST 120c. Dissolution of the igneous apatite, SP-3, always yielded clear solutions.

At low pH, phosphate in solution is predominantly present as H_3PO_4 and should not bind to cation exchange resin (O'Neil et al., 2003; Figure 1). Therefore, a set of quartz columns were prepared to separate H_3PO_4 from matrix cations using 1.0 mL of cation resin (AG50W-X12, 200-400 mesh). Column stems were 105 mm long with 9.55 mm internal diameters and 60 ml reservoirs. The column and reservoir were first cleaned with 60 mL of 6.0 M HCl, followed by a rinse with 10 mL of ultrapure water to remove Cl^- ions. Care must be taken to avoid Cl^- contamination in the H_3PO_4 elutant, or insoluble AgCl salt (K_{sp} = 1.8 x 10^{-8} M^2) will form during the Ag_3PO_4 precipitation. The columns were equilibrated with 10 mL of 0.05 M HNO_3 before use. The dissolved apatite was concentrated into a 0.4 mL

volume of ~0.5 M HNO_3 acid, and loaded onto the columns. The H_3PO_4 elutes quickly from the cation column (Figure 3.1), while Ca, Sr, and REEs (Sm and Nd) are retained by the resin. If insufficient resin is used, or the strength of the HNO_3 acid in the loading solution is greater than 0.5 M, breakthrough of Ca may occur, which will interfere with the precipitation of the Ag_3PO_4. Following the elution of the H_3PO_4, 60 mL of 6.0 M HCl are passed through the column to elute Ca, Sr, and REEs (Figure 3.2), followed by conventional chromatographic techniques that ultimately allow for determination of $\delta^{44}Ca$, $^{87}Sr/^{86}Sr$ and $^{143}Nd/^{144}Nd$ values, respectively, on the same apatite sample as $\delta^{18}O$. In addition, if Ca isotopes are to be measured, and double-spiking performed after the column separation, then 100% yields of Ca are necessary to guard against potential isotope fractionation effects occurring on the resin (e.g., Russell and Papanastassiou, 1978). The procedure for making Ca isotope measurements in the Saskatchewan Isotope Laboratory is described in Holmden (2005). For Sr isotope measurements, see Holmden and Hudson (2005), and for Sm-Nd see Fanton et al. (2002). If Ca, Sr, and REEs are not collected, columns should be cleaned with 60 mL of 6.0 M HCl prior to re-use, to prevent build-up of Ca, Sr, and REEs on cation resin that would ultimately contaminate subsequent H_3PO_4 aliquots. Fossil apatite require particular caution as they contain relatively high (1000 ppm) levels of Sr and REE.

Purified H_3PO_4 was evaporated on a hot plate at a temperature of 70°C until less than 1 mL remained (approximately 1 hour). The remaining solution is transferred to a 1.5 mL centrifuge tube and diluted to 1 mL with ultra pure H_2O. Silver ions were added to the H_3PO_4 solution in the form of an aqueous solution of $AgNO_3$. The amount added was three times the stoichiometric amount of PO_4^{3-} in solution, according to equation (1).

$$3Ag^{+} + PO_4^{-3} \rightarrow Ag_3PO_4 \qquad (1)$$

$$K_{sp} = 8.89 \times 10^{-17}\ M^4$$

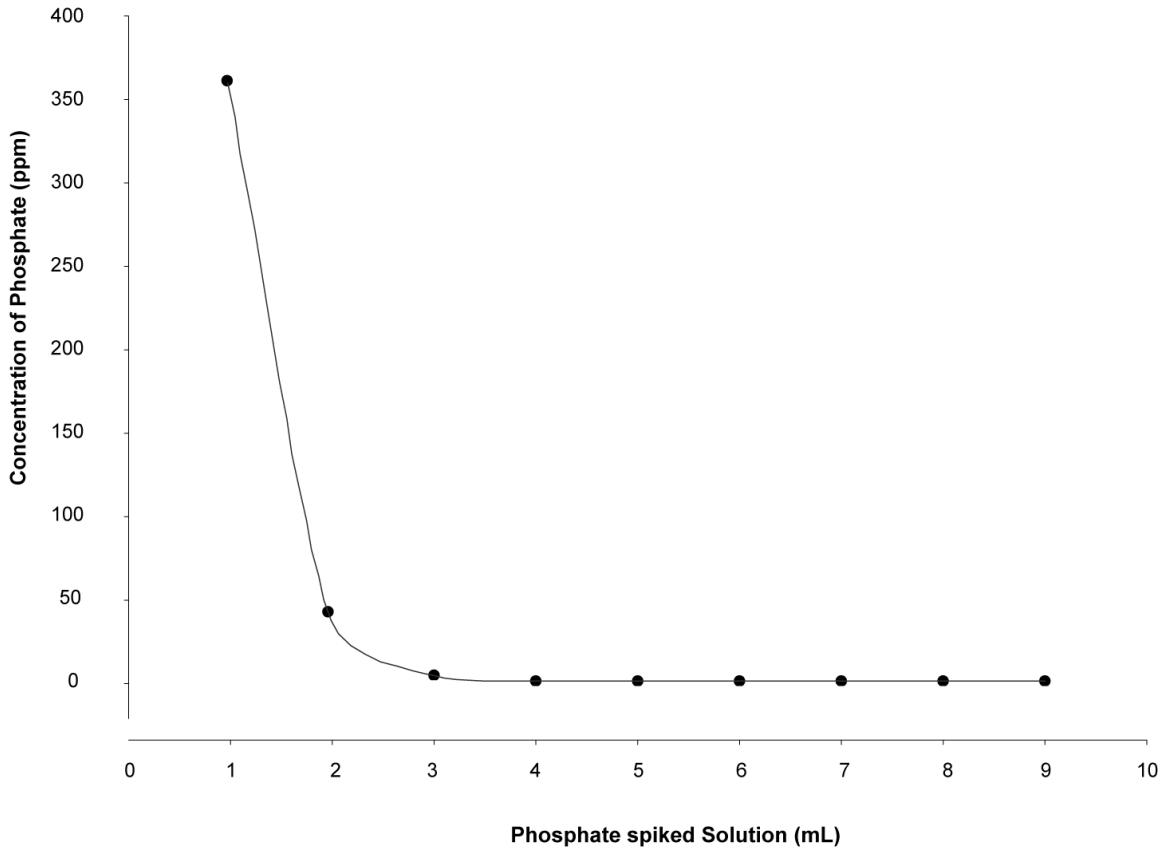

Figure 3.1. Elution curve for PO_4^{-3} in 0.5 N HNO_3 from the AG50W-X12 cation resin column. Because the phosphate is in H_3PO_4 form, it passes quickly through the resin. Concentrations were analysed using atomic absorption spectrometry. Samples were concentrated in a 0.5 N HCl solution prior to analysis.

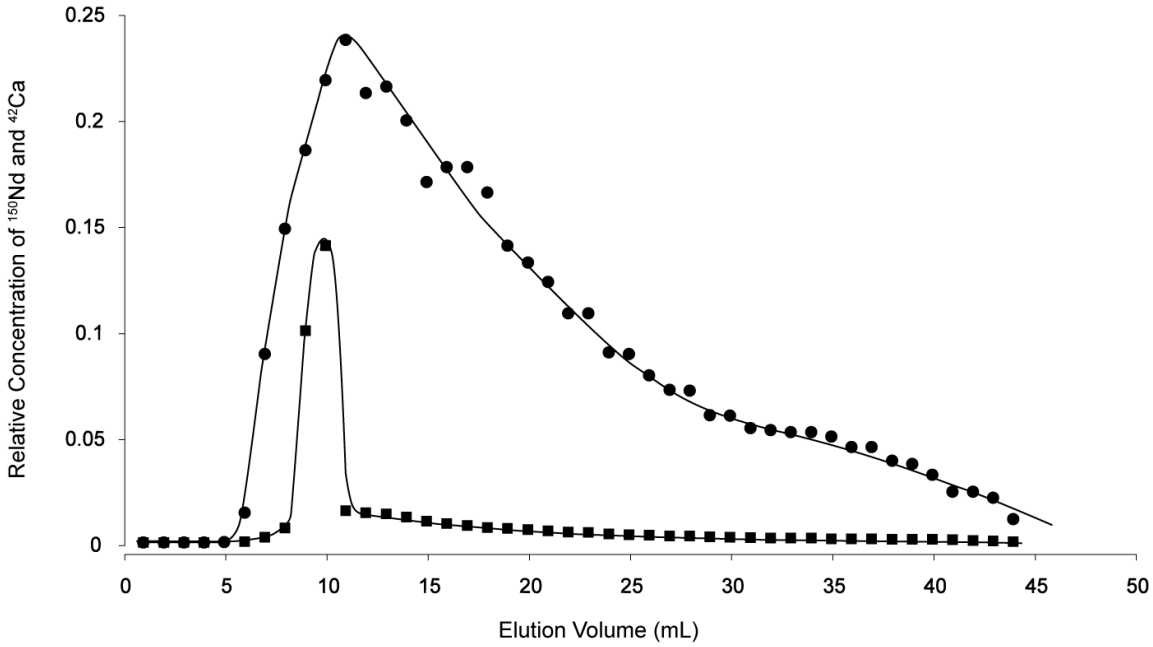

Figure 3.2. Elution curve for relative intensities of ^{150}Nd (circles) and ^{42}Ca (squares) from the AG50W-X12 cation resin column. Intensities were measured using a plasma mass spectrometer. Collection of Sr, Ca, and REEs allows for multi-isotope studies from single samples of apatite.

Although excess Ag^+ ions remain after the complete precipitation of Ag_3PO_4, no precipitation of $AgNO_3$ and AgOH occurs under these conditions. The ammoniacal solution was prepared by adding 60 µl of 37% (by vol.) NH_4OH to the 1.0 mL mixed H_3PO_4 and $AgNO_3$ solutions. The slow evaporation of NH_3 from the solution lowers the pH resulting in the slow growth of mm-scale Ag_3PO_4 crystals from solution (Firsching, 1961). Solutions are left to precipitate Ag_3PO_4 in open centrifuge tubes at 70°C for ~30 hours, at which time calculations indicated ~100% of the PO_4^{-3} in solution had precipitated. Ultra-pure water was added to keep the volume of the solution close to 1.0 mL throughout this time. Once precipitation of silver phosphate was complete, samples were centrifuged and rinsed four times using ultra-pure H_2O, and then dried at 70°C on a hotplate for two to four hours. Ag_3PO_4 crystals formed by this process are consistently dark yellow, acicular, and between 0.2 and 1 mm in length. It made no difference to the size, geometry, or color of the crystals whether the starting material was an igneous apatite, biogenic apatite, or synthetic standard. Process yields were determined by gravimetry using a microbalance.

3.3.3 Thermal conversion elemental analyzer (TC/EA)

Before the $^{18}O/^{16}O$ ratio of the phosphate-bound oxygen can be measured by the mass spectrometer, the P—O bond must be broken, and released oxygen reacted to form CO gas in the TC/EA. The conversion to CO (pyrolysis) occurs in a glassy carbon tube (459 mm x 12 mm x 8.6 mm) that is fitted inside a ceramic insulator (470 mm x 17 mm x 13 mm) held at a temperature of 1,450°C. The glassy carbon tube is packed with glassy carbon fragments (3,150 – 4,000 µm in diameter) up to the level of the hot spot in the reactor, minus the length of the crucible, where the most efficient pyrolysis occurs (Figure 3.3). Ag_3PO_4 samples are packed into small silver capsules (3.3 mm x 5 mm) so that they may be dropped into the reactor from an automated carrousel. Different packing depths and pyrolysis temperatures were tested to optimize CO yields from pyrolysis with the goal of producing the most rapid reaction possible that will in turn produce narrow elution peaks from the GC column. Narrower elution peaks provide a more reliable basis, ultimately, for calculating isotopic ratios. Three chromatograms (Figure 3.4) demonstrate how peak shape is degraded when temperature and packing depth are not optimized.

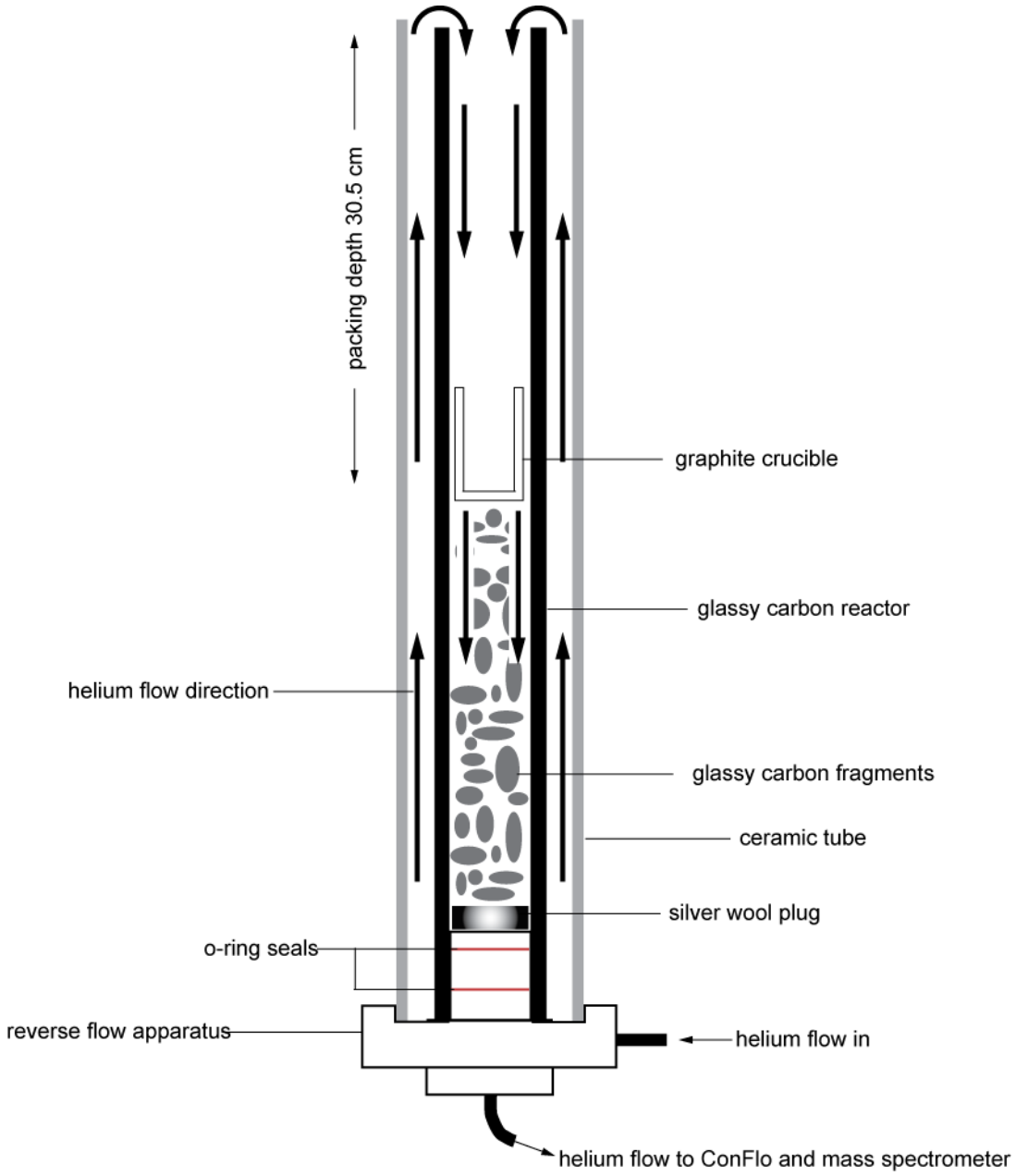

Figure 3.3. Diagram (not to scale) of the 'reverse plumbed' TC/EA reactor showing the flow of He carrier gas. The purpose of the He flow is to carry the produced CO through the reactor, into a gas chromatograph (not shown), and then into the mass spectrometer. The reverse flow adaptor, carbon reactor, and ceramic outer tube can all be purchased through IVA Analysentechnik e.k.

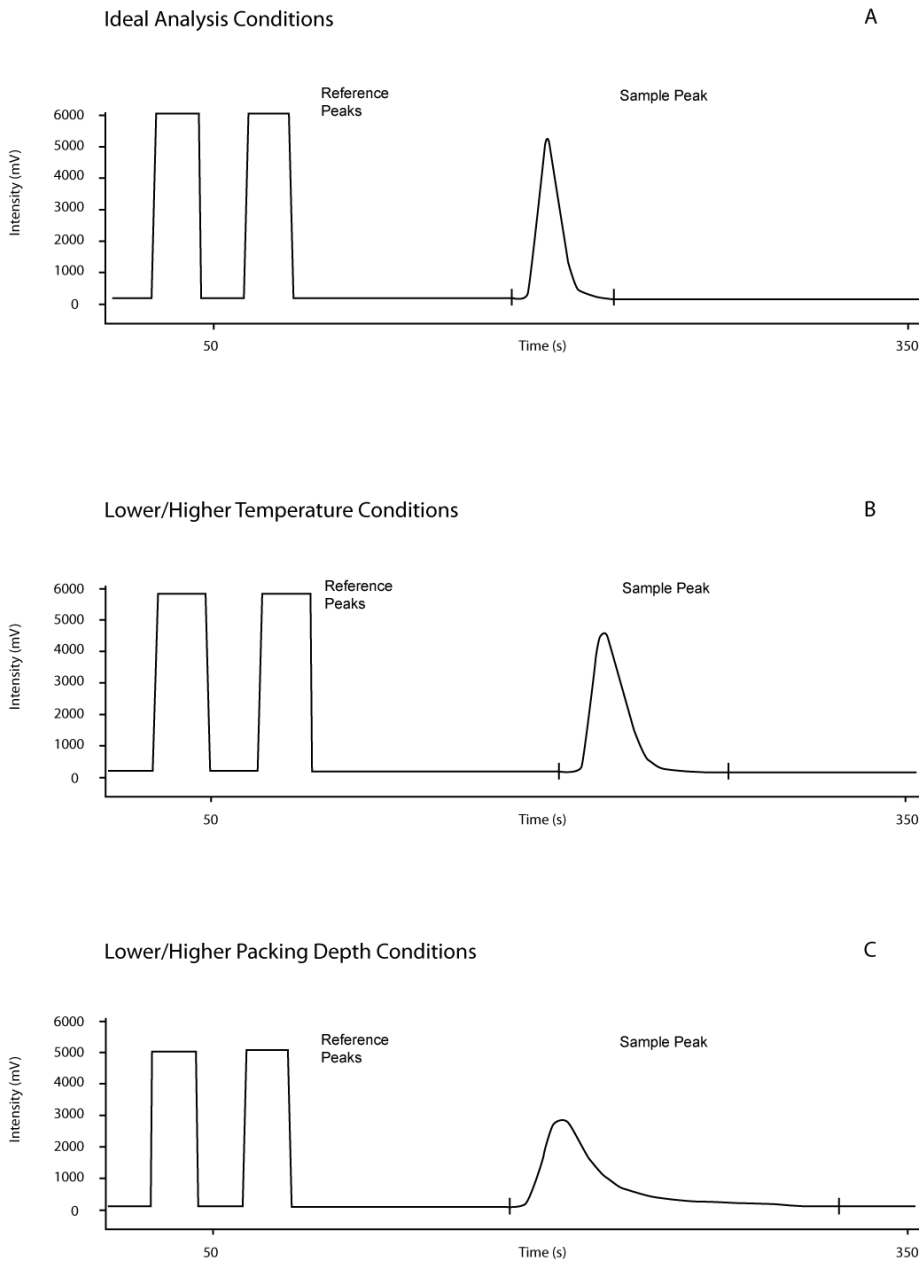

Figure 3.4. Mass 28 chromatograms of the reference gas and CO^+ sample gas are shown for the ideal versus poor analysis conditions. Dashes on sample elution peaks represent the selected peak used in the calculation of $\delta^{18}O_{Measured}$. Different packing depths and temperature were experimented with until the ideal conditions were found (A). Lower or higher temperature (B) and packing depth (C) resulted in wider peaks eluting from the GC column and poorer precision.

A packing depth of 30.5 cm from the top of the column to the top of the glassy carbon fragments was found to be optimal for our system. A graphite crucible (30 mm x 7.7 mm x 2.5 mm) is placed on top of the glassy carbon fragments to collect the silver metal residue that forms as a by-product of the reaction. Silver wool is used at the base of the reactor to capture sulfur and halogen gases that may form during the pyrolysis, and as a plug to hold the glassy carbon fragments in place.

CO is carried from the reactor using a He carrier gas flowing at a rate of 100-120 mL/min. It passes through an ascarite trap to remove any by-products (sulfur, halogens, etc.) that are not trapped in the silver wool at the base of the reactor, and a desiccant (magnesium perchlorate) to adsorb water vapour (cf., Brooks et al., 2003). The CO is then passed through a 0.6m 5Å molecular sieve gas chromatograph (GC) held at a constant temperature of 90°C in order to further purify the CO gas from small amounts of air that enter the reactor by way of the silver capsule (N_2), and trace amounts of CO_2 produced along with the CO during the pyrolysis reaction.

The graphite crucible that collects silver residue was changed after every sequence of 50 samples to ensure that accumulating Ag did not influence the reproducibility of the pyrolysis reaction. The column was repacked after running approximately eight sequences (300 - 400 analyses). After this number of samples pyrolysis slows, evidenced by broader CO elution peaks from the GC column due to exhaustion of reactive glassy carbon surfaces in the hot zone. No issues with the accumulation of sticky residue in the capillary tubing, or in the ConFlo interface, such as was noted by Vennemann et al. (2002), were encountered during this work. However, residues did collect over time in the GC column. It is expected that ascarite trap modification will eliminate this issue.

3.3.4 Mass Spectrometry

The oxygen isotope ratio of the CO gas was measured on a Thermo-Electron Delta Plus XL mass spectrometer in continuous flow mode. Pyrolysis of 0.4 mg of Ag_3PO_4 yields $2.3x10^{18}$ molecules of CO. However, the size of the gas pulse entering the ion source of the mass spectrometer is regulated using a ConFlo III device that bleeds off ~95% of sample gas

to waste when dilution is not inserted. About 5% of the gas pulse enters the ConFlo open split. The pressure differential between the open split and the capillary line to the mass spectrometer causes CO to be drawn into the capillary, where it flows to the electron impact ion source. Inevitably, an unknown amount of gas entering the ConFlo open split is also lost because of the size difference between the open split and the capillary to the mass spectrometer. The efficiency of producing CO^+ ions in the electron impact source is 1:1500 molecules of CO. Only the CO^+ ions that enter the flight tube of the mass spectrometer are mass analyzed. Assuming approximately 50% of the gas that enters the ConFlo open split is lost, the transmission efficiency (CO^+ ions measured: CO produced) is $3.83x10^{13}/2.3x10^{18}$ or $\leq 0.002\%$. Clearly, far greater amounts of sample are required by the TC/EA than is needed by the mass spectrometer to make quality measurements. If the transmission could be improved, the sample size could be dramatically reduced. As a point of comparison, the N-TIMS method is approximately five orders of magnitude more sensitive (Holmden et al., 2007). At the present time, however, it is not possible to increase transmission through the TC/EA and ConFlo without major modifications to factory-designed components. Clearly, increasing the transmission of CO through the instrument is the key to future increases in sensitivity and sample size reduction.

The $^{18}O/^{16}O$ ratio of samples corresponds to the ratio of the peak areas of molecular CO^+ at masses 30 and 28, corrected for the small contribution of $^{13}C^{17}O$ on mass 30 by the proprietor's software. Because of the transient nature of the CO eluted from the TC/EA, the intensity of the CO^+ ion beams corresponding to masses 30 and 28 are determined by counting all of the ions that hit their individual Faraday collectors over the duration of the peak. From beginning to end, it takes between 100 and 150 seconds for the CO/CO^+ elution peak to be produced in the TC/EA and mass analyzed in the spectrometer.

The $^{18}O/^{16}O$ ratio of each sample is normalized to a measurement of the $^{18}O/^{16}O$ ratio of an in-house reference CO gas that does not pass through the TC/EA or ConFlo, but rather is introduced directly to the ion source from an adjustable storage volume (bellows). The volume of the bellows was adjusted periodically during a sequence in order to precisely replicate the reference gas pressure from sample to sample, as it is the backing pressure that ultimately controls the intensity of the ion beam signals from the reference gas, which will

decay as the gas in the bellows is depleted. If the reference gas pressure is allowed to decrease too much through a sequence of analyses, this can lead to a time-dependent drift in the measured $^{18}O/^{16}O$ ratio of the reference gas due to changes in the linearity of the ion source to lower pressures of CO. The measurement of each sample begins with two measurements of the $^{18}O/^{16}O$ ratio of the reference gas, with each injection of reference gas from the bellows lasting 20 seconds. The reference gas measurements are averaged and the $^{18}O/^{16}O$ ratio of the sample is compared to the $^{18}O/^{16}O$ ratio of the reference gas through the construction of the delta (δ) value: $\delta^{18}O_{reference} = \left[\left({}^{18}O / {}^{16}O \right)_{sample} / \left({}^{18}O / {}^{16}O \right)_{reference} - 1 \right] x1000$, which yields the permil difference in the $^{18}O/^{16}O$ ratio of the sample relative to that of the reference gas. The $\delta^{18}O$ value of the reference CO gas used in the Saskatchewan Isotope Laboratory is approximately –5.5‰ (VSMOW).

3.3.5 Calibration of $\delta^{18}O$ values to the VSMOW scale

Two different international standards with internationally agreed upon $\delta^{18}O$ values on the VSMOW scale are ideally analyzed along with sample unknowns in order to prepare a calibration line (Figure 3.5) that will allow raw $\delta^{18}O_{sample\text{-}reference}$ values from each laboratory to be compared on a common reference scale. This practice effectively negates the influence of CO reference gases that have different isotope values in each laboratory. So as not to deplete the supply of international standards, the general practice is for each laboratory to produce bulk supplies of internal (in-house) standards that are precisely calibrated against international standards. For oxygen isotopes, the international standard is Vienna Standard Mean Ocean Water (VSMOW). Aliquots of VSMOW may be purchased from the International Atomic Energy Association (IAEA), and this water used, in turn, to calibrate bulk waters with different isotope values for use as internal standards in laboratories. For practical reasons, a solid standard is needed for phosphate oxygen work because the sample introduction system used does not toggle between solid and liquid samples.

For calibration, some workers have prepared a range of Ag_3PO_4 standards calibrated against VSMOW (cf. Vennemann et al., 2002; Lécuyer et al., 2007). I have taken a different approach, choosing instead to use in-house benzoic acid standards that were prepared and

calibrated against international standards USGS 34 ($\delta^{18}O$ = -27.9‰ ±0.6‰ (1σ) VSMOW) and USGS 35 ($\delta^{18}O$ = 57.5‰ ±0.6‰ (1σ) VSMOW). The IAEA NO_3 standard (25.6‰ ±0.4‰ (1σ) VSMOW) was used as a check–standard during calibration of the in-house benzoic acid standards to VSMOW. A 'check–standard' is defined as one that, when analyzed along with a suite of samples and reference standards calibrated against the VSMOW scale, is not itself used to construct the calibration line that relates $\delta^{18}O_{sample\text{-}reference}$ values to $\delta^{18}O_{sample\text{-}VSMOW}$ values. Long-term reproducibility of a check-standard provides an estimate of long-term reproducibility of $\delta^{18}O_{sample\text{-}VSMOW}$ measurements that include any uncertainties introduced by calibration procedures.

3.3.6 Preparation and calibration of benzoic acid standards to VSMOW

In-house benzoic acid standards should bracket the typical range of $\delta^{18}O$ values in biogenic apatite (Figure 3.5). Two were prepared: the first by mixing ^{18}O-enriched water ($\delta^{18}O$ = ~500‰ VSMOW) with deionized Saskatoon tap water ($\delta^{18}O$ = -17‰ VSMOW); the second, using Saskatoon winter precipitation ($\delta^{18}O$ = -40‰ VSMOW). The above waters were mixed with benzoic acid in sealed flasks, and left on a hotplate at 75°C for 72 hours to facilitate oxygen isotope exchange between water and benzoic acid, according to the isotope exchange reaction:

$$C_6H_5{}^{16}O^{16}OH + H_2{}^{18}O \leftrightarrow C_6H_5{}^{16}O^{18}OH + H_2{}^{16}O \qquad (2)$$

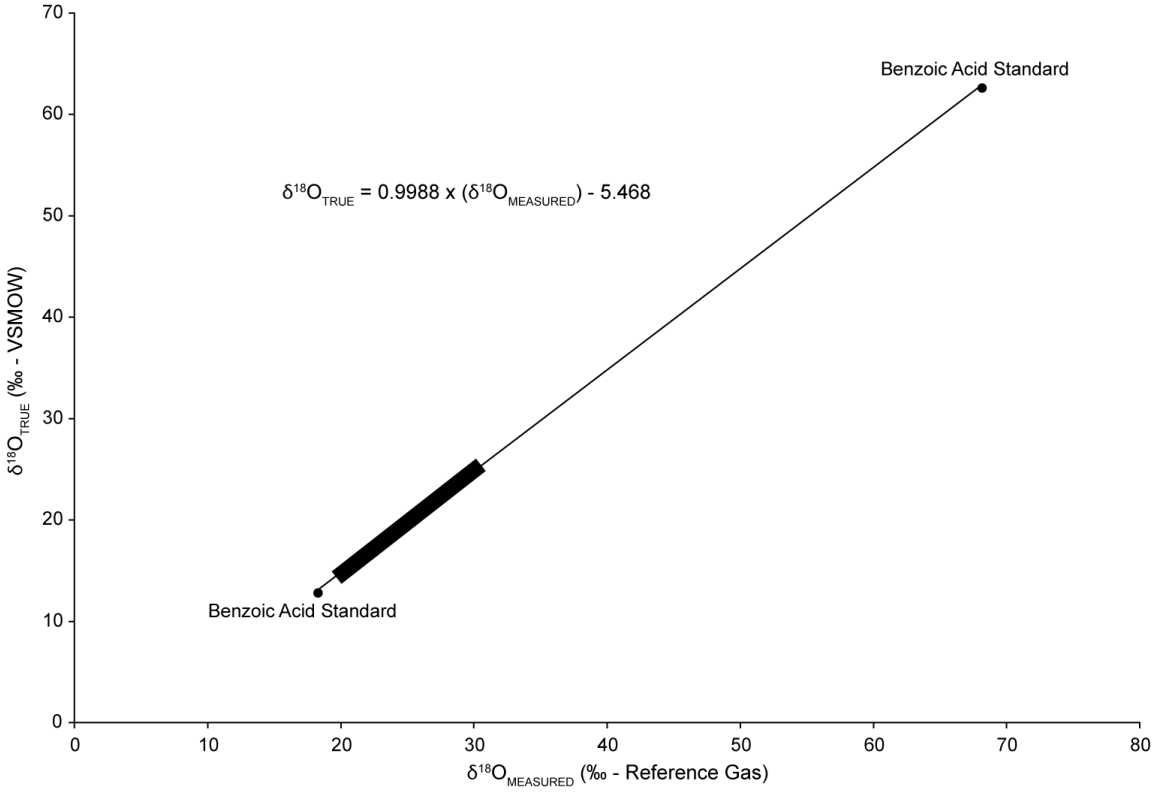

Figure 3.5. Example of a two end-member calibration line using the in-house benzoic acid standards. Measured $\delta^{18}O$ values are corrected using the equation for the regression of a straight line between the $\delta^{18}O_{Measured}$ and $\delta^{18}O_{True}$ values of the two standards. The rectangle represents the approximate range of $\delta^{18}O$ values for biogenic apatites.

Flasks were removed from the hot plate and refrigerated at 4°C until the benzoic acid crystallized from solution. Benzoic acid crystals were separated by vacuum filtration and freeze-dried over night. The dried crystals were powdered with a mortar and pestle to ensure isotopic homogeneity.

The calibration of the benzoic acid standards against VSMOW utilized data from five sequences, totaling 140 analyses of the benzoic acids (70 each). A 'sequence' is defined as a set of standards and sample unknowns filling a 'carrousel' (i.e. 49 individual analyses). The 'carrousel' is the automated sample introduction device that drops samples—loaded in silver capsules—into the reactor of the TC/EA. An 'analysis' is defined as the measurement of a single sample (or standard) within the sequence. Each sequence (carrousel) is loaded with enough standards to allow for the construction of a calibration line that relates $\delta^{18}O_{sample\text{-}reference}$ values to $\delta^{18}O_{sample\text{-}VSMOW}$ values. The sequence used to calibrate the in-house benzoic acid standards against the VSMOW scale is shown in Table 3.1. Also shown, is the sequence for the measurement of sample unknowns against the VSMOW–calibrated benzoic acid standards. The VSMOW–calibrated $\delta^{18}O$ values of the benzoic acid standards are 12.81 ±0.12‰ (1σ) and 62.61 ±0.15‰ (1σ).

Table 3.1. TC/EA carrousel sequence for calibration of the benzoic acid standards and for analysis of sample unknowns. Each sequence (carrousel) consists of a specific number (n) of analyses of each standard and sample as indicated. Samples and standards are listed in the order that they were analyzed in the calibration and sample unknown sequences. The (+) and (-) represent the high and low in-house $\delta^{18}O$ benzoic acid standards respectively.

Sample	Carrousel	
	Calibration Sequence (n)	Sample Unknown Sequence (n)
Flush	2	2
Blank	2	2
USGS 35	5	
USGS 34	5	
IAEA NO3	3	
Benzoic (+)	14	3
IAEA NO3	2	
Benzoic (-)	14	3
IAEA NO3	2	
Aesar		3
Unknowns		16
Aesar		2
Unknowns		16
Aesar		2

3.4 Results

3.4.1 Reproducibility of $\delta^{18}O$ values in synthetic standards

Forty-five analyses of the Aesar Ag_3PO_4 standard, representing five sequences (i.e., five carrousels, and five individual calibration curves), were analyzed against the international standards. The average $\delta^{18}O$ value obtained was 19.57 ±0.15‰ (1σ) VSMOW (Table 3.2). The Ag_3PO_4 powder is considered to be isotopically homogenous at sample sizes analyzed (200–450 μg), and as such the uncertainty of ±0.15‰ (1σ) represents the uncertainty of the instrumental portion of the measurement procedure, including all potential sources of isotopic fractionation that might occur during the production of CO gas in the TC/EA, and including non-linearity in detector response between samples and standards, focusing of the mass spectrometer, imperfections in the shape of the CO elution peaks, and differences in backgrounds.

To test for potential isotopic fractionation effects introduced during the purification chemistry, 58 samples of the SIL-P standard (pure H_3PO_4) were analyzed in six sequences over a period of five months. Silver phosphate was precipitated from half of the H_3PO_4 samples directly, while the other half were first passed through the cation exchange columns. The mean $\delta^{18}O$ value for all samples was 8.42 ±0.14‰ (1σ) (VSMOW) (Table 3.3). As expected, there is no evidence that the cation exchange column fractionates isotopomers of PO_4^{-3} if the yields from the column are close to 100%. Combining the results of Aesar and SIL-P measurements, the calculated overall reproducibility of $\delta^{18}O_{PO4}$ is ±0.15‰ (1σ), on 200 to 500 μg samples of Ag_3PO_4.

Reproducibility of $\delta^{18}O_{PO4}$ values in SP-3 (natural igneous apatite) and NBS 120c (Florida Rock Phosphate) were much worse than the standards described above(Aesar and SIL-P). Initially, no special effort was made to ensure isotopic homogeneity among the individual aliquots of Ag_3PO_4 salts that were prepared from these standards.

Table 3.2. Results from the calibration of the in-house Aesar standard. The mean, standard error, and 1σ are reported for the $\delta^{18}O_{Measured}$ and $\delta^{18}O_{True}$ values of each sequence. NIST standards USGS 34 and 35 were used for the construction of sequence-specific calibrations lines. Note that only minor changes in the 1σ are seen between sequences regardless of the number of runs of Aesar in the sequence.

Run	Mass (mg)	CO Yield (%)	δ18O	
			Raw Data	VSMOW
1	0.4532	14.9	25.60	19.66
	0.4423	15.2	25.70	19.80
	0.4758	15.1	25.13	19.63
	0.4267	15.0	25.21	19.56
	0.4092	14.3	25.06	19.50
	0.4194	15.7	25.23	19.31
	0.4862	14.3	25.38	19.50
	0.4062	14.7	25.36	19.56
	0.4579	14.8	25.39	19.50
	0.4103	14.8	25.51	19.62
Mean			25.36	19.56
Standard Error			0.07	0.04
1σ			0.21	0.13
2	0.4124	13.9	25.13	19.57
	0.4092	15.4	25.28	19.72
	0.4079	15.7	25.24	19.54
	0.4021	15.4	25.27	19.70
	0.4507	15.5	25.22	19.38
	0.4764	14.7	25.17	19.52
	0.4605	14.2	25.44	19.80
	0.5335	14.6	25.11	19.46
	0.4818	14.5	25.36	19.70
	0.4213	14.4	25.78	19.86
Mean			25.30	19.63
Standard Error			0.06	0.05
1σ			0.20	0.15
3	0.4934	15.0	25.21	19.58
	0.4605	14.5	25.38	19.43
	0.45	15.1	25.60	19.64
	0.5284	15.0	25.46	19.56
	0.4591	15.5	25.47	19.57
	0.4578	15.3	25.45	19.55
	0.4535	14.5	25.36	19.46
	0.4744	14.9	25.39	19.49
Mean			25.41	19.53
Standard Error			0.04	0.02
1σ			0.11	0.07
4	0.4646	14.6	25.38	19.43
	0.5325	14.1	25.36	19.81
	0.5505	14.6	25.06	19.48
	0.4558	14.7	25.18	19.58
	0.4586	14.7	25.39	19.36
	0.4522	15.3	25.58	19.53
	0.4537	15.1	25.34	19.35
	0.4591	15.3	25.35	19.76
	0.4503	15.2	25.34	19.52
Mean			25.33	19.54
Standard Error			0.05	0.05
1σ			0.14	0.16
5	0.4491	15.5	25.21	19.34
	0.4598	15.4	25.45	19.63
	0.4528	14.7	25.41	19.52
	0.4504	14.2	25.70	19.84
	0.416	14.6	25.36	19.46
	0.4478	14.5	25.60	19.70
	0.4433	15.2	25.23	19.33
	0.5076	14.5	25.54	19.82
Mean			25.44	19.58
Standard Error			0.06	0.07
1σ			0.17	0.20
Total Mean				**19.57**
Total Standard Deviation				**0.15**

The mean $\delta^{18}O_{PO4}$ for 16 analyses of NBS 120c was 22.4‰ ±0.3‰ (1σ) VSMOW. That is, 16 samples of 100 to 450 µg each were processed and analyzed in four sequences (Table 3.4). For the SP-3 measurements, two to five (millimeter–scale) crystals of apatite were taken from a hand sample, and homogenized by dissolution. The average $\delta^{18}O_{PO4}$ value was 7.4‰ ±0.3‰ (1σ) VSMOW, on nine analyses representing two sequences (Table 3.4). Another set of analyses on individual crystals yielded $\delta^{18}O_{PO4}$ values between 6.7 and 9‰ (Table 3.4), measured over two sequences.

The $\delta^{18}O_{PO4}$ value of the modern monkfish tooth, measured just once, yielded 23.20‰ VSMOW. A collection of Pennsylvanian conodonts from the same hand sample yielded a mean $\delta^{18}O_{PO4}$ value of 20.64 ± 0.12‰ VSMOW, based on two measurements of separately processed aliquots (one contained elements of only *Streptognathodus sp.*, and the other was a mixture of elements comprising different species). A suite of late Ordovician conodonts from two stratigraphic sections spanning the Hirnantian glaciation event yielded $\delta^{18}O_{PO4}$ values from 16.75 to 18.42‰ VSMOW (Table 3.4).

Over the course of measuring $\delta^{18}O_{PO4}$ values of our synthetic standards, the modern monkfish tooth, and the fossil conodonts, the Aesar check-standard yielded an average $\delta^{18}O$ value of 19.53‰ ±0.14‰ (1σ) (VSMOW) n= 45, measured over 15 sequences.

3.4.2 Memory Effects

Memory effects—defined as the influence of the isotopic signature of a preceding sample on subsequent samples—were evaluated by comparing consecutive samples with vastly different $\delta^{18}O$ values. This was monitored routinely for each sequence by comparing the last benzoic acid standard measured near the beginning of a sequence ($\delta^{18}O$ = 62.61‰) with the first Aesar check-standard ($\delta^{18}O$ = 19.57‰) analyzed subsequently. Consecutive measurements of the two Ag_3PO_4 standards (Aesar and SIL-P) that differ by ~11‰ were also compared. No memory effect was observed in either case.

Table 3.3. Results from the calibration of SIL-P standard. The mean, standard error, and 1σ are reported for the $\delta^{18}O_{Measured}$ and $\delta^{18}O_{True}$ values of each sequence. In-house benzoic acids were used for construction of the sequence-specific calibration lines. Note that only minor changes in the 1σ are seen between sequences regardless of the number of runs of SIL-P in the sequence.

Run	Mass (mg)	CO Yield (%)	δ18O	
			Raw Data	VSMOW
1	0.2591	13.7	14.38	8.49
	0.3671	13.9	14.24	8.35
	0.2222	12.8	14.13	8.24
	0.3348	13.4	14.40	8.51
	0.3135	13.4	14.47	8.57
	0.3349	13.0	14.05	8.06
	0.4038	13.8	14.42	8.53
	0.365	14.1	14.39	8.50
	0.4587	14.2	14.10	8.20
	0.3333	14.1	14.27	8.38
Mean			14.29	8.38
Standard Error			0.05	0.05
2	0.3122	14.9	13.91	8.45
	0.2687	15.5	13.97	8.51
	0.3814	14.7	13.97	8.51
	0.4097	14.8	14.16	8.70
	0.3314	15.2	13.83	8.37
	0.217	14.8	13.99	8.53
	0.3293	13.6	14.17	8.62
	0.3433	15.3	13.74	8.28
	0.3176	14.7	13.84	8.37
	0.3689	15.1	13.93	8.47
	0.3022	13.8	13.87	8.41
	0.3398	15.3	13.73	8.27
	0.2936	14.3	14.03	8.57
	0.3944	13.3	13.90	8.44
Mean			13.93	8.46
Standard Error			0.04	0.03
3	0.4676	14.6	14.13	8.58
	0.3934	14.8	14.21	8.66
	0.3582	12.8	14.07	8.52
	0.2874	15.0	13.78	8.23
	0.3564	15.0	14.14	8.59
Mean			14.06	8.52
Standard Error			0.07	0.07
4	0.3791	15.4	14.29	8.41
	0.3872	15.4	14.37	8.49
	0.4113	15.3	14.26	8.38
	0.3373	14.9	14.31	8.44
	0.447	15.3	14.11	8.23
	0.3996	15.1	14.28	8.41
	0.4339	15.1	14.26	8.39
	0.4152	15.6	14.39	8.52
	0.3421	14.6	14.25	8.38
	0.4169	15.2	14.16	8.28
Mean			14.27	8.39
Standard Error			0.03	0.03
5	0.4339	15.6	13.97	8.24
	0.4678	15.6	14.16	8.43
	0.4409	15.5	14.09	8.36
	0.3545	15.4	14.04	8.31
	0.3772	15.5	14.20	8.47
	0.4097	15.3	13.93	8.20
	0.3323	15.4	13.60	8.24
	0.3056	15	13.97	8.14
	0.4424	15.5	14.14	8.41
Mean			14.01	8.31
Standard Error			0.06	0.04
6	0.4572	14	13.92	8.39
	0.2874	14.1	13.95	8.42
	0.3606	15.3	13.84	8.31
	0.4305	15	14.16	8.63
	0.393	15	13.93	8.40
	0.4367	15.2	13.99	8.46
	0.3767	14.1	14.19	8.66
	0.3948	15	14.10	8.57
Mean			14.01	8.48
Standard Error			0.04	0.04
Total Mean				**8.42**
Total Standard Deviation				**0.14**

Table 3.4. Results from $\delta^{18}O$ analysis of NBS 120c, SP – 3, Ordovician conodonts, and multi-isotope study of a modern monkfish tooth and Pennsylvanian conodonts. The "*" represents individually processed Ag_3PO_4 from the same collection of conodonts.

Standard	Sequence	Mass (mg)	Ag_3PO_4 Yield (%)	Transfer Method	CO Yield (%)	$\delta^{18}O$ (‰ - VSMOW)	Crystal Size (mm)
NBS 120c	1	0.3213	90.4	Direct	14.6	22.3	
				Direct	14.7	22.4	
		0.3845	89.3	Direct	14.7	22.2	
		0.2056	94.2	Direct	15.4	22.1	
	2	0.4519	97.0	Direct	15.0	22.3	
		0.1948	91.3	Direct	14.9	22.5	
		0.1683	88.1	Direct	14.6	22.6	
		0.3708	92.5	Direct	14.7	21.7	
	3	0.3888	96.2	Direct	14.4	22.3	
				Direct	13.8	22.5	
		0.1774	92.7	Direct	15.1	22.6	
		0.3933	91.5	Direct	14.8	22.7	
	4	0.3822	87.4	Direct	15.1	22.6	
		0.5387	85.9	Direct	13.8	22.6	
		0.2237	90.8	Direct	15.3	22.9	
		0.4479	91.8	Direct	14.8	22.7	
Total Average						**22.4**	
Total Standard Deviation						**±0.3**	
SP - 3	1	0.4280	99.7	Direct	15.4	7.6	
		0.5474	100	Direct	15.2	7.1	
		0.4562	97.5	Direct	13.7	7.2	
		0.4763	96.3	Direct	14.5	7.8	
	2	0.3959	98.0	Direct	14.5	7.2	
		0.3947	98.4	Direct	13.9	7.1	
		0.4113	97.3	Direct	15.2	7.9	
		0.3819	97.4	Direct	15.2	7.1	
				Direct	14.5	7.1	
Total Average						**7.4**	
Total Standard Deviation						**±0.3**	
SP - 3	1	0.4113	98.5	Direct	14.8	8.6	1-2
		0.4156	99.6	Direct	14.9	8.7	1-2
		0.4349	98.6	Direct	14.9	9.0	1-2
	2	0.3819	98.7	Direct	14.8	6.7	2-3
		0.4032	99.4	Direct	14.5	7.1	0.5-1

Table 3.4

Results from $\delta^{18}O$ Analysis of NBS 120c, SP – 3, Conodonts and Monk Fish (continued)

Sample	Sequence	Mass (mg)	CO Yield (%)	$\delta^{18}O$ (‰ - VSMOW)	$^{143}Nd/^{144}Nd$	$\delta^{44}Ca$ (‰ - seawater)	$^{87}Sr/^{86}Sr$
Monk Fish	1	0.1924	14.3	23.13		–1.29	0.709190
Pennsylvanian Conodonts		0.4202	14.8	20.56*	0.512293	-1.29	0.708437
		0.4107	14.9	20.73*			
Ordovician Conodonts							
Nevada	2	0.3924	14.3	16.75			
		0.4023	14.9	16.99			
		0.3547	15.3	17.09			
		0.3956	14.7	18.20			
Arctic Canada	3	0.4056	15	18.23			
		0.4079	15.1	18.38			
		0.3874	14.5	18.37			
		0.3569	14.6	18.42			

3.4.3 Transfer Techniques

Two techniques were evaluated for quantitative transfer of Ag_3PO_4 salt from the 1.5 mL centrifuge tubes to silver capsules. The first, involving dry transfer of crystals using weighing paper, was used exclusively to determin the reproducibility of $\delta^{18}O_{PO4}$ analyses. However, smaller crystals of Ag_3PO_4 readily stick to the walls of the centrifuge tube and are difficult to recover. If, as suggested by Stuart-Williams et al. (1995), isotopic fractionation can occur between early and late formed crystals during precipitation from ammoniacal solutions, then failure to transfer all crystals might result in an apparent oxygen isotope fractionation. A similar effect may result from the process of splitting large samples of Ag_3PO_4 for $\delta^{18}O_{PO4}$ analysis, if different splits contain different proportions of small and large crystals (Stuart-Williams et al. 1995). To avoid this potential problem, a strategy of preparing only as much Ag_3PO_4 as can be processed in one analysis was adopted. A slurry transfer technique was also evaluated to convey very small amounts of Ag_3PO_4 salt quantitatively to silver capsules using a drop of water protruding from a clear transfer pipette. Using a binocular microscope, and a thin-tipped translucent transfer pipette, it was found that all crystals could be transferred to silver capsules by sweeping them into suspension with the water drop. Water was evaporated from the crystals by placing the silver capsules in an oven at 70°C for four hours.

Using the slurry transfer technique, the $\delta^{18}O_{PO4}$ value of the SIL-P standard was found to be indistinguishable from $\delta^{18}O_{PO4}$ values measured using dry transfer, even though a visual inspection revealed that some crystals were not transferred by the dry method (Table 3.3). No peak tailing from the TC/EA, or other effects such as higher blanks or lower yields, were observed.

3.5 Discussion

Using the methodology described herein, an external precision (reproducibility) for apatite $\delta^{18}O$ analysis of ±0.15‰ (1σ) was achieved. This uncertainty takes into account preparation of Ag_3PO_4 salt, preparation of CO gas in a reverse–plumbed TC/EA, and mass spectrometric analysis of oxygen isotopes using a CF-IRMS instrument. It also takes into

account uncertainty in constructing the calibration curve that relates measured $\delta^{18}O_{sample-reference}$ values to $\delta^{18}O_{sample-VSMOW}$ values. Based on a literature review, it is common practice in many laboratories to measure sample unknowns in duplicate or triplicate, and present $\delta^{18}O_{PO4}$ values that are means of several measurements. In most cases, however, it is impossible to discern whether: (1) the replicate measurements that were combined to determine the mean were collected from the same sequence (that is, using the same calibration line), (2) outliers were retained or removed, and (3) each replicate analysis included new preparations of Ag_3PO_4 salt, or splits of a larger aliquot. Although clear difficulties persist in making robust comparisons between laboratories, uncertainties quoted herein are about twice as precise as those found in the literature over the past nine years. This degree of improvement is consistent with measurements of an Ag_3PO_4 salt produced by one of the authors (C.H.) at the Finnigan MAT factory in Bremen, Germany in December, 2000, using a conventionally plumbed TC/EA coupled via helium flow to the same model mass spectrometer used in this study. Nine consecutive measurements of reagent grade Ag_3PO_4 gave a standard deviation ±0.35‰ (1σ): a second run of nine measurements on a different Ag_3PO_4 salt, performed weeks later, yielded ±0.38‰ (1σ). These data were not transformed to the VSMOW scale. A year earlier, Kornexl et al. (1999) reported ±0.2‰ (1σ) on the basis of five measurements of an Ag_3PO_4 salt. In 2002, Vennemann et al. reported precisions ranging from ±0.09 to 0.62‰ (1σ) based on a large number of repeated samples and standards. Joachimski et al. (2004 and 2006) report an overall reproducibility of ±0.25‰ (1σ). More recently, Lécuyer et al. (2007) reported ±0.28‰ (1σ), and Bassett et al. (2007) reported ±0.62 to 0.77‰ (1σ).

Two reasons are envisioned for improved precision of $\delta^{18}O_{PO4}$ analyses in this work relative to other studies: (1) reverse plumbing of the He flow through the TC/EA (e.g., Gehre et al., 2004), and (2) precise location of the packing of the reactor relative to the hot spot in the furnace. Locating the precise level of the hot spot is more important for pyrolysis of Ag_3PO_4 than other materials measured (e.g. water, cellulose, benzoic acid). If the glassy carbon fragments are not packed to the precise level of the hot spot each time the reactor is cleaned out and re-packed, CO peaks eluting from the TC/EA will broaden. This is an indication of sluggish pyrolysis in the TC/EA, and peak-tailing that results from this means

that the entire signal cannot be integrated. This, in turn, leads to errors in the determination of isotope ratios. Reverse plumbing of the He carrier gas also produces narrower peaks with reduced peak tailing, compared to conventional He flow. It is believed that the reverse flow of He allows for more 'reproducible' conditions in the reactor over the longer term, and that the bulk of the improvement in precision of $\delta^{18}O_{PO4}$, compared to measurements made with conventionally plumbed TC/EA's (Figure 3.6), is most likely due to a more symmetrical peak shape. The reduced peak tailing is most likely the result of increased He flow through the carbon reactor (Gehre et al., 2004). Because the flow of He is forced to pass first between the outer ceramic and inner carbon reactor, it forces the downward flow of He through the carbon reactor and ultimately to the mass spectrometer more effectively than the conventionally plumbed TC/EA where downward flow to the mass spectrometry can occur through the carbon reactor and between the reactor and outer ceramic tube. With the conventional plumbing, restricted flow can occur in the carbon reactor (e.g., silver build-up from multiple analyses) that will result in greater He flow between the ceramic and carbon reactor instead of through the carbon reactor. This lower flow rate inside the carbon reactor means the CO produced during pyrolization is not flushed to the mass spectrometer as a single pulse and can result in greater peak tailing.

The Saskatchewan Isotope Laboratory has a greater body of work, and experience, performing $\delta^{18}O$ analyses of natural waters in the TC/EA. No increase in precision was seen in water $\delta^{18}O$ analyses resulting from the reversed He flow. However, the memory effect is greatly reduced as noted by Gehre et al. (2004). Before switching to reverse plumbing, water samples were analyzed seven consecutive times to remove the isotopic memory of the previous sample from the reactor. After switching the flow of He carrier gas through the TC/EA, the memory effect was diminished to the point where only three consecutive analyses of a sample are required. Although memory is less of a problem for solids, the previously mentioned narrower elution peaks suggest that conditions in the reactor are more reproducible from sample to sample when the stream of the He carrier gas is reversed through the TC/EA.

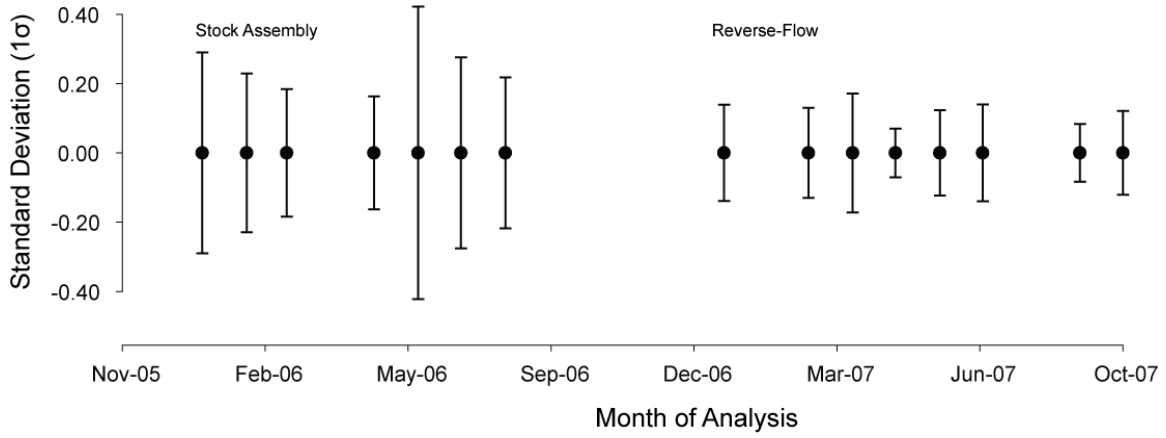

Figure 3.6. Change in precision (1σ) of the in-house Aesar standard from the stock assembly to the reverse-flow plumbed TC/EA. Monthly standard deviations were taken from Aesar samples analysed during sample unknown sequences. An approximately two-fold improvement in the precision was obtained after the modification was made.

Isotopic heterogeneity is another source of uncertainty that may explain some of the large uncertainties reported in the literature (c.f., Venneman et al. 2002), especially for those samples where the uncertainty was based on replicate measurements, and where the sample may not have been homogenized prior to analysis. I found 2.5‰ variation amongst individual crystals of apatite sampled from an igneous rock that I believed was isotopically homogeneous based on a previous study using conventional nickel bomb fluorination and dual inlet G-IRMS (Farquhar et al. 1993). But a closer look reveals the average $\delta^{18}O_{PO4}$ value of 7.28‰ obtained by Farquhar et al. (1993) was based on aliquots of 4 to 10 mg of crystal. I did not expect this range of $\delta^{18}O$ for apatite from a single hand sample because of the high crystallization temperature of the igneous anorthosite, determined to be ~820^{o}C using the plagioclase–apatite oxygen isotope paleothermometer (Farquhar et al., 1993). After homogenizing a large aliquot of the sample, I determined a value of 7.2‰ VSMOW, in excellent agreement with the value reported by Farquhar et al. (1993). The nearly 3‰ range in $\delta^{18}O_{PO4}$ values of the apatite crystals in this rock have some bearing on the precision with which igneous paleotemperatures can be determined, and the closure temperature of apatite.

The poor precision of NBS 120c is more difficult to explain as an artifact of isotopic heterogeneity in the sample because it is distributed by NIST as a fine powder, albeit, an impure powder containing silicates, oxides, and organic matter. Most workers point to these impurities as the principle reason for poor reproducibility between laboratories using this standard. Reduced phosphates, like P_2O_7 and organically bound phosphorous, may react to form PO_4^{-3} ions during the purification chemistry, thus, taking on the isotope value of water in acids used during the dissolution procedure (Keisch et al., 1958). Typically, these acids would be ^{16}O enriched by some 20 to 40‰ compared to phosphate bound oxygen in marine apatite. Microbes can also play a role in promoting isotopic heterogeneity in natural apatite. As phosphate is an essential nutrient, certain microbes can break P–O bonds, thus promoting oxygen isotopic exchange with environmental or diagenetic waters (Blake et al., 1997). There is little consensus on the importance of these natural and laboratory induced isotopic exchange effects because it is not always clear to what extent the widely varying precisions reported in the literature for $\delta^{18}O_{PO4}$ analyses are a reflection of analytical

difficulties or original isotopic heterogeneity in samples. The range in $\delta^{18}O_{PO4}$ values reported for NBS 120c is ~1.2‰ (Crowson et al., 1991; Joachimski et al., 2004; Lécuyer et al., 2007; Vennemann et al., 2002).

The additional benefit of using cation exchange columns for the purification of phosphate is the potential to explore multi-isotope applications. In this study, a modern monkfish tooth and Pennsylvanian conodonts were selected for analysis of $\delta^{18}O_{PO4}$, $\delta^{44}Ca$, $^{87}Sr/^{86}Sr$, and $^{143}Nd/^{144}Nd$ (conodonts only). Late Ordovician conodonts were also processed and analyzed for $\delta^{18}O_{PO4}$. The modern monkfish tooth yielded a $\delta^{18}O_{PO4}$ of 23.20‰ VSMOW, $^{87}Sr/^{86}Sr$ of 0.709190 ± 0.000012 ($2\sigma_m$), and a $\delta^{44}Ca$ of –1.29‰ ± 0.03 ($2\sigma_m$) relative to seawater. Using the phosphate paleo-temperature equation of Kolodny et al. (1983), the monkfish, harvested from coastal waters of the Pacific Northwest near Seattle, yields a habitat water temperature range of 11.0 to 12.3°C, based on our long-term reproducibility of ± 0.15‰. The average yearly temperature for Pacific coastal seawater near Seattle is 10.6 ±2.4°C based on NOAA/National Ocean Services tide stations and NOAA/National Data Buoy Center buoys. The $\delta^{18}O$ value of 20.63‰ for the Pennsylvanian conodont is consistent with previously reported $\delta^{18}O$ values of Pennsylvanian conodonts from the Oread cyclothem (Joachimiski et al. 2006). The $^{87}Sr/^{86}Sr$ ratio is 0.708437 ±0.000033 ($2\sigma_m$), the $\delta^{44}Ca$ value is -1.29‰ ±0.026 ($2\sigma_m$) relative to seawater, and the $^{143}Nd/^{144}Nd$ is 0.512293 ±0.000006 ($2\sigma_m$). The late Ordovician conodonts yielded higher $\delta^{18}O$ values than those determined for middle Ordovician conodonts (15.6 to 16.7‰ VSMOW) by Bassett et al. (2007). The higher $\delta^{18}O$ values suggest cooler climates in the late Ordovician, consistent with their stratigraphic position below the sea level lowstand deposits formed during the Hirnantian glaciation. Global scale ice volume effects may also be implicated, as well as local differences in the $\delta^{18}O$ value of epeiric seawater masses owing to evaporation effects or dilution with meteoric waters.

In their recent paper, Lécuyer et al. (2007) suggested that precision was improved (±0.28‰, 1σ) using only Ag_3PO_4 standards that matched the matrix of the samples. Vennemann et al. (2002) also prepared Ag_3PO_4 standards for this purpose. Both workers calibrated their standards against VSMOW using conventional nickel bomb fluorination and

dual inlet G-IRMS. By contrast, I have shown that a two-point calibration using benzoic acid standards or nitrates (IAEA standards) works just as effectively. Our technique is also demonstrated to be accurate with respect to conventional fluorination and dual inlet isotope ratio mass spectrometry, as I have determined the same $\delta^{18}O$ value for the igneous apatite sample (SP – 3) as Farquhar et al. (1993) when care is taken to homogenize many individual crystals. I conclude that no matrix matching interference is observed when analyzing benzoic acid, nitrates, and phosphates together, and that precise and accurate $\delta^{18}O_{PO4}$ analyses can be achieved as long as standards used are isotopically well-characterized and homogeneous. Because very few laboratories today operate nickel-bomb fluorination lines, and many lack dual inlet G-IRMS, the calibration technique presented herein is better suited to the vast majority of laboratories that are equipped with modern continuous flow instrumentation. Furthermore, if HNO_3 acid is used for dissolution of apatite rather than HF, and cation exchange resin is used instead of anion exchange resin for purification of PO_4^{-3}, then it becomes rather straightforward to extend the reach of $\delta^{18}O_{PO4}$ as a paleothermometer and potential tracer of water masses, with additional measurements of $\delta^{44}Ca$, $^{87}Sr/^{86}Sr$ and $^{143}Nd/^{144}Nd$ (Table 3.4).

3.6 Conclusions

I demonstrate that with a simple modification to a commercially available thermal conversion elemental analyzer (TC/EA), and with careful attention to the location of the reactor hot spot, a two-fold increase in precision of $\delta^{18}O_{PO4}$ measurements can be achieved with coupling to a continuous flow isotope ratio mass spectrometer (CF-IRMS). Reversing the flow of He carrier gas through the TC/EA also reduces the memory effect for water isotope analyses, presumably because the sweep of reversely flowing He clears the TC/EA of CO and H_2 gases more completely than conventional flow. In order to limit the potential for oxygen isotope fractionation during wet chemistry procedures, I employ nitric acid dissolution of apatite and avoid anion exchange resins. Instead, I employ cation exchange resin where the PO_4^{-3} ions pass through the column without interacting with resin, and Ca, Sr and REEs are retained on the resin. An advantage to this approach, compared with dissolutions involving HF, is that precipitation of insoluble metal fluorides is avoided, and

Ca, Sr, and Nd can be eluted from the column and processed further for multi-isotope studies using $\delta^{44}Ca$, $^{87}Sr/^{86}Sr$, and $^{143}Nd/^{144}Nd$ tracers on the same sample aliquot.

The preparation of homogeneous, in-house standards for conversion of raw $\delta^{18}O$ measurements to the VSMOW scale, was described. Calibration was done with the same instrument used for $\delta^{18}O_{PO4}$ measurements. This effectively demonstrates that matrix matching of Ag_3PO_4 samples, with VSMOW calibrated Ag_3PO_4 standards, is not required if benzoic acids nitrates are used. Precise and accurate $\delta^{18}O_{PO4}$ analyses are achieved with either standard. Adopting analytical protocols described herein should allow for a reproducible precision of ±0.15‰ (1σ) to be achieved in any laboratory. This is essentially the instrumental precision as I have found no isotopic fractionation associated with the purification chemistry described herein. The quoted uncertainty also takes into account errors in constructing the calibration line, as each calibration line is constructed from in-house standards analyzed within a given sequence (i.e., the calibration line will 'float' from day to day). I find no compelling reason to run samples multiple times as a strategy for improving the 1σ precision of analyses, unless all sources of systematic error have been eliminated, and the sample is processed in such a way that original isotope heterogeneity is not confounded by analytical artifacts. It is not uncommon to find standard deviations calculated from multiple measurements that are worse than the long-term reproducibility reported herein for a single measurement (e.g., Vennemann et al. 2002; Table 2; Lécuyer et al. 2007; Table 1). This points to sources of uncertainty that have not been fully resolved.

3.7 Acknowledgements

The author would like to thank Ngat Mee Choo for work done at the Saskatchewan Isotope Laboratory. Dr. Walt Sweet and Dr. Sandy McCracken are thanked for donating some of their Ordovician conodont collections.

3.8 References

Bassett, D., MacLeod, K.G., Miller, J.F., and Ethington, R.L. 2007. Oxygen isotopic composition of biogenic phosphate and the temperature of early Ordovician seawater. Palaios, v. 22, p. 98-103.

Blake, R.E., O'Neil, J.R., and Garcia, G.A. 1997. Oxygen isotope systematics of biologically mediated reactions of phosphate. 1. Microbial degradation of organophosphorus compounds. Geochimica et Cosmochimica Acta, v. 61, p. 4411-4422.

Brooks, P.D., Geilmann, H., Werner, R.A., and Brand, W.A. 2003. Letter to the Editor: Improved precision of coupled $\delta^{13}C$ and $\delta^{15}N$ measurements from single samples using an elemental analyzer/isotope ratio mass spectrometer combination with a post-column six port valve and selective CO_2 trapping: improved halide robustness of the combustion reactor using CeO_2. Rapid Communications in Mass Spectrometry, v. 17, p.1924-1926.

Crowson, R.A., Showers, W.J., Wright, E.K., and Hoering, T.C. 1991. Preparation of phosphate samples for oxygen isotope analysis. Analytical Chemistry, v. 63, p. 2397-2400.

Epstein, S., Buchsbaum, R., Lowenstam, H., and Urey, H.C. 1951. Carbonate-water isotopic temperature scale. Geological Society of America Bulletin, v. 62, p. 417-426.

Fanton, K.C., Holmden, C., Nowlan, G.S., and Haidl, F.M. 2002. $^{143}Nd/^{144}Nd$ and Sm/Nd stratigraphy of Upper Ordovician epeiric sea carbonates. Geochimica et Cosmochimica Acta, v. 66, p. 241-255.

Farquhar, J., Chacko, T., and Frost, B.R. 1993. Strategies for high-temperature oxygen-isotope thermometry – A worked example from the Laramie Anorthosite Complex, Wyoming, USA, Earth and Planetary Science Letters, v. 117, p. 407-422.

Firsching, F. 1961. Precipitation of silver phosphate from homogeneous solution. Analytical Chemistry, v. 33, p. 873.

Gehre, M., Geilmann, H., Richter, J., Werner, R.A., Brand, W.A., 2004, Continuous flow $^{2}H/^{1}H$ and $^{18}O/^{16}O$ analysis of water samples with dual inlet precision. Rapid Communications in Mass Spectrometry, v. 18, p. 2650-2660.

Holmden, C., Papanastassiou, D.A., and Wasserburg, G.J. 1997. Negative thermal ion mass spectrometry of oxygen in phosphates. Geochimica et Cosmochimica Acta, v. 61, p. 2253-2263.

Holmden, C., and Hudson, J.D. 2003. $^{86}Sr/^{86}Sr$ and Sr/Ca investigation of Jurassic mollusks from Scotland: Implications for paleosalinities and the Sr/Ca ratio of seawater. Geological Society of America Bulletin, v. 115, p. 1249-1264.

Holmden, C. 2005. Measurement of $\delta^{44}Ca$ using a ^{43}Ca-^{42}Ca double spike TIMS technique In: Summary of Investigations 2003, volume 1, Saskatchewan Geological Survey, Saskatchewan Industry and Resources, Miscellaneous Report 2005-1, CD-ROM, Paper A-4, p. 7.

Joachimski, M.M., van Geldern, R., Breisig, S., Buggisch, W., and Day, J. 2004. Oxygen isotope evolution of biogenic calcite and apatite during the Middle and Late Devonian. International Journal of Earth Sciences, v. 93, p. 542-553.

Joachimski, M.M., von Bitter, P.H., and Buggisch, W. 2006. Constraints on Pennsylvanian glacioeustatic sea-level changes using oxygen isotopes of conodont apatite. Geology, v. 34, p. 277-280.

Kolodny, Y., Luz, B., and Navon, O. 1983. Oxygen isotope variations in phosphate of biogenic apatites, I. Fish bone apatite – rechecking the rules of the game. Earth and Planetary Science Letters, v. 64, p. 398-404.

Keisch, B., Kennedy, J.W., and Wahl, A.C. 1958. The exchange of oxygen between phosphoric acid and water. Journal of the American Chemical Society, v. 80, p. 4778-4782.

Kornexl, B.E., Gehre, M., Hofling, R., and Werner, R.A. 1999. On-line $\delta^{18}O$ measurement of organic and inorganic substances. Rapid Communications in Mass Spectrometry, v. 13, p. 1685-1693.

Lécuyer, C., Grandjean, P., O'Neil, J.R., Cappetta, H., and Martineau, F. 1993. Thermal excursions in the ocean at the Cretaceous-Tertiary Boundary (Northern Morocco) - $\delta^{18}O$ record of phosphatic fish debris. Palaeogeography, Palaeoclimatology, Palaeoecology, v. 105, p. 235-243.

Lécuyer, C., Grandjean, P., and Emig, C.C. 1996. Determination of oxygen isotope fractionation between water and phosphate from living lingulids: Potential application to palaeoenvironmental studies. Palaeogeography, Palaeoclimatology, Palaeoecology, v. 126, p. 101-108.

Lécuyer, C., Fourel, F., Martineau, F., Amiot, R., Bernard, A., Daux, V., Escarguel, G., and Morrison, J. 2007. High-precision determination of $\delta^{18}O$ ratios of silver phosphate by EA-pyrolysis-IRMS continuous flow technique. Journal of Mass Spectrometry, v. 42, p. 36-41.

Longinelli, A., and Nuti, S. 1973. Revised phosphate-water isotopic temperature scale. Earth and Planetary Science Letters, v. 19, p. 373-376.

Luz, B., Kolodny, Y., and Kovach, J. 1984. Oxygen isotope variations in phosphate of biogenic apatite, III. Conodonts. Earth and Planetary Science Letters, v. 69, p. 255-262.

O'Neil, J.R., Roe, L.J., Reinhard, E., and Blake, R.E. 1994. A rapid and precise method of oxygen isotope analysis of biogenic phosphate. Israel Journal of Earth-Sciences, v. 43, p. 203-212.

O'Neil, J.R., Vennemann, T.W., and McKenzie, W.F. 2003. Effects of speciation on equilibrium fractionations and rates of oxygen isotope exchange between $(PO_4)(aq)$ and H_2O. Geochimica et Cosmochimica Acta, v. 67, p. 3135-3144.

Russell, W.A., and Papanastassiou, D.A. 1978. Isotope fractionation of Ca in ion-exchange chromatography. Bulletin of the American Physical Society, v. 23, p. 103-103.

Stephan, E. 2000. Oxygen isotope analysis of animal bone phosphate: Method refinement, influence of consolidants, and reconstruction of palaeotemperatures for Holocene sites. Journal of Archaeological Science, v. 27, p. 523-535.

Stuart-Williams, H.L.Q., and Schwarcz, H.P. 1995. Oxygen isotopic analysis of silver orthophosphate using a reaction with bromine. Geochimica et Cosmochimica Acta, v. 59, p. 3837-3841.

Vennemann, T.W., Fricke, H.C., Blake, R.E., O'Neil, J.R., and Colman, A. 2002. Oxygen isotope analysis of phosphates: a comparison of techniques for analysis of Ag_3PO_4. Chemical Geology, v. 185, p. 321-336.

3.9 Relevance of Manuscript to Thesis

This chapter presents an innovative approach to the analysis of $\delta^{18}O$ from phosphates that results in better precision, small sample sizes, and a chemical process that allows for multiple isotopes systems to be analyzed simultaneously. Although no reference is made to the previous chapter, the chemical and analytical procedure presented allows for the study of oxygen isotopes in epeiric sea settings using conodonts that can be coupled with carbon and nutrient cycling to gain a better understanding of changes in climate and how that relates to stratigraphic changes in stratigraphic isotope profiles.

CHAPTER 4 DISCUSSION AND RELATION OF THE MANUSCRIPTS TO THE THESIS

Each chapter in the main body of the thesis (Chapters 2 and 3) offers a detailed examination of different aspects of using isotope profiles, specifically those from epeiric sea stratigraphic sections. Not only do these manuscripts focus on understanding changes in isotope proxies as they relate to local changes in epeiric seawater characteristics, but they provide novel ways to study multiple isotope systems simultaneously.

Chapter 2, *Carbon and Nitrogen Cycling During the Hirnantian Glaciation: Implications for Epeiric Sea Gradients, Productivity and Calcite Dust Deposition*, provides the most detailed study yet presented of epeiric sea C-cycling during the Hirnantian. Based on the deepest water sections studied thus far (Nevada, Cape Phillip's, Estonia), the global positive $\delta^{13}C$ excursion during the Hirnantian is determined to be $2.6 \pm 0.4‰$. This value is significant since it allows for predictive models to more accurately determine the cause for the change in the global carbon cycle during the Hirnantian. Additionally, this study suggests an explanation for the differences in $\delta^{13}C_{org}$ profile variance seen between Hirnantian stratigraphic sections. A $\delta^{15}N$ profile through the Hirnantian glacial interval records a 2‰ positive shift in the Vinini Creek section, Nevada. Its interpretation as a major late Ordovician upwelling zone makes this section a suitable candidate for the preservation of original sedimentary $\delta^{15}N$ records. A conceptual model of ocean nitrogen cycling is presented that highlights the dual role of cyanobacteria as primary producers and nitrogen fixers. In greenhouse climates, deepwater fixed nitrogen inventories decline due to denitrification in the ocean's expansive oxygen minimum zones, and algal productivity becomes tightly coupled to cyanobacterial productivity as the main source of fixed nitrogen to the photic zone. The cooler climate of the Hirnantian icehouse led to increased ocean ventilation, greater partitioning of atmospheric oxygen into downwelling surface waters, oxygen minimum zone shrinkage, and declining denitrification rates. This in turn allowed for upwelling of recycled nitrogen with high $\delta^{15}N$ values into the photic zone, thus, shifting the export production of organic carbon from the photic zone to higher $\delta^{15}N$ value, consistent with the observed positive shift during the Hirnantian glaciation.

The 2.6‰ shift in the $\delta^{13}C$ value of the Hirnantian global ocean is attributed to increased carbonate weathering during the glacio-eustatic sea level lowstand. Increased productivity may, however, be partly responsible for the much larger shifts recorded in the epeiric seas (5-7‰). Weathering of carbonates is expected to transfer nutrients to the epeiric seas, and some of this nutrient may have been delivered in the form of calcite dust. Because the supply of calcite dust drops off rapidly with increasing distance from the paleo-shoreline, any ^{13}C enriched alkalinity addition, or ^{13}C increase from primary productivity, will decrease towards the ocean—a pattern consistent with the orientation of the inferred seawater gradient in $\delta^{13}C$ values. The absence of vascular plants, the predictable increase in the velocity of the trade winds in icehouse climates, and the large quantities of calcite sediment exposed by the glacio-eustatic lowering of sea level, all point to a prominent role for calcite dust as a component of the early Paleozoic carbon cycle.

Chapter 3, *Oxygen isotope analysis of phosphate: Improved precision using TC/EA CF-IRMS*, provides a detailed description of the chemical and analytical technique developed by the author. The chemical technique for apatite focuses primarily on oxygen isotopes and is the first study to implement the collection of multiple isotopes. This method allows for small sample sizes of apatite (200 µg) to be used for a single analysis that limits the potential fractionation of PO_4^{-3} isotopomers, and yields precise (0.15‰, 1σ) oxygen isotope values. The simultaneous collection of Ca, Sr, and REE by using a cation exchange column approach allows for multiple isotope systems to be studied from a single sample. This chemical technique is ideal for the study of biogenic apatite from preserved epeiric sea sediment (e.g., conodonts).

APPENDIX 1

Stratigraphic Data from Vinini Creek, Monitor Range, and Blackstone River

Section Depth (m)	$\delta^{13}C_{Carb}$ (‰, V-PDB)	$\delta^{13}C_{Org}$ (‰, V-PDB)	$\delta^{18}O_{Carb}$ (‰, V-PDB)	$\delta^{15}N_{TN}$ (‰, Air)	%TOC	%TN	%Calcite	C_{org}/N_{tn}
Vinini Creek								
0.85	-1.00	-30.69	-6.76	0.25	1.62	0.148	36.4	13
1.08	0.63	-30.52	-5.71	0.04	0.35	0.044	72.5	10
1.30	1.15	-30.57	-5.75	0.07	0.91	0.056	75.5	20
1.47	-0.61	-30.56	-6.88	-0.23	1.28	0.068	81.4	22
1.75	0.77	-30.14	-6.48	0.24	0.32	0.036	78.4	11
1.86	0.54	-30.47	-5.91	0.33	0.37	0.030	84.8	15
2.08	0.73	-30.74	-6.33	0.10	0.59	0.051	72.3	13
2.31	-0.34	-30.37	-6.01	0.13	0.90	0.103	50.6	11
2.53	0.18	-30.56	-6.79	0.17	0.59	0.062	68.0	12
2.75	0.56	-30.32	-6.19	0.34	0.36	0.032	79.5	13
2.98	-1.33	-30.5	-7.06	0.03	1.04	0.121	43.4	11
3.20	0.35	-30.54	-6.38	0.26	0.33	0.041	77.1	10
3.43	0.66	-30.35	-5.87	0.32	0.33	0.037	78.9	10
3.65	-0.22	-30.2	-5.98	0.44	0.60	0.060	70.6	13
3.87	-0.41	-30.41	-5.74	0.21	0.24	0.027	85.6	11
4.10	0.30	-30.32	-6.65	0.26	0.40	0.037	78.8	13
4.43	0.04	-30.2	-7.06	0.27	0.44	0.054	70.7	10
4.66	0.93	-30.7	-5.97	0.14	0.43	0.046	76.4	12

4.77	0.37	-30.05	-6.36	-0.84	0.20	0.044	90.4	5
4.99	-1.50	-30.49	-4.34	0.44	0.26	0.023	87.5	14
5.21	0.58	-29.96	-6.26	-0.02	0.21	0.042	75.6	6
5.72	-2.16	-30.48	-3.67	0.37	0.24	0.024	88.4	11
5.94	-1.85	-30.52	-4.12	0.43	0.23	0.022	88.0	13
6.28	-2.29	-30.63	-3.55	0.38	0.17	0.019	89.7	11
6.50	-2.80	-30.41	-3.98	0.52	0.24	0.021	88.9	14
6.72	-4.87	-29.68	-10.24	0.92	0.71	0.099	48.3	9
6.95	0.75	-30.69	-5.89	0.23	0.33	0.038	81.4	11
7.28	0.00	-30.86	-7.18	0.15	0.71	0.043	83.8	19
7.51		-30.79		-0.05	3.10	0.208	13.1	19
7.79	1.52	-30.83	-5.97	0.23	0.27	0.030	83.5	11
8.07	-1.84	-31.15	-5.23	0.23	3.53	0.219	9.1	19
8.29	-2.91	-30.91	-7.29	0.24	2.69	0.184	15.6	18
8.51	-2.74	-31.87	-7.65	-0.18	12.55	0.438	25.5	36
8.74		-31.91		-0.22	20.00	0.651	10.3	36
8.96		-32		-0.05	21.49	0.689	9.1	39
9.18	-2.74	-31.56	-9.42	-0.73	1.62	0.051	15.5	39
9.41	-4.21	-31.61	-13.09	-0.30	2.60	0.078	15.2	39
9.63	-1.26	-31.9	-9.22	0.39	1.58	0.055	89.9	36
9.74	-1.07	-31.7	-8.50	0.14	1.60	0.042	69.0	48
9.97	0.09	-31.73	-7.51	0.19	1.32	0.052	89.0	29
10.02	-1.92	-31.3	-8.34	-0.02	1.49	0.043	8.8	43
10.25	-2.47	-31.31	-10.10		0.93		85.9	

10.47	-0.89	-31.44	-7.90	0.02	1.13	0.058	10.0	23
10.69	-2.81	-31.19	-9.54	0.15	2.22	0.080	19.7	35
10.92	-3.83	-31.1	-11.06	0.08	1.57	0.052	2.2	38
11.14	-3.76	-31.09	-11.10	0.03	3.45	0.092	10.6	44
11.37		-31.43		0.03	25.24	0.773	4.3	41
11.59		-31.53		-0.25	3.93	0.097		50
11.81	-2.64	-31.46	-11.22	-0.26	2.63	0.079	7.0	39
12.04	-4.71	-31.48	-11.87	-0.10	3.55	0.096	30.6	46
12.26	-2.57	-31.28	-17.02		1.07			
12.60	-2.59	-31.27	-10.77		0.79			
12.82	-1.10	-31.49	-8.51	0.64	1.38	0.053	88.1	33
13.15	-1.33	-31.06	-7.77	0.48	1.50	0.051	88.3	37
13.38	-0.31	-31.59	-8.49	0.51	1.84	0.068	88.0	31
13.60	-4.77	-30.93	-14.19	0.76	1.56	0.060	75.6	32
13.83	-3.12	-31.2	-10.59	0.26	5.89	0.202	19.8	36
14.05	-3.92	-30.81	-13.02	0.83	3.40	0.100	-2.8	40
14.27	-2.64	-31.12	-12.81	0.22	2.67	0.085	-1.2	39
14.50		-31		0.18	2.69	0.083	4.9	41
14.56	-4.49	-31.08	-14.55	0.07	2.75	0.078	7.5	41
14.79	-3.31	-31.24	-11.47	-0.18	2.56	0.075	16.2	43
15.01	-4.70	-31.1	-14.29	0.12	1.98	0.059	17.5	42
15.23		-31.13		-0.02	2.10	0.066	4.6	37
15.46	-3.24	-31.09	-10.72	-0.29	1.94	0.044	95.3	55
15.61	-3.20	-30.82	-11.21	-0.23	4.57	0.098	89.2	58

15.84	-4.94	-31.05	-15.20		0.72			
16.06	-3.34	-31.33	-9.28	-0.57	3.28	0.091	7.7	45
16.23		-31.31		-0.43	3.06	0.098	7.2	39
16.45		-31.34		-0.54	2.33	0.076	6.4	36
16.73		-31.45		-0.57	3.09	0.104	5.7	37
16.96		-31.44		-0.28	3.33	0.104	4.6	40
17.18		-31.16		-0.18	25.04	0.834	16.2	35
17.29		-31.56		-0.31	5.02	0.157	4.2	40
17.46		-31.54		-0.51	3.76	0.119	4.4	39
17.68	-3.34	-31.68	-6.56	-0.62	3.87	0.123	4.9	37
17.85		-31.66		-0.33	8.94	0.274	2.7	41
18.07		-31.74		-0.46	6.40	0.209	3.2	38
18.30		-31.3		-0.06	10.44	0.324	18.5	38
18.52		-31.25		0.33	4.33	0.169	37.9	32
18.69	-0.39	-30.81	-2.98	0.02	5.16	0.173	43.6	37
18.97	-0.19	-29.28	-2.83	0.05	2.59	0.102	68.4	30
19.19	-0.45	-29.01	-3.35	0.43	3.00	0.112	55.6	33
19.42	-0.25	-29.78	-3.44	0.13	2.57	0.099	57.8	32
19.64	-1.42	-29.17	-9.34	0.30	0.73	0.030	84.9	28
19.86	-0.72	-29.58	-8.94	0.37	0.53	0.016	91.3	41
20.09	-0.67	-29.23	-4.42	0.14	1.61	0.063	60.7	32
20.31	-0.60	-29.08	-4.23		2.19			
20.54	-0.24	-30.05	-3.56	0.36	1.65	0.066	62.0	31
20.76	-0.63	-30.69	-5.68	0.35	1.90	0.070	61.0	34

20.93	0.37	-29.7	-6.42	0.17	0.35	0.025	74.0	16
21.04	1.78	-30.1	-5.89	0.43	0.81	0.038	72.7	26
21.15	0.34	-30.35	-6.65	0.43	0.85	0.046	71.3	23
21.32	0.17	-29.54	-6.07	0.54	0.68	0.043	64.1	19
21.54	1.11	-30.07	-5.84	0.51	0.40	0.019	84.0	26
21.77	1.46	-30.08	-6.59	0.76	0.39	0.016	90.3	31
21.99	2.01	-30.2	-5.82	0.70	0.31	0.013	90.8	28
22.21		-29.92		0.60	0.99	0.053	68.6	24
22.32		-29.89		0.55	0.54	0.033	75.5	20
22.55	1.42	-29.88	-7.39	0.87	0.23	0.014	89.5	19
22.77	2.30	-29.9	-6.72	0.55	0.24	0.013	87.5	23
23.00		-29.94		0.80	0.78	0.049	71.9	20
23.11	2.35	-29.04	-6.24	0.84	0.18	0.015	87.3	14
23.44	2.49	-29.12	-5.29	0.67	0.17	0.014	90.1	16
23.67	2.55	-29.34	-5.93	0.76	0.35	0.025	77.7	18
24.00		-29.56		0.66	0.98	0.060	65.4	19
24.23		-29.38		0.73	0.93	0.051	65.9	23
24.45	3.92	-29.46	-5.61	0.64	0.22	0.016	90.0	17
24.78		-28.73		0.61	2.06	0.046	70.6	21
25.01	3.64	-28.67	-5.59	0.40	0.77	0.025	83.2	25
25.23	3.24	-29.37	-5.66	0.62	0.49	0.021	84.5	27
25.46	3.05	-29.15	-5.35	0.63	0.48	0.011	93.2	25
25.79	1.58	-29.44	-6.35	0.55	0.22	0.030	77.5	24
26.01	2.06	-28.19	-6.34	1.27	0.58	0.009	93.8	19

26.24	2.04	-28.45	-6.27	0.61	0.14	0.009	93.7	24
26.46	0.03	-29.5	-6.83	0.53	0.17	0.037	76.3	26
26.69	1.84	-28.73	-6.42	0.58	0.76	0.007	94.9	19
26.91	1.19	-29.29	-5.96	0.75	0.11	0.011	92.3	20
27.13	1.79	-29.1	-6.09	0.41	0.18	0.007	94.3	17
27.30	1.11	-29.72	-5.17	0.73	0.10	0.009	94.2	24
27.47	1.72	-29.78	-4.74	0.40	0.18	0.013	92.5	33
27.69	1.85	-28.19	-5.97	0.51	0.35	0.005	96.1	23
27.92	-1.10	-28.94	-5.79	0.72	0.10	0.017	77.1	72
28.14	-3.25	-30.6	-6.82		1.06			
28.70		-30.03			2.08			

Section Depth (m)	$\delta^{13}C_{Carb}$ (‰, V-PDB)	$\delta^{13}C_{Org}$ (‰, V-PDB)	$\delta^{18}O_{Carb}$ (‰, V-PDB)	$\delta^{15}N_{TN}$ (‰, Air)	%TOC	%TN	%Calcite	Corg/Ntn
Monitor Range								
126	2.08	-25.32	-6.08		0.16		50.9	
127	1.90	-26.66	-5.39	0.93	0.15	0.002	90.9	98
128	2.19	-29.07	-6.14	3.24	0.17	0.004	96.6	54
129	1.70	-29.65	-4.80	3.22	0.22	0.006	98.3	40
130	1.83	-29.28	-5.30	2.99	0.14	0.005	97.6	35
131	2.00	-28.73	-5.25	3.11	0.06	0.009	99.4	8
132	1.67	-29.06	-5.69	0.75	0.04	0.002	99.6	21
133	1.71	-29.05	-5.55	1.17	0.04	0.002	99.6	17

134		-27.14		1.70	0.06	0.002	99.4	46
135	1.73	-28.13	-6.04		0.08		89.1	
136	1.66	-29.20	-5.70	2.05	0.17	0.003	98.9	67
137	1.35	-29.33	-5.59	4.98	0.12	0.008	98.4	18
138	0.84	-28.83	-6.30	3.25	0.20	0.004	97.0	62
139	1.64	-28.71	-7.93	3.19	0.10	0.003	97.0	38
140	1.66	-28.65	-9.38	4.06	0.12	0.008	98.8	17
141	1.26	-28.38	-5.54	2.94	0.09	0.002	97.7	41
142	1.18	-28.97	-5.36	2.85	0.15	0.005	97.8	37
143	1.13	-28.98	-6.18	2.24	0.08	0.002	98.5	38
144	0.95	-28.26	-7.62	3.87	0.07	0.003	98.5	32
145	0.81	-28.88	-5.84	2.94	0.16	0.002	98.5	101
146	0.42	-28.71	-4.37	1.25	0.17	0.003	98.2	70
147	0.08	-29.43	-6.41	2.83	0.18	0.003	98.3	65
148	0.59	-30.40	-5.62	1.86	0.47	0.018	89.6	30
149	1.29	-30.02	-5.68	-0.67	0.50	0.011	61.4	54
150	1.49	-29.94	-5.21	0.76	0.59	0.016	81.6	42
151	1.74	-28.97	-3.39	-0.13	0.55	0.024	75.3	27
152	1.68	-29.20	-2.99	0.59	0.66	0.025	78.3	31
153	3.27	-28.02	-5.47	1.17	0.30	0.009	95.9	40
154	3.65	-27.63	-5.70	1.48	0.23	0.007	96.5	40
155	3.84	-27.71	-5.43	0.76	0.16	0.009	94.1	21
156	4.27	-27.20	-5.48	1.62	0.09	0.006	94.5	17
157	5.18	-26.47	-5.42	0.39	0.07	0.004	96.3	20

158	6.70	-25.88	-4.41	0.76	0.04	0.003	98.1	19
159	6.06	-25.77	-6.03	0.45	0.04	0.002	98.1	24
160	6.56	-26.19	-5.21	1.72	0.05	0.002	98.5	38
160.5	6.96	-25.97	-4.39		0.03		99.0	
161	7.22	-25.59	-4.48		0.02		99.2	
162.8	7.20	-25.49	-4.09		0.02		99.2	
164.5	6.87	-26.99	-5.01	2.02	0.07	0.005	98.8	18
165.5	6.34	-29.03	-6.02	0.45	0.11	0.005	99.0	26
166.5	6.64	-29.80	-6.91	0.05	0.20	0.006	98.9	43
167.5	6.97	-27.08	-6.47		0.05		99.1	
168.5	6.47	-26.48	-6.59	3.56	0.08	0.006	98.1	15
169.3	6.85	-28.33	-5.91		0.04		99.6	
171.5	6.29	-29.04	-7.01	0.71	0.15	0.004	98.8	48
172.9	1.38	-29.97	-6.41	0.05	0.98	0.040	80.1	28
173.8	6.22	-29.33	-7.88	0.66	0.12	0.004	99.0	36
175	6.26	-29.40	-6.75	0.05	0.09	0.002	99.4	46
176.5	6.28	-29.32	-6.72		0.08		99.5	
178.4	6.57	-27.48	-5.72		0.03		99.5	
180.5	5.74	-28.94	-8.09	1.93	0.08	0.003	99.4	34
181.5	5.66	-26.79	-5.94		0.02		99.7	
182.5	4.89	-29.42	-8.26	-0.41	0.13	0.003	99.1	42
183.2	5.54	-29.11	-7.06		0.04		99.4	
184	4.95	-26.50	-7.90		0.03		99.2	
185	4.88	-28.38	-7.84	-0.47	0.06	0.001	99.0	55

186	4.93	-26.16	-8.18		0.03		98.9	
187	4.79	-25.63	-7.79		0.02		99.2	
188	4.11	-25.79	-7.61		0.04		98.6	
191	2.76	-27.25	-7.30	0.30	0.02	0.003	99.1	23
193.4	2.58	-28.42	-7.41	-0.90	0.11	0.005	93.8	27
194.4	-0.44						94.1	
197	2.69	-30.41	-5.60		0.11		97.4	
198	0.98	-30.42	-9.21	1.51	0.19	0.004	98.3	57
202	0.84	-30.48	-9.25		0.21		29.7	
204	0.57	-30.78	-6.08	0.12	0.07	0.002	99.6	43
205	0.11	-29.94	-5.98	0.87	0.70	0.035	83.3	23
206	0.82	-30.23	-6.42		0.09		98.7	
207	0.04	-30.74	-6.32		0.02		99.8	
208	0.05						100.0	
209	0.04						99.2	
211	0.07	-29.81	-7.45	0.03	0.04	0.000	99.2	117
212	0.17	-29.32	-6.67	3.50	0.04	0.003	99.7	27
213	0.00	-29.11	-7.69		0.06		97.9	
214	-0.24	-29.43	-7.40	0.29	0.04	0.002	99.3	44
215	-0.16	-29.50	-6.52		0.08		98.7	
216	-0.03	-29.73	-8.41		0.05		98.9	
217	-0.19	-30.40	-6.62		0.10		98.9	
217.9	-0.083						97.5	
218	-0.108						98.2	

219	-0.18	-29.41	-7.42	0.58	0.07	0.001	98.8	65
220	-0.10	-30.32	-6.39		0.07		99.2	
221	-0.395						94.5	
223	-0.457						96.8	
224	-0.71	-28.49	-5.95		0.27		27.5	
226.3	-0.76	-28.47	-5.35	6.31	0.07	0.005	99.7	24
227	0.28	-29.42	-6.02	1.47	0.11	0.004	99.6	50
228	-0.288						98.2	
229	0.17	-29.61	-8.29		0.16		98.2	
231	-1.48	-28.58	-6.16	-0.70	0.16	0.001	98.5	23
232	-1.95	-28.61	-6.54		0.02		99.8	
233	-1.49	-30.09	-7.08	-2.60	0.36	0.273	96.7	0

Section Depth (m)	**$\delta^{13}C_{Carb}$ (‰, V-PDB)**	**$\delta^{13}C_{Org}$ (‰, V-PDB)**	**$\delta^{18}O_{Carb}$ (‰, V-PDB)**	**$\delta^{15}N_{TN}$ (‰, Air)**	**%TOC**	**%TN**	**%Calcite**	**Corg/Ntn**
Blackstone River								
0.05	0.78	-30.25	-7.13		2.31		22.4	
0.5	0.99	-29.97	-6.58		2.46		17.4	
1	0.94	-30.76	-6.27		1.15		20.8	
1.5	1.04	-30.08	-6.51		1.66		29.9	
2	1.14	-30.28	-7.07		2.72		38.3	
2.5	1.29	-29.93	-6.70		1.18		49.7	
3	1.77	-29.96	-6.96		0.92		70.5	

3.5	2.03	-30.19	-6.83	1.14	83.7
4	1.82	-30.19	-7.18	1.52	80.1
4.5	1.70	-29.96	-6.58	0.65	80.1
5	1.20	-30.32	-7.74	2.15	65.6
5.5	1.23	-30.40	-6.67	2.68	47.7
6	1.41	-29.77	-6.98	1.85	70.0
6.5	1.36	-30.10	-6.86	1.21	71.9
7	1.98	-30.48	-6.63	1.24	86.4
7.5	2.14	-30.60	-6.73	0.99	92.0
8	0.29	-30.40	-7.28	1.46	71.8
8.5	1.33	-30.27	-7.09	1.98	74.5
9	1.99	-30.44	-6.79	3.04	69.2
9.5	1.83	-30.46	-6.76	1.28	84.0
10	2.05	-30.27	-6.45	0.99	91.1
10.5	1.92	-30.42	-6.62	0.92	92.2
11	1.79	-30.47	-6.50	0.59	94.3
11.5	1.62	-30.25	-6.76	1.81	80.9
12	1.48	-30.44	-6.75	1.36	76.8
12.5	0.98	-30.25	-7.12	3.56	70.1
12.67	0.53	-30.37	-6.12	4.08	63.3
13	0.44	-30.48	-6.92	3.19	71.3
13.5	-0.09	-30.20	-6.75	2.26	55.1
14	-0.10	-30.14	-6.55	5.45	39.2
14.5	-0.77	-30.33	-7.41	4.62	34.1

15	-0.32	-30.17	-6.61	4.28	27.9
15.5	0.18	-30.56	-6.81	3.08	39.9
16	0.01	-30.67	-7.00	3.44	46.6
16.5	0.01	-30.71	-6.45	3.28	51.4
17	1.49	-30.62	-6.85	3.32	52.3
17.5	-0.32	-30.85	-7.09	3.18	56.0
18	-0.29	-30.59	-7.10	4.15	57.9
18.5	0.09	-30.81	-6.57	4.52	66.0
18.85	0.01	-30.78	-7.17	4.31	68.9
19	0.10	-30.55	-7.58	5.08	65.1
19.2	2.41	-28.91	-7.76	4.82	55.6
19.5	3.58	-26.36	-6.75	0.30	90.1
20	4.13	-27.69	-7.09	0.40	86.0
20.5	4.57	-28.52	-5.73	0.55	76.9
21	4.51	-28.73	-5.71	0.71	77.8
21.5	3.54	-27.46	-6.97	0.25	87.1
22	4.99	-27.84	-6.08	0.30	89.5
22.5	4.96	-28.36	-6.42	0.54	80.7
23	4.30	-27.56	-6.05	0.48	88.8
23.5	4.50	-26.86	-6.34	0.16	86.5
24	4.56	-27.19	-6.03	0.29	87.1
24.5	5.08	-27.30	-7.02	0.65	77.3
25	5.28	-26.24	-7.24	0.68	76.1
25.5	5.31	-27.61	-6.22	0.66	80.7

26	4.94	-27.01	-5.72	0.28	88.6
26.5	5.23	-26.33	-7.23	0.47	76.0
27	5.03	-26.48	-6.91	0.39	79.2
27.5	4.68	-26.33	-7.40	0.47	80.9
28	3.74	-27.49	-6.80	0.50	88.7
28.25	3.92	-25.70	-6.73	0.16	96.4
28.5	4.06	-27.74	-6.89	0.77	87.4
29	4.26	-24.87	-4.88	0.12	95.9
29.5	5.20	-24.84	-4.49	0.11	97.7
30	5.03	-28.33	-7.82	0.79	75.8
30.5	4.64	-27.92	-6.82	0.56	79.0
31	4.36	-27.52	-5.72	0.44	88.3
31.5	4.34	-27.55	-5.68	0.22	93.7
32	4.74	-25.53	-4.79	0.12	97.7
32.5	2.26	-28.99	-6.83	0.35	89.6
32.8	1.14	-30.72	-7.69	2.91	55.3
33	1.93	-29.91	-7.28	2.53	75.9
33.5	0.30	-30.93	-7.49	2.57	51.0
34	0.80	-31.20	-7.40	2.68	45.0
34.5	0.54	-30.84	-7.00	1.76	38.2
35	0.45	-30.92	-6.93	1.81	43.6
35.5	0.06	-31.46	-8.20	2.01	51.0
36	0.72	-30.86	-8.63	0.57	15.8
36.5	0.21	-30.94	-7.32	1.52	31.4

37	0.13	-30.47	-7.85	1.07	52.5
37.5	0.19	-30.97	-7.31	1.38	49.5
38	0.55	-30.84	-7.28	0.57	21.3
38.5	0.39	-30.29	-7.64	1.14	27.8
39	0.19	-30.97	-7.36	1.13	26.0
39.5	0.31	-31.11	-7.07	1.72	59.9
40	1.86	-31.07	-7.37	0.94	72.7
40.5	-0.36	-30.58	-8.11	0.63	42.3
41	0.10	-30.45	-7.39	1.69	30.7
41.5	-0.11	-30.32	-7.52	1.10	44.0
42.5	-0.36	-30.27	-7.80	0.85	33.2
43	-0.03	-30.48	-7.58	1.04	23.1
43.5	-0.05	-30.41	-7.35	1.81	33.7
44		-30.19		1.07	10.4
44.5	-0.17	-30.43	-7.31	2.54	28.9
45	-0.20	-30.29	-7.18	3.05	29.9
47	0.36	-30.36	-7.49	4.63	21.7
47.5	0.51	-30.47	-7.27	3.57	21.0
48	0.17	-30.27	-7.03	2.85	28.5
48.5	-0.43	-30.44	-8.28	3.64	36.0
49	-0.66	-30.24	-8.81	3.01	35.8
49.5	0.05	-30.48	-7.64	4.06	40.4